

***Synthesis, catalytic and electrochemical  
studies of manganese oxides, OMS-2***

**A thesis**

**Submitted to**

**Goa University**

**For the degree of**

**DOCTOR OF PHILOSOPHY**

**In**

**CHEMISTRY**

**By**

***Jeanette S. Rebello***

**Department of Chemistry,**

**Goa University,**

**Taleigao Plateau,**

**Goa - 403 206.**



*Examined & Accepted*

*BH... 9/9/06*

*(External Referee)*

**JUNE 2006**

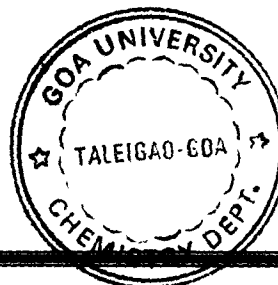
*547*  
*REB/Syn*

*T-339*

*Examined & Accepted*

*[Signature]*

*9/9/06*




## STATEMENT

I hereby state that this thesis entitled, "Synthesis, Catalytic and Electrochemical studies of manganese oxides, OMS-2" is my original work and it has not previously formed the basis for the award of any degree, diploma, associateship, fellowship or any other similar titles to the best of my knowledge.



Jeanette S. Rebello


(candidate)



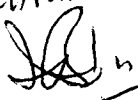
Prof. Julio B. Fernandes

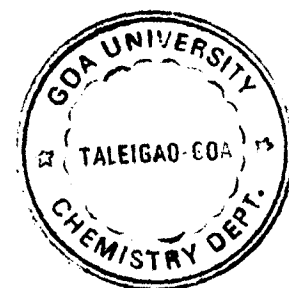
(Research Guide)



 9/9/06  
(External Referee)  
Dr. B.H. Mehta.  
Univ. of Mumbai

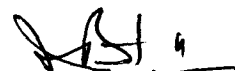
Examined & accepted

  
9/9/06



## CERTIFICATE

As required under the University ordinance, I certify that the thesis entitled, "Synthesis, Catalytic and Electrochemical studies of manganese oxides, OMS-2" submitted by **Miss Jeanette S. Rebello** for the award of Doctor of Philosophy in Chemistry is a record of research work done by the candidate during the period of study and it has not previously formed the basis for the award of any degree, diploma, associateship, fellowship or any other similar titles.



Prof. Julio B. Fernandes

Research Guide

Department of Chemistry,

Goa University.

## ACKNOWLEDGEMENTS

*I cannot begin to express my pleasure for the opportunity to work with one of the best I've known – Prof. Julio B. Fernandes. I am honoured to have been a part of his research group. Without his encouragement, patience, guidance, overwhelming wealth of knowledge and inspiration throughout, this would still be a dream. Thank you Sir, for believing in me enough and helping me last right through the end.*

*I sincerely thank Prof. J.S. Budkuley and Prof. K.S. Rane for the constant encouragement throughout the course of this investigation.*

*Thanks to Prof. Newman Fernandes, Principal, St. Xavier's College, Mapusa and the 'Xavier's Family' for the encouragement.*

*I am greatly indebted to Dr. Sajo P. Naik, University of Tokyo, Japan, for the valuable suggestions, scientific discussions and all the help rendered to me especially the XRD, FESEM, catalytic studies and teaching me to use the GC.*

*Special thanks to Dr. M. Sudersanan, Rtd. Scientist, Analytical Chemistry Division, BARC, Mumbai for allowing me to use the facilities; Mr. Ashish Satpati, ACD, BARC, for helping me immensely with the CV measurements and constantly encouraging me whenever needed and the discussions as well. And not to forget Mr. Thomas and Mr. Dalvi for waving the 'magic wand' whenever the instrument was down.*

*I am also grateful to Prof. J.L. Figueiredo, University of Porto for permitting me to use BET and TPD instruments; Dr. Carmen Rangel, INETI, Lisbon for electrochemical studies and to Fundação Oriente for the scholarship and making this visit to Portugal possible for me. I appreciate and cherish all the friendships developed in Portugal.*

*To all my teachers at the Department of Chemistry, who have positively affected my life in all these years that I have spent at the University and for providing useful suggestions and constructive criticism especially during the annual research presentations.*

*Thanks are also due to the non-teaching staff of Department of Chemistry, Goa University library and office for always being very helpful and kind. I am grateful to Mr. Jai Prakash and Mr. Lopes, USIC, Goa University for the help rendered to me.*

*To all research colleagues from our group, research scholars in the different branches of the Department of Chemistry, as well as the research fraternity at the Goa University, I do cherish the pleasant moments we've had.*

*How can I forget Dr. Asha D'Souza, a great friend and ex-research colleague? I can never thank you enough Ash, for helping me especially when I had just begun research, the fun times we've shared, as well as for introducing me to chai.*

*And Dr. Purnakala Samant (Purna), I will forever remain indebted to you. Thanks for your constant encouragement, support, suggestions and valuable discussions. Despite the many obstacles you had yourself, you were yet available to assist me at a moments notice.*

*Thanks to Mitendra Alve, DIKSHA Education Centre, Margao, for the timely and prompt help rendered to me all the time.*

*To those friends, who have unknowingly rejuvenated my pleasure in the "simple things", many thanks for sharing parts of your lives with me. And I cannot forget the welcome "wuffs" and doggy tales of my dearest Snoopy; at the end of an exhausting day were the most soothing of all.*

*I owe all of this and much more to my entire family for their love, prayers, constant support and assistance in ways I cannot tell, despite all odds and ends that have aided me to this point of my life.*

*Finally, I am grateful to my Lord Jesus Christ, who continues to be my refuge and my guiding light.*

**Jeanette S. Rebello**

# INDEX

<b>CONTENTS</b>	<b>Page</b>
List of Figures .....	v
List of Tables.....	viii
List of Schemes .....	x
<b><i>SUMMARY/GENERAL CONCLUSIONS.....</i></b>	<b><i>xi</i></b>
<b>CHAPTER I – Introduction and literature status.....</b>	<b>1-39</b>
1.1 Introduction to OMS-2.....	1
<i>1.1.1 Manganese Oxides; Structural Chemistry.....</i>	<i>2</i>
<i>1.1.2 Classification of Molecular sieves .....</i>	<i>7</i>
<i>1.1.3 Synthesis of OMS-2 materials.....</i>	<i>8</i>
<i>1.1.4 Characterization Techniques.....</i>	<i>14</i>
<i>1.1.5 What makes Octahedral Molecular sieves so interesting?.....</i>	<i>14</i>
<i>1.1.6 Putting the OMS materials to use .....</i>	<i>16</i>
1.2 Introduction to Fuel Cells.....	18
<i>1.2.1 Why DMFC? An Overview.....</i>	<i>20</i>
<i>1.2.2 Conventional Electrocatalysts: A glimpse at the methanol oxidation     mechanism.....</i>	<i>22</i>
<i>1.2.3 Drawbacks .....</i>	<i>26</i>
<i>1.2.4 Move towards other catalysts .....</i>	<i>26</i>
<i>1.2.5 Transition metal oxides as promising catalysts.....</i>	<i>32</i>
<i>1.2.6 Supported Metal catalysts .....</i>	<i>35</i>
<i>1.2.7 Objectives .....</i>	<i>37</i>
1.3 Summary .....	38

<b>CHAPTER II – Synthesis of OMS-2 using anion template.....</b>	<b>40-56</b>
2.1 Introduction .....	40
2.2 Synthesis of OMS-2 .....	41
2.2.1 By $KMnO_4$ oxidation .....	41
2.2.2 By Chlorate oxidation .....	41
2.3 Characterization of the samples.....	46
2.3.1 Powder X-ray Diffraction studies (XRD).....	46
2.3.2 infrared Spectroscopy (IR) .....	50
2.3.3 Chemical analysis (Average Oxidation State).....	51
2.3.4 Chemical activity studies.....	52
2.3.5: Effect of $SO_4^{2-}$ on manganese oxide formation with Mn(II) nitrate precursor .....	54
2.4 Conclusions .....	56
<b>CHAPTER III – Oxidation of benzyl alcohol.....</b>	<b>57-86</b>
3.1 Introduction .....	57
3.2 Effect of Al on OMS-2 .....	60
3.2.1 Catalyst Synthesis.....	60
3.2.2 Characterization .....	60
3.2.3 Oxidation of benzyl alcohol.....	66
3.2.4 Thermal analysis.....	69
3.2.5 $H^+$ ion exchange capacity.....	72
3.2.6 Temperature Programmed Desorption (TPD) studies.....	72
3.2.7 Chemical analysis .....	74
3.3 Effect of $Fe^{3+}$ and $Ti^{4+}$ on catalytic activity of OMS-2.....	75
3.3.1 Catalyst synthesis.....	75

3.3.2 Catalyst characterization .....	75
3.4 Conclusions .....	86
<b>CHAPTER IV – Electrochemical reduction studies.....</b>	<b>87-98</b>
4.1 Introduction .....	87
4.2 Experimental.....	89
4.2.1 Catalyst synthesis.....	89
4.2.2 Electrochemical reduction studies (Cell preparation).....	89
4.3 Results and discussion .....	94
4.4 Conclusions .....	98
<b>CHAPTER V – Electrocatalytic oxidation of methanol.....</b>	<b>99-131</b>
5.1 Introduction .....	99
5.2 Effect of 5% Ru-C support.....	100
5.2.1 Catalyst synthesis.....	100
5.2.2 Catalyst characterization .....	100
5.2.3 Electrode preparation .....	101
5.2.4 Electrocatalytic activity studies .....	101
5.3 Results and Discussion.....	103
5.4 Conclusions .....	108
5.5 Effect of temperature .....	109
5.6 Effect of amount of OMS-2 on activity of Ru-C.....	110
5.7 Effect of H <sub>2</sub> reduction on activity of 50% mixture of 5% Ru-C supported OMS-2.....	112
5.8 Effect of reduction on activity of OMS-2 .....	114
5.8.1 Sample treatment.....	114
5.8.2 Sample characterization.....	115



5.9 Cyclic Voltammetry studies on some OMS-2 catalysts.....	123
5.9.1 Cyclic Voltammetry Experiment .....	123
5.9.2 Results and Discussion.....	123
5.10 Conclusions .....	131
References.....	132

## **LIST OF FIGURES**

<b>Figure 1.1:</b> Representation of [MnO <sub>6</sub> ] octahedron	<b>2</b>
<b>Figure 1.2:</b> Polyhedral representations of some crystal structures of manganese dioxide	<b>4</b>
<b>Figure 1.3:</b> Three different phases of layered manganese oxides: (a) the dehydrated phase, (b) birnessite phase and (c) buserite phase	<b>6</b>
<b>Figure 1.4:</b> Comparative graph of pore sizes between Tetrahedral Molecular sieves (zeolites) and Octahedral Molecular sieves (manganese dioxides)	<b>8</b>
<b>Figure 1.5:</b> A representation of a Direct Methanol Fuel Cell (DMFC)	<b>22</b>
<b>Figure 1.6:</b> Volcano Plot for different metals active for HER	<b>23</b>
<b>Figure 1.7:</b> Ru assisting Pt in the oxidation of poisonous residues (CO)	<b>28</b>
<b>Figure 1.8:</b> Possible mechanism of back bonding from filled $\pi$ orbital of Pt to vacant $\pi^*$ orbital in CO	<b>29</b>
<b>Figure 2.1:</b> Scheme of the synthesis of OMS-2 by KMnO <sub>4</sub> oxidation method	<b>43</b>
<b>Figure 2.2:</b> XRD profiles of; (a) S1, (b) S2, (c) S3 and (d) S4	<b>48</b>
<b>Figure 2.3:</b> Infrared spectra of; (a) S1, (b) S2, (c) S3 (d) S4 and (e) S5	<b>51</b>
<b>Figure 2.4:</b> XRD profiles of OMS-2 by reflux method (S1); Mn(II) nitrate decomposed at 200 °C (N1); Mn(II) salt + K <sub>2</sub> SO <sub>4</sub> in 1:1 ratio (N2); Mn(II) salt + Na <sub>2</sub> SO <sub>4</sub> in ratio 1:1 (N3)	<b>55</b>
<b>Figure 3.1:</b> XRD profiles of pure OMS-2 sample, S and Al <sup>3+</sup> containing OMS-2 sample, SA	<b>61</b>
<b>Figure 3.2:</b> Infra-Red profiles of stoichiometric manganese dioxide (Pyrolusite), P; pure OMS-2 sample, S and Al <sup>3+</sup> - doped OMS-2, SA	<b>64</b>
<b>Figure 3.3:</b> FESEM micrograph of pure OMS-2 (S) sample	<b>65</b>
<b>Figure 3.4:</b> Scheme for the oxidation of Benzyl alcohol	<b>68</b>

<b>Figure 3.5:</b> TG/DSC profiles of stoichiometric manganese dioxide (Pyrolusite), P; pure OMS-2 sample, S and Al <sup>3+</sup> - doped OMS-2, SA	<b>71</b>
<b>Figure 3.6:</b> TPD profiles of stoichiometric manganese dioxide (Pyrolusite), P; pure OMS-2 sample, S and Al <sup>3+</sup> - doped OMS-2, SA	<b>73</b>
<b>Figure 3.7:</b> XRD profiles of pure OMS-2, S; 0.5% Fe modified catalyst, Sf1; 5% Fe modified catalyst, Sf2 and 15% Fe modified catalyst, Sf3	<b>77</b>
<b>Figure 3.8:</b> XRD profiles of pure OMS-2, S; 5% Ti modified catalyst, ST5; 10% Ti modified catalyst, ST10 and 20% Ti modified catalyst, ST20	<b>79</b>
<b>Figure 3.9:</b> Infra-red profiles of pure OMS-2, S; 0.5% Fe modified catalyst, Sf1; 5% Fe modified catalyst, Sf2 and 15% Fe modified catalyst, Sf3	<b>80</b>
<b>Figure 3.10:</b> Thermogravimetric patterns of the various Fe modified catalysts	<b>81</b>
<b>Figure 3.11:</b> Correlation plot of % weight loss for the temperature interval 300-570 °C v/s % Conversion	<b>84</b>
<b>Figure 4.1:</b> Structures of (a) α- MnO <sub>2</sub> (OMS-2) and (b) γ-MnO <sub>2</sub> (nsutite) showing intergrowth of pyrolusite and ramsdellite.	<b>88</b>
<b>Figure 4.2:</b> Scheme for the preparation of a manganese dioxide electrochemical cell	<b>91</b>
<b>Figure 4.3:</b> Experimental circuit diagram for the electrochemical reduction of manganese oxides	<b>93</b>
<b>Figure 4.4:</b> Discharge curves of the various MnO <sub>2</sub> samples in 9 M KOH	<b>95</b>
<b>Figure 4.5:</b> Discharge curves comparing half the amount of OMS-2 (50 mg) in 9 M KOH	<b>97</b>
<b>Figure 4.6:</b> Discharge curves of the nsutite and OMS-2 samples during Li <sup>+</sup> insertion in alkaline medium	<b>97</b>

<b>Figure 5.1:</b> Experimental set-up to study Tafel Relationship	<b>102</b>
<b>Figure 5.2:</b> Tafel plots to study effect of pyrolusite (P) on OMS-2 (S) and nsutite (IC8)	<b>103</b>
<b>Figure 5.3:</b> Tafel plots to study effect of RuC support on OMS-2 (S)	<b>106</b>
<b>Figure 5.4:</b> Tafel plots to study effect of temperature on S/RuC	<b>109</b>
<b>Figure 5.5:</b> Tafel plots to study effect of amount of S on RuC	<b>110</b>
<b>Figure 5.6:</b> Tafel plots to study effect of reduction on S/RuC	<b>112</b>
<b>Figure 5.7:</b> X-ray diffractograms of the various treated samples; (a) S1, (b) S300, (c) S550, (d) SH120, (e) SH300 and (f) SBH	<b>120</b>
<b>Figure 5.8:</b> Infra-red spectra of the treated samples; S1, S300, S550, SH120, SH300 and SBH	<b>121</b>
<b>Figure 5.9:</b> Cyclic Voltammograms of Pt/C catalyst in (2.5 M) H <sub>2</sub> SO <sub>4</sub> (—) and (2.5 M) H <sub>2</sub> SO <sub>4</sub> + (1M) methanol (—)	<b>124</b>
<b>Figure 5.10:</b> Cyclic Voltammograms of Pt/C catalyst at various scan rates of 10, 50 and 100 mVs <sup>-1</sup>	<b>125</b>
<b>Figure 5.11:</b> Cyclic Voltammograms of Pt-NR + Ru-C catalyst in (2.5 M) H <sub>2</sub> SO <sub>4</sub> (—) and (2.5 M) H <sub>2</sub> SO <sub>4</sub> + (1M) methanol (—)	<b>126</b>
<b>Figure 5.12:</b> Cyclic Voltammograms of Pt-NR + S catalyst in (2.5 M) H <sub>2</sub> SO <sub>4</sub> (—) and (2.5 M) H <sub>2</sub> SO <sub>4</sub> + (1M) methanol (—)	<b>127</b>
<b>Figure 5.13:</b> Cyclic Voltammograms of OMS-2 (S) + Ru-C catalyst in (2.5 M) H <sub>2</sub> SO <sub>4</sub> (—) and (2.5 M) H <sub>2</sub> SO <sub>4</sub> + (1M) methanol (—)	<b>128</b>
<b>Figure 5.14:</b> Correlation between peak potentials obtained from cyclic voltammetry and exchange current densities from Tafel plots of various catalysts	<b>130</b>

## **LIST OF TABLES**

<b>Table 1.1:</b> Synthetic procedures adopted by various workers	<b>13</b>
<b>Table 1.2:</b> Various tools used by the workers in the characterization of OMS-2 materials	<b>14</b>
<b>Table 1.3:</b> The different types of fuel cells that have been realized and currently in use	<b>19</b>
<b>Table 1.4:</b> Some common fuels and their corresponding maximum voltage and energy density	<b>20</b>
<b>Table 1.5:</b> Effect of catalyst promoters on methanol oxidation	<b>34</b>
<b>Table 2.1:</b> Synthesis of OMS-2 by chlorate method	<b>44</b>
<b>Table 2.2:</b> Simple codes for the synthesized samples	<b>45</b>
<b>Table 2.3:</b> Characteristic X-Ray diffraction data of OMS-2	<b>46</b>
<b>Table 2.4:</b> Characteristic X-Ray diffraction data of $\gamma$ -MnO <sub>2</sub>	<b>47</b>
<b>Table 2.5:</b> Typical X-ray powder diffraction pattern of the samples.	<b>47</b>
<b>Table 2.6:</b> Synthesis of manganese oxides in relation to its crystal phase and H <sup>+</sup> ion exchange capacity	<b>54</b>
<b>Table 3.1:</b> X-Ray diffraction data of the OMS-2 catalysts	<b>62</b>
<b>Table 3.2:</b> BET surface areas of the samples	<b>66</b>
<b>Table 3.3:</b> % Conversion of Benzyl alcohol over the various catalysts	<b>67</b>
<b>Table 3.4:</b> Percent weight losses of the samples in three different temperature intervals	<b>70</b>
<b>Table 3.5:</b> Catalytic activity of the Mn(IV) oxides in relation to their physicochemical characteristics	<b>74</b>
<b>Table 3.6:</b> X-ray diffraction data of Fe OMS-2 samples	<b>76</b>
<b>Table 3.7:</b> Thermogravimetric weight losses of Fe <sup>3+</sup> modified manganese oxides	<b>81</b>

<b>Table 3.8:</b> Physico-chemical characteristics of various metal cation modified manganese oxides	<b>83</b>
<b>Table 4.1:</b> Discharge characteristics of the various manganese oxides in 9 M KOH solution	<b>95</b>
<b>Table 5.1:</b> Chemical reactivity of the Mn(IV) oxides in relation to their physicochemical characteristics	<b>104</b>
<b>Table 5.2:</b> Electrocatalytic activity of the various samples investigated expressed in terms of current produced at an arbitrarily chosen overpotential of 150 mV.	<b>106</b>
<b>Table 5.3:</b> Electrocatalytic activity at 60 °C of the various samples investigated expressed in terms of current produced at a chosen overpotential of 150 mV	<b>109</b>
<b>Table 5.4:</b> Electrocatalytic activity of the various samples investigated expressed in terms of current produced at an arbitrarily chosen overpotential of 150 mV	<b>111</b>
<b>Table 5.5:</b> Electrocatalytic activity of the various samples investigated expressed in terms of current produced at an arbitrarily chosen overpotential of 150 mV	<b>113</b>
<b>Table 5.6:</b> Samples treated in various ways and their corresponding codes	<b>115</b>
<b>Table 5.7:</b> Catalytic activity of OMS-2 in relation to its chemical characteristics in relation to the different treatment procedures	<b>116</b>
<b>Table 5.8:</b> Typical X-ray powder diffraction data of the samples	<b>119</b>
<b>Table 5.9:</b> BET surface areas of the treated samples	<b>122</b>
<b>Table 5.10:</b> Methanol oxidation peak potentials of forward scan from CV data for various catalysts at scan rate of 10 mVs <sup>-1</sup>	<b>129</b>

## **LIST OF SCHEMES**

<b>Scheme 1.1:</b> Comparison between energy conversion in conventional technology and fuel cells	<b>18</b>
<b>Scheme 1.2:</b> Methanol oxidation over a platinum catalyst	<b>24</b>
<b>Scheme 1.3:</b> A six-step methanol oxidation mechanism on conventional Pt catalysts	<b>25</b>
<b>Scheme 1.4:</b> The different pathways (and a number of identified intermediates) in the oxidation of methanol	<b>37</b>
<b>Scheme 3.1:</b> Mechanism of benzyl alcohol oxidation via lattice oxygen vacancy in OMS-2 catalysts	<b>85</b>
<b>Scheme 5.1:</b> Formation of adsorbed CO as a result of incomplete oxidation of methanol over OMS-2 (S) catalyst	<b>105</b>
<b>Scheme 5.2:</b> Methanol oxidation over OMS-2 catalyst by lattice oxygen participation followed by its regeneration	<b>105</b>
<b>Scheme 5.3:</b> Methanol oxidation over S/Ru-C catalyst	<b>107</b>

## SUMMARY/GENERAL CONCLUSIONS

### 1. Introduction:

(i) Manganese oxides display a remarkable diversity of atomic architectures because Mn occurs in oxides in three different oxidation states: +2, +3 and +4, giving rise to a range of multivalent phases. The basic building block for most of the manganese oxides is the  $[\text{MnO}_6]$  octahedron. These octahedra can be assembled by sharing edges and/or corners into a large variety of different structural arrangements viz. Pyrolusite, nsutite, bixbyite, *Octahedral Molecular Sieves (OMS)*, Octahedral layers (OL), etc.

OMS-2 materials are currently considered as 'hot materials' and find use in various areas from catalytic materials, detergents, to battery materials and sensors as well as ion exchangers. Their pore sizes are considered to be analogous to zeolites. Their acidities can be varied by altering the method of preparation, by specific activation, and by doping with transition metal cations either before or after crystallization. By inserting divalent cations into OMS it is possible to alter electronic, catalytic and structural properties. All this results in outstanding materials for various catalytic oxidation reactions.

(ii) Recent years has seen increased interest in fuel cells for a range of applications, including transport and small-scale static power, they being a fantastic source of clean alternative energy. Hydrogen the most promising fuel has storage, handling and transportation hazards. Liquid fuels like methanol, ethanol, etc. are better alternatives. Of the very few metals that are able to adsorb methanol in acidic medium, platinum is an excellent catalyst for the oxidation of methanol. But platinum poses CO poisoning as a major problem besides being very expensive. Thus, in general, the move is



(a) to reduce catalyst cost for direct methanol fuel cells by reducing noble metal content, and

(b) to identify potential non-noble metal catalytic systems.

## **2. Objectives of this work:**

Manganese oxides are well known to have appreciable electrochemical activity. *They are* used as oxidation catalysts for preparation of a wide variety of specialty chemicals. Thus, in this work it was intended to test the OMS-2 materials;

(i) to improve the oxidation ability of these catalysts by modifying with cations,

(ii) as cathode materials for use in batteries, and

(iii) as anode catalysts for oxidation of methanol.

## **3. Contents of the Thesis:**

The present work has been described in 5 chapters.

i. **Chapter I** – Introduction, has been divided into 2 sections – one introducing Octahedral Molecular Sieve (OMS-2), its applications in various fields especially catalysis and second - the current literature status in the area of anode catalysts in direct methanol fuel cells. Thus the salient features are <sup>as</sup> follows:

(a). Octahedral molecular sieves are currently ‘hot’ materials, which can find use in various applications.

(b). The ability to adjust their pore sizes and activities make them great materials for separation and sorption applications.

(c). Fine-tuning the valence states of the active sites gives the ability to perform selective catalytic reactions and conductivity changes for sensors.

(d). Fuel cells are in high demand in the area of energy/power generation.

(e). Various catalysts have been tried out so far with platinum and its alloys being the best.

(f). Thus the search is on for new materials, which will use lesser amount of expensive noble metals, but one which will not compromise on efficiency.

(g). This calls for a study of designing electrodes with specific structures using the catalytic material if one needs to develop high performance electrodes.

(h). Electrocatalyst studies are thus directed to establishing the nature of the species formed during adsorption, understanding the mechanism of the reaction, studying surface structural effects and invariably *a search for new catalysts*.

ii. **Chapter II** – deals with the synthesis of OMS-2 materials via a simple method using  $\text{KClO}_3$  *vis-à-vis* the conventionally used  $\text{KMnO}_4$ . OMS-2 is known to form in the presence of specific tunnel cations like  $\text{K}^+$ ,  $\text{Ca}^{2+}$ ,  $\text{Pb}^{2+}$ , etc. In this work OMS-2 has been synthesized showing the importance of  $\text{SO}_4^{2-}$  in the phase formation. Some aspects regarding this have been discussed as follows;

(a).  $\text{SO}_4^{2-}$  ion has a crucial role in OMS-2 phase formation,

(b). OMS-2 could be synthesized without the presence of  $\text{K}^+$  ion,

(c). OMS-2 could be formed in a facile manner by use of chlorate as oxidizing agent in place of permanganate and

(d). OMS-2 samples could be successfully characterized both by IR and XRD techniques.

iii. **Chapter III** – describes the application of synthesized catalysts for oxidation of benzyl alcohol to benzaldehyde. Also activities of OMS-2 materials

modified with some transition metal cations have been studied. A mechanism has been proposed explaining the enhanced activity of these materials.

- (a). Adding transition metal cations (Fe and Ti) has resulted in improved catalytic activity thus showing increasing % conversion with increase in transition metal content in the samples. The effect with  $\text{Fe}^{3+}$  was found to be more as compared to that by  $\text{Ti}^{4+}$ .
  - (b). Corresponding increase in chemical reactivity and % weight loss in the three temperature intervals, with metal content is seen.
  - (c). The higher activity is associated with the extent of participation of lattice oxygen of the catalyst and a mechanism is proposed.
- iv. **Chapter IV** – Cathodic reduction studies have been carried out on the OMS-2 materials and the results discussed in relation to other forms of manganese oxides. OMS-2 showed synergistic interactions with pyrolusite resulting in improved performance.  $\text{Li}^+$  insertion behaviour of OMS-2 catalysts are also studied in comparison to a synthesized nsutite material.
- v. **Chapter V** – For the first time OMS-2 is investigated as anode material for use in fuel cells. The activity of the materials has been discussed in comparison to some manganese oxides as well as in combination with carbon supported Ruthenium. Effect of temperature and reduction of OMS-2 composites have been studied. The results are as follows;
- (a). Manganese octahedral molecular sieves have been found to be active for methanol electrooxidation.
  - (b). Pyrolusite in combination with manganese octahedral molecular sieves gave a higher current (more than twice) than the current produced by a combination of

pyrolusite with the international sample (IC8), thus suggesting that it produced a synergistic interaction with OMS-2 thus improving its activity towards methanol oxidation.

- (c). In case of OMS-2 materials in combination with 5% Ru-C (whether *in situ* generated phase on the Ru-C or 1:1 mechanical mixture), Ru enhances oxidation of CO to CO<sub>2</sub> significantly.
- (d). Methanol oxidation kinetics improved with temperature.
- (e). Increasing amount of OMS-2 in a mixture with 5% Ru-C showed increase in exchange current density.
- (f). Reduction studies revealed that OMS-2 shows maximum activity under reducing atmosphere by hydrogen upto 120 °C and is not stable beyond 300 °C.
- (g). The high activity of the manganese oxide was associated with presence of Mn<sup>4+</sup>/Mn<sup>3+</sup> redox couple. The extent of participation of lattice oxygen played an important role in methanol oxidation reaction.
- (h). Cyclic voltammetry studies showed that active OMS-2 composites showed oxidation of methanol at a lower positive potential.

*CHAPTER – I*

*INTRODUCTION AND LITERATURE*

*STATUS*

## 1.1 Introduction to OMS-2:

Ever since the discovery of aluminosilicate materials at Mobil in 1992 [1], synthesis of molecular sieves has captured the interest of many scientists and innumerable research papers have been published [2-4]. Recently, much attention has been focused on transition metal oxides since transition metal atoms are multi-valent thus showing better advantages over aluminosilicate materials for use in electromagnetics, photo electronics and catalysis [5-7]. However, it is quite difficult to synthesize transition metal oxides with stable porous structures because of their multitude of different coordination numbers and oxidation states.

Manganese oxides have been exploited since times immemorial – by the ancients as pigments and to clarify glass [8] and today as ores of manganese metal, catalysts and battery materials [8-13], besides forming an essential component in the making of hard-steel alloys [14]. More than 30 manganese oxide minerals occur in a wide variety of geological settings as coatings and in massive deposits [9]. They form major components of Mn nodules that pave the huge areas of the ocean floor and are also ubiquitous in soils and sediments and participate in a variety of chemical reactions that affect ground water and bulk soil composition [15].

*What accounts for the complexity and impressive variety of these manganese oxide minerals?*

Mn occurs as its major oxides in three different oxidation states: +2, +3 and +4 [9], giving rise to a range of multivalent phases. Manganese oxides also display a remarkable diversity of atomic architectures, many of which easily accommodate a wide assortment of other metal cations.

The ability to successfully model and predict the chemical and thermodynamic properties of manganese oxide minerals and to prepare synthetic analogues depends to a large degree on a detailed understanding of their crystal structures.

### 1.1.1 Manganese Oxides; Structural Chemistry

The basic building block for most of the manganese oxides is the  $[\text{MnO}_6]$  octahedron (Figure 1.1). These octahedra can be assembled by sharing edges and/or corners into a large variety of different structural arrangements as shown in Figure 1.2. These structures usually contain relatively freely accessible tunnels and/or interlayer spaces of various sizes, occupied by water molecules and other cations.

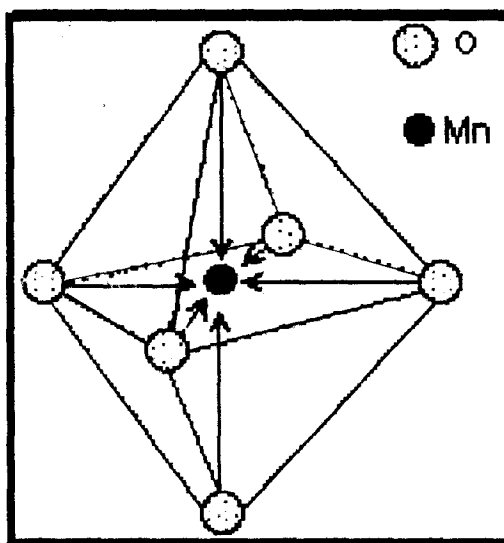


**Figure 1.1:** Representation of  $[\text{MnO}_6]$  octahedron

Summarized below are descriptions of the atomic structures for some of the most important manganese oxides.

Manganese oxides with tunnel structures [9]

**(i) *Pyrolusite:***

Single chains of edge-sharing  $[\text{Mn(IV)O}_6]$  octahedra share corners with neighbouring chains to form a framework structure containing tunnels with square

cross sections that are one octahedron by one octahedron (1×1) on a side as shown in Figure 1.2. The tunnels in pyrolusite are too small (its size is usually 2.3×2.3 Å) to accommodate other chemical species, and chemical analyses indicate that the composition deviates very slightly from pure MnO<sub>2</sub>. It is the only stoichiometric form of manganese oxide. The average oxidation state of Mn is +4 and is almost practically inactive.

**(ii) Ramsdellite:**

In this form of Mn oxides, the [Mn(IV)O<sub>6</sub>] octahedra are linked into double chains, each of which consists of two adjacent single chains that share octahedral edges. The double chains, in turn, link corners with each other to form a framework having tunnels with rectangular-shaped cross sections that are 1×2 octahedra on a side [16].

**(iii) Nsutite:**

It is a disordered structure consisting of alternating intergrowths of pyrolusite and ramsdellite [17] as well as numerous defects and grain boundaries. All these complexities affect the chemical and electrical properties of the material, which makes it an interesting material for battery cathodes.

**(iv) Other Mn oxides:**

(a) Mn<sub>2</sub>O<sub>3</sub> also called as Bixbyite.

(b) Mn<sub>3</sub>O<sub>4</sub> also called as Hausmannite

**(v) Manganese oxides with micro and mesopores:**

(a) *Molecular Sieves:*

Several complex manganese oxides have been synthesized and some find potential applications as octahedral molecular sieve (OMS) materials. These substances also exhibit ion-exchange properties and some are microporous just like



zeolites. Their large surface areas (upto  $250 \text{ m}^2/\text{g}$ ) give them possibilities for catalytic applications.

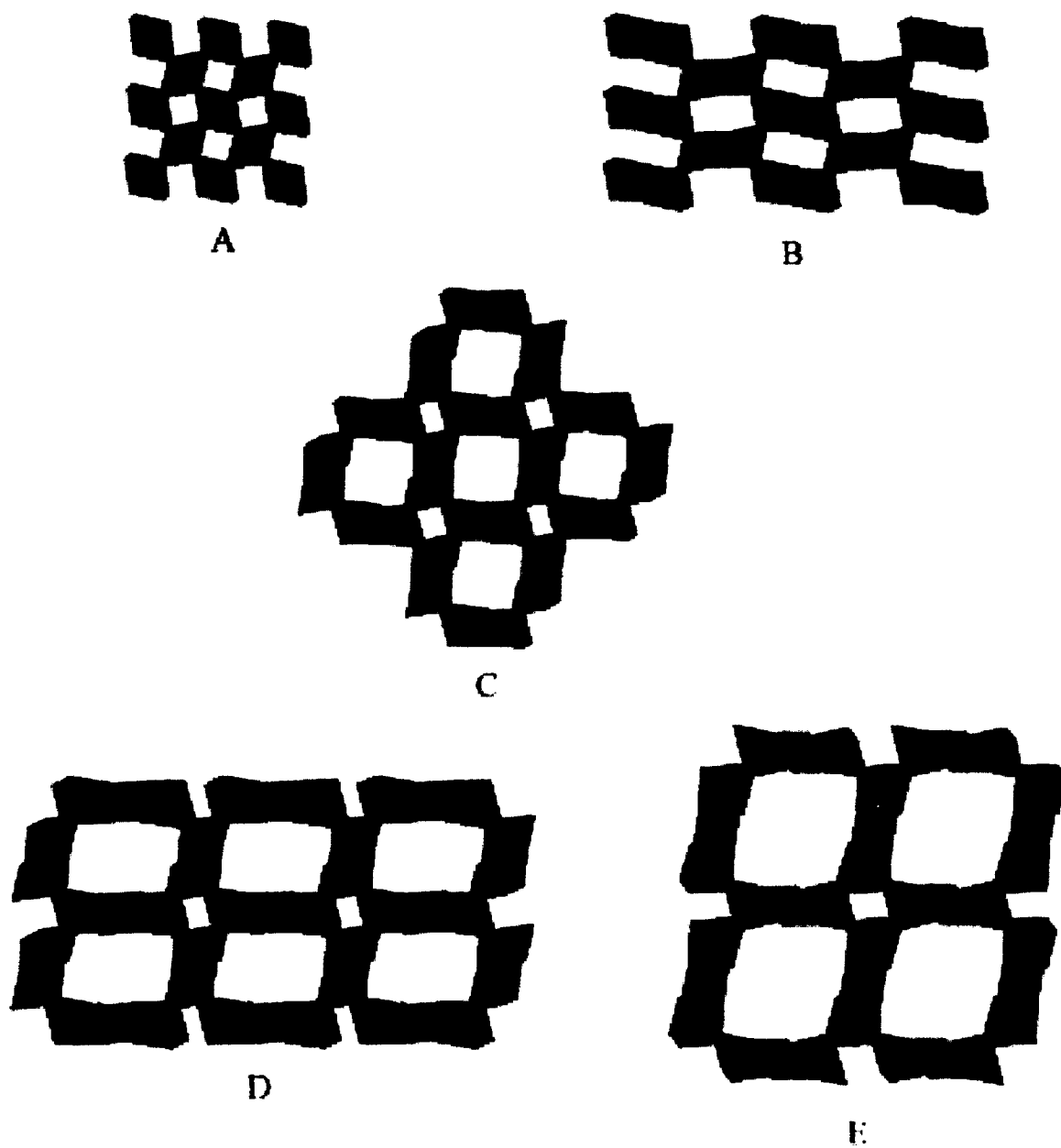


**Figure 1.2:** Polyhedral representations of the crystal structures of (A) pyrolosite, (B) ramsdellite, (C) hollandite, (D) romanechite, and (E) todorokite [9]

*i. Todorokite:*

It constitutes one of the major components of sea-nodules. The tunnel structure is constructed of triple chains of  $[\text{MnO}_6]$  octahedra, which share corners with each other to form large tunnels with square cross sections that measure three octahedra on a side ( $3 \times 3$ ). Its synthetic analogue is called as OMS-1 (Octahedral Molecular Sieves-1). It has a tunnel edge size of 6.9 Å whereas a diagonal pore size of 9.6 Å. It is due to the presence of such large zeolites-like tunnels, which is why it has attracted considerable interest for use in catalysis [22].

*ii. Hollandite Group:*

The hollandite structure is constructed of double chains of edge-sharing  $[\text{MnO}_6]$  octahedra, which are linked in such a way as to form tunnels with square cross sections, measuring two octahedra on a side (Figure 1.2). The tunnels are partially filled with large uni- or divalent cations and water molecules. These large cations are believed to be necessary to prevent collapse of the framework. The charges on the tunnel cations are balanced by substitution of lower valence cations of manganese in order to maintain electrical neutrality. The different minerals in the hollandite group are named on the basis of the predominant tunnel cation: Hollandite (Ba), cryptomelane (K), coronadite (Pb) and manjiroite (Na). Its synthetic analogue is called OMS-2 [9,22]. The synthetic forms of hollandite, pyrolusite or nsutite are also identified by Greek symbols  $\alpha$ ,  $\beta$  or  $\gamma$  respectively. The  $\alpha$  – variety is now called the OMS-2.

*(b) Octahedral Layered materials:*

As the name suggests these materials are made up of stacks of sheets of  $[\text{MnO}_6]$  octahedra alternating with either (a) sheets of  $\text{Al}(\text{OH})_6$  octahedra (e.g. Lithiophorite,  $\text{LiAl}_2\text{Mn}_3\text{O}_6(\text{H})_6$ ) [18] or (b) layers of Zn cations and water molecules

(e.g.  $\text{ZnMn}_3\text{O}_7 \cdot 3\text{H}_2\text{O}$ ) [19] or (c) interlayer cations like Na or K or Mg along with water molecules e.g. Birnessite [20] (Figure 1.3).

Birnessites are a class of layered manganese oxides, which are found in nature as well as produced synthetically. It is a layered structure comprising of edge sharing  $[\text{MnO}_6]$  octahedral, with water molecules and metal cations occupying the interlayer region and has an interlayer distance of  $7.1 \text{ \AA}$  (also called OL-1). Other forms of Na-birnessite include a dehydrated form with an interlayer spacing of  $5.5 \text{ \AA}$ , and an extrahydrated phase, called buserite, with a spacing of  $10 \text{ \AA}$ , expanded by the presence of an extra layer of water [21].

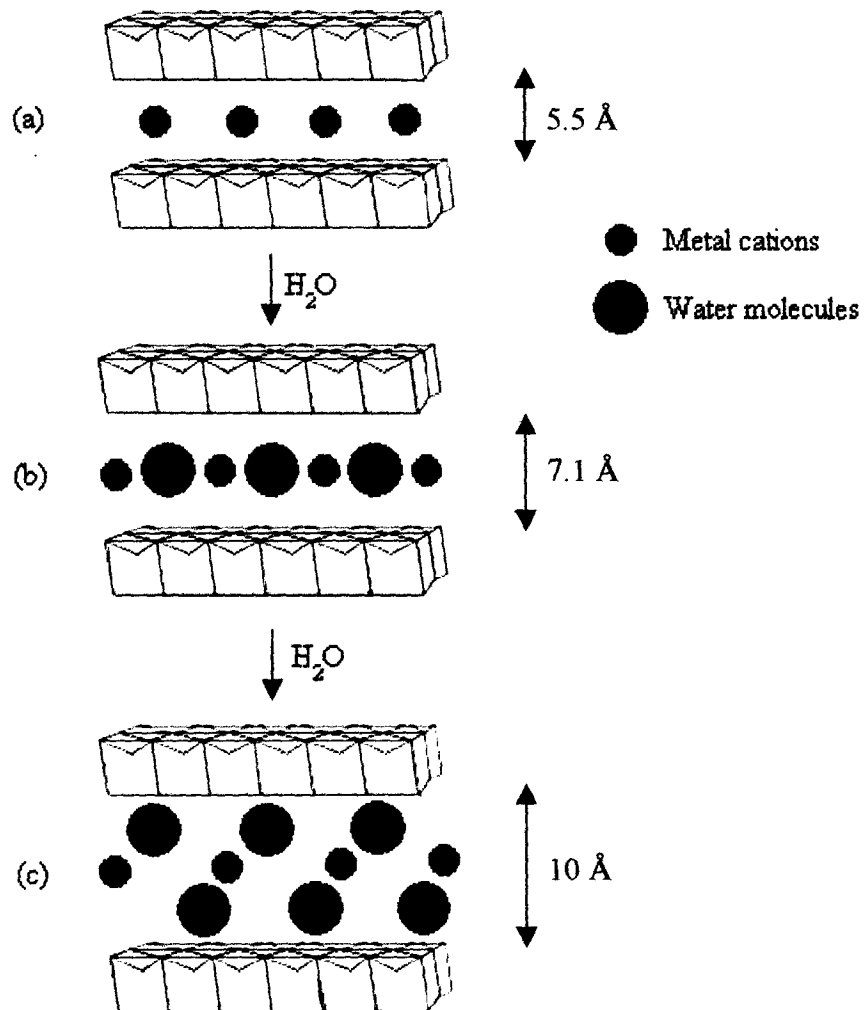


**Figure 1.3:** Three different phases of layered manganese oxides: (a) the dehydrated phase, (b) birnessite phase and (c) buserite phase

### 1.1.2 Classification of Molecular sieves:

Based on the basic structural unit, molecular sieves can be classified as tetrahedral molecular sieves (TMS), octahedral molecular sieves (OMS) and mixed molecular sieves. Most common molecular sieves, such as zeolites,  $\text{AlPO}_4$ , SAPO, MeAPO and MeAPSO are tetrahedron based molecular sieves. Todorokite, hollandite and pyrolusite are octahedron based molecular sieves. Titanosilicates (ETS-4 and ETS-10) and phosphomolybdates are mixed molecular sieves, which have tetrahedra and octahedra to form the frameworks. The pore sizes of some representative TMS and OMS together with the kinetic diameters of some molecules are shown in Figure 1.4. OMS-2 has a pore size of 4.6 Å between Na-A and ZSM-5 zeolites; OMS-1 has a pore size of 6.9 Å between ZSM-5 and Na-X zeolites. The tunnels of OMS-1 are big enough to adsorb most hydrocarbons; OMS-2 can only adsorb straight chain but not branched chain hydrocarbon molecules. A hypothetical OMS (4×4) structure has a pore size of 9.2 Å, between  $\text{AlPO}_4$ -8 and VPI-5. The tunnels of pyrolusite are too small to adsorb any hydrocarbon.

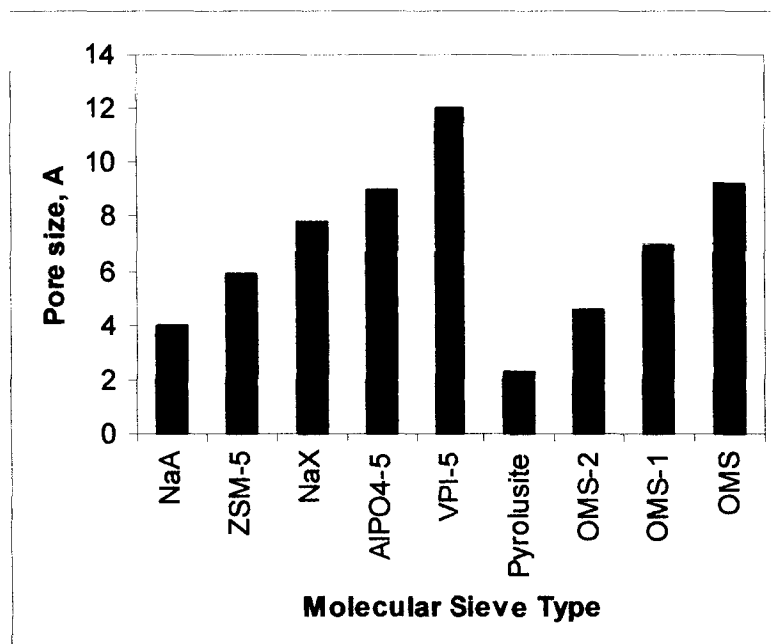


**Figure 1.4:** Comparative graph of pore sizes between Tetrahedral Molecular sieves (zeolites) and Octahedral Molecular sieves (Manganese dioxides)

### 1.1.3 Synthesis of OMS-2 materials:

Microporous and mesoporous materials are prepared via a variety of routes. Many of the oxides with gross similar structural features nevertheless show a diversity of properties depending upon the specific synthetic route. These differences can be attributed to variations in crystal type, particle size, the type and amount of defects in the structures, etc. For this reason, small changes in synthetic parameters can result in materials with novel catalytic, electrochemical and ion exchange properties.

#### (i) *Precipitation, Ion exchange and hydrothermal routes:*

Many workers have carried out synthesis of OMS-2 materials by precipitation routes involving redox reactions of  $Mn^{7+}$  (permanganate) and/or  $Mn^{2+}$  salts since suitable  $Mn^{4+}$  salts are rare. A typical preparation involves heating of an aqueous solution of  $MnSO_4$  as the Mn(II) salt in nitric acid medium and dropwise addition of hot solution of  $MnO_4^-$  amidst continuous and vigorous stirring. This results in a dark

brown Mn oxide (birnessite), which can be converted to OMS-2 by refluxing for 24 hours [23].

Giovanoli and Balmer [24] at first prepared the layered buserite in alkaline (NaOH) medium, followed by ion exchange with  $K^+$ , partial dehydration to K-birnessite and then calcined it at high temperature to give the desired product. DeGuzman *et al.* [23] have slightly modified this procedure by skipping the ion exchange step. Aqueous KOH was added to  $MnSO_4$  solution and oxygen was bubbled vigorously (12 L/min) through it for 5 hours. The black buserite formed was washed and calcined at 600 °C for 24 hours.

Recently Luo *et al.* [25] have performed a detailed investigation on the contribution of various synthetic parameters to the crystallinity and ion exchange properties of resulting materials. An interesting observation was made that the pore size of the tunnel obtained depended on the cation that was present. Also, Feng *et al.* have prepared OMS-2 by hydrothermal treatment of sodium birnessite at 150 °C for 2 days under autogenous pressure [26], as well as materials obtained by ion exchange with Li, K and Mg [27]. A dependence of the product on the ion size and the basicity of the hydrothermal solution were observed. Increasing basicity increased the crystallinity of Na and K, while Li birnessite was found to transform into the more stable spinel structure. At neutral pH, for preparation involving use of  $Mg^{2+}$  cations, the 3×3 OMS-1 phase was obtained, while in acidic solution, Na in HCl and Mg in  $H_2SO_4$  both yielded 1×1 pyrolusite, whereas K in  $H_2SO_4$  medium predominantly formed the 2×2 OMS-2 phase. Thus, structural transformations from birnessite appeared to occur more readily to OMS-2 in neutral to acidic solutions, and resulting products showed some dependence on the identity of the cation.

Rhiza, Gies and Rius have synthesized OMS-2 [28] using Rb, Na and K birnessites as starting materials, all prepared by treatment of basic  $\text{Mn}^{2+}$  with oxygen. They have studied the effect of combinations of the mentioned cations on the phase formation and it was found that potassium when not in presence of sodium, directs preferentially toward the  $2 \times 2$  OMS-2 structure.

Dai *et al.* [29] have reported synthesis of  $\alpha$ - $\text{MnO}_2$  without tunnel cations. In a typical synthesis, a 1:1 mixture of oxygen and ozone was bubbled through a solution containing 0.1 M  $\text{MnSO}_4$  and 10 M  $\text{H}_2\text{SO}_4$  at 80 °C for 24 hours, amidst constant stirring. The black product obtained was washed till free of all sulphate ions, dried at 80 °C and then annealed at different temperatures in air. The hydronium ion is expected to be the stabilizing tunnel ion. These materials are reported to exhibit enhanced Li-intercalation properties as compared to cation-stabilized  $\alpha$ - $\text{MnO}_2$ .

$\alpha$ - $\text{MnO}_2$  has been reported to be modified by ion exchange of cerium ions and also by the wet impregnation technique [30]. Though the ion exchange method succeeded in incorporating Ce into the tunnels, the wet impregnation technique failed to do so. Instead, the Ce particles agglomerated and were dispersed on the external surface of the fibrous structure.

*(ii) Sol-gel techniques:*

Ching and co workers [31,32] have investigated the synthesis of OMS-2 material by sol-gel technique using two different groups of organic species as reducing agents: multifunctional carboxylic acids (fumaric acid and maleic acid) and polyols (glucose). In both cases, the organic species were mixed with  $\text{KMnO}_4$  in various proportions, which resulted in formation of dark gels. These were calcined at appropriate temperatures and the resultant oxides were washed. Interesting results were obtained, wherein it was observed that, in case of glucose precursors, a high

glucose/KMnO<sub>4</sub> ratio yielded K-birnessite whereas, a low ratio gave cryptomelane or amorphous manganese oxide as the final product. Also, high reactant concentrations yielded the cryptomelane and/or bixbyite phase while K-birnessite was formed at low concentrations. While in the carboxylic acid synthesis, different metal cations (Li, Na, Mg, Ca) were studied it was found that only Ca<sup>2+</sup> yielded a pure hollandite material.

Garces *et al.* [33] have studied the effect of using polyvinyl alcohol (PVA) and polyvinyl pyrrolidone (PVP) in the synthesis of OMS-2 films and report interesting results in properties like crystallinity, particle sizes, surface areas and hardness of the films in comparison to those prepared by standard routes.

*(iii) Microwave treatment:*

Recently Zhang *et al.* [34] have used microwave radiations as an effective technique for the fast and selective synthesis of OMS materials. MnO<sub>2</sub> has a large dielectric constant ( $\epsilon = 10^4$ ), which is believed to have a pronounced effect on the synthesis of porous manganese oxides with the influence of microwave irradiation. Here maleic acid and KMnO<sub>4</sub> have been used as precursors. It was seen that cryptomelane begins to form at 320 °C, which was much lower than 390 °C required by the conventional heating sources. It also showed positive additional effects on crystallization with the peaks appearing much faster (after shorter time) and being sharper.

Another method involves phase transformations induced by microwave radiation, as in the production of OMS from OL systems via oxygen evolution [10].

*(iv) Disproportionation*

Synthesis of OMS-2 has been reported to be formed by disproportionation of Mn<sub>2</sub>O<sub>3</sub> in sulphuric acid medium via a simple route without the use of any stabilizing cation [35,36]. Johnson *et al.* [37] also report a similar synthesis wherein



commercially prepared EMD and CMD of the  $\alpha$ -MnO<sub>2</sub> type have been heated at 700 °C to convert to Mn<sub>2</sub>O<sub>3</sub> followed by disproportionation at 105 °C in 4-8 M H<sub>2</sub>SO<sub>4</sub> solution. The resulting products were dehydrated at 300 °C.

(v) *Electrochemical synthesis:*

In contrast to the high temperature required for most of the previously reported syntheses, Liao *et al.* [38] reported synthesis of  $\alpha$ -MnO<sub>2</sub> by a combination of electrochemical oxidation of Mn(II) salt in acidic medium to MnO<sub>4</sub><sup>-</sup>, followed by self assembly via a hydrolysis process at a relatively low temperature of 80 °C. Also it was seen that the structure was independent of the cation sizes Li, Mg, Na, K and Cs were used in the hydrolysis step. This method has also seemed to allow the preparation of  $\alpha$ -MnO<sub>2</sub>, free of alkali-earth metal tunnel cation.

Recently Hill *et al.* [39] have come up with yet another electrochemical synthesis claiming formation of OMS-2 at a higher temperature, low pH and a current density of 0.36 mAcm<sup>-2</sup>. They suggest H<sub>3</sub>O<sup>+</sup> (or Li<sup>+</sup> in case of MnSO<sub>4</sub>/Li<sub>2</sub>SO<sub>4</sub> solutions) to have a structure directing effect in this case, since no potassium salts have been used in the synthesis.

(vi) *Green method?*

Villegas *et al.* [40] report synthesis of nanosize (particle size 7 – 9 nm) OMS-2, based on the use of H<sub>2</sub>O<sub>2</sub> to reduce MnO<sub>4</sub><sup>-</sup> under acidic conditions to produce Mn<sup>2+</sup> in situ, which avoids necessity of excessive washing and calcinations to remove any organic material. Thus forming OMS-2 nanofibres. Here the particle size of the nanofibres is believed to be controlled by the concentration of hydrogen peroxide in the medium.

**Table 1.1: Synthetic procedures adopted by various workers:**

Route/method	Precursor	Reactant/reaction conditions	Intermediate	Phase	Ref.
1. Precipitation	Mn <sup>2+</sup> salts	KMnO <sub>4</sub>	Birnessite (reflux)	OMS-2	23
	-do-	KOH	K-birnessite (O <sub>2</sub> )→	OMS-2	23
2. Ion-exchange	-do-	NaOH	Na-birnessite (I.E.) O <sub>2</sub> →	OMS-2	24
3. Hydrothermal	-do- (Li, Mg, K, Na)	150 °C under autogenous pressure	Mg (neutral) Na, Mg (acidic) K (acidic)	OMS-1 Pyrolusite OMS-2	26, 27
	-do- (Rb, Na, K)	O <sub>2</sub>	Birnessites →	K without Na gave OMS-2	28
	MnSO <sub>4</sub> , H <sub>2</sub> SO <sub>4</sub>	1:1 O <sub>2</sub> /O <sub>3</sub>	-	OMS-2 without tunnel cations	29
4. Sol-gel method	KMnO <sub>4</sub>	Fumaric acid Maleic acid (Na, Li, Mg, Ca)	Gel (calcination) →	Only Ca gave OMS-2	31
	KMnO <sub>4</sub>	Glucose	Low glucose/MnO <sub>4</sub> <sup>-</sup> ratio High reactant conc.	OMS-2 ±AMO OMS-2/Mn <sub>2</sub> O <sub>3</sub> ,	32
	KMnO <sub>4</sub>	PVA or PVP + MnAc <sub>2</sub>	Reflux (calcination at 400 °C)	OMS-2	33
5. Microwave treatment	KMnO <sub>4</sub>	Maleic acid	-	OMS-2	34
	OL	Microwave	via O <sub>2</sub> evolution	OMS-2	10
6. Disproportionation	Mn <sub>2</sub> O <sub>3</sub>	H <sub>2</sub> SO <sub>4</sub>	-	OMS-2	35, 36
	EMD, CMD	$\xrightarrow{700^\circ\text{C}}$ Mn <sub>2</sub> O <sub>3</sub>	-	OMS-2	37
7. Electrochemical synthesis	Mn(II) salt	Electrochemical oxidation to MnO <sub>4</sub> <sup>-</sup>	Self-assembly via Hydrolysis at 80 °C	OMS-2	38
	-do-	High temp, low pH, i <sub>0</sub> = 0.36 mAcm <sup>-2</sup>	-	OMS-2	39
8. Green method	KMnO <sub>4</sub>	H <sub>2</sub> O <sub>2</sub> +AcOK (H <sup>+</sup> )	Reflux (15 h)	OMS-2	40

#### 1.1.4 Characterization Techniques:

Various methods have been used in the characterization of OMS-2 compounds like chemical as well as instrumental techniques. These have been able to throw much light on the structural and activity properties of the materials.

**Table 1.2: Various tools used by the workers in the characterization of OMS-2 materials [41]**

<b>Instrumental Techniques</b>	<b>Information</b>
ICP-AES	Elemental composition
XRD	Crystallinity, particle size
Electron Microscopy (TEM, SEM)	Modifications in structures caused by doping, etc.
Thermal Techniques (DSC, TG, DTA)	Structural and physisorbed water, thermal stability
TPD/TPR	Acid/base sites, reducibility
Electrochemical characterization (Slow-scan cyclic voltammetry, constant-current intermittent discharge, Electrochemical Impedance Spectroscopy)	As characterization tools for insertion electrodes, electrocatalytic parameters

#### 1.1.5 What makes Octahedral Molecular sieves so interesting?

##### *i. As adsorbents:*

The building blocks of OMS materials, the  $\text{MnO}_6$  octahedra, share corners and/or edges to form chainlike slabs and further cross-link to build one-dimensional tunnels. These pores harbour various cations, which help to support the framework and to maintain charge balance. The pores that are formed are square tunnels and the

diagonal distances across the opposite sides of the tunnels are significantly larger (6.3 Å) than the tunnel edge size (4.6 Å). Such porosity is retained up to about 600 °C. Hydrocarbon uptake studies have revealed much higher uptake in case of dehydrated materials thus confirming that they contain water in the tunnels which get dislodged from the pores when heat-treated. The pore size distributions of OMS materials are quite different from that of zeolitic materials and also the adsorption capacity of these materials is of the order of 18 – 20 g of adsorbate per 100 g of adsorbent. Such adsorption capacity rivals zeolitic type materials [10-13].

*ii. As catalysts:*

They are small particle size materials having large surface areas up to 250 m<sup>2</sup>/g with cation exchange properties and are microporous. Their acidities can be varied by altering the method of preparation, by specific activation, and by doping with transition metal cations either before or after crystallization. By inserting divalent cations into OMS it is possible to alter electronic, catalytic and structural properties. The choice of cations is dictated by sizes, charges and polarisabilities that are similar to Mn<sup>2+</sup> for which these cations may substitute [22,23,30-34]. Since OMS-2 materials can have variable composition and can be prepared by a variety of methods, the resultant degree of mixed valence varies. All this results in outstanding materials for various catalytic oxidation reactions.

*iii. As ion-exchangers:*

Also it has been found that hollandite materials formed by different methods have different thermal properties. There seems to be a significant difference in the temperatures at which phase transformation occurs and the amount of oxygen evolution for hollandites synthesized by reflux and calcination methods [23]. Studies also show that materials with lower average manganese oxidation state have higher

cation exchange capacity [10,30-34]. This is probably due to presence of  $Mn^{3+}$ , which is associated with acidic protons.

*iv. As Intercalation materials:*

Manganese oxides having good electrochemical performance are attractive as cathode materials for lithium cells [38] because manganese has economic and environmental advantages over compounds based on cobalt or nickel. The largest part of electrochemical studies has been related to lithium intercalation.

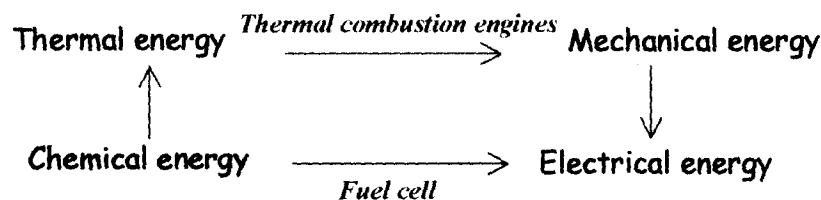
#### **1.1.6 Putting the OMS materials to use**

Ceaseless search for greener chemical processes has become one of the most important tasks of today's researchers. Many ways have been used to achieve this such as use of alternative solvents, feed stocks, reagents, products, catalysts and so on. Since heterogeneous catalysts are resistant to leaching, are recyclable and readily available from catalyst manufacturers in various compositions and forms, they play an important role in environmentally clean processes.

OMS-2 systems have various potential uses hence their synthesis, characterization and applications have gained considerable interest. Suib in a recent article [10] has deemed them as "HOT" materials for the same reason. Octahedral molecular sieves of manganese exhibit good conductivity, high porosity and good thermal stability. The dimensions of the channels in these materials can be adjusted to fit various applications, and chemical reactions at the active sites can be varied by substituting different metals into the structure or by changing the valence of the manganese ions. This adaptability opens up possibilities for several potential applications and catalysis is one area in which these materials have been exploited to the maximum.

## 1.2 Introduction to Fuel Cells:

The fuel cell – a nineteenth century invention, twentieth century technology development and now the twenty first century energy demand!!! A fuel cell is an electrochemical device, which continuously and directly converts chemical energy of a fuel and oxidant to electrical energy (Scheme 1.1) unlike combustion engines [62]. Thus a fuel cell theoretically is supposed to continually generate energy as long as the fuel and oxidant are provided in the cell. This is distinctly different from batteries, which are merely energy storage devices.



**Scheme 1.1:** Comparison between energy conversion in conventional technology and fuel cells.

Fuel cells have been classified into various types; either according to their temperature (high, medium and low temperature fuel cells) or by the fuels and/or oxidants used (solid, liquid and gaseous fuels). But the more often followed classification is by the type of electrolyte used: Alkaline fuel cells (AFC), proton exchange membrane fuel cells (PEMFC), phosphoric acid fuel cells (PAFC), molten carbonate fuel cells (MCFC) and solid oxide fuel cells (SOFC). Table 1.3 summarizes the properties of the different commercially viable fuel cells.

**Table 1.3:** The different types of fuel cells that have been realized and currently in

use

Parameters	Alkaline fuel cell (AFC)	Polymer electrolyte fuel cell (PEFC)	Direct methanol fuel cell (DMFC)	Phosphoric acid fuel cell (PAFC)	Molten carbonate fuel cell (MCFC)	Solid oxide fuel cell (SOFC)
Operating temperature (°C)	60 - 90	60-120	60-120	160-220	600-800	800 - 1000
Electrolyte	Sodium hydroxide/potassium hydroxide	Proton exchange membrane (Nafion/Dow)	Aqueous acid or alkali	Concentrated phosphoric acid	Molten carbonate melts (Li <sub>2</sub> CO <sub>3</sub> /Na <sub>2</sub> CO <sub>3</sub> )	Yttrium-stabilized Zirconia (ZrO <sub>2</sub> /Y <sub>2</sub> O <sub>3</sub> )
Charge carrier in the electrolyte	OH <sup>-</sup>	H <sup>+</sup>	H <sup>+</sup>	H <sup>+</sup>	CO <sub>3</sub> <sup>2-</sup>	O <sup>2-</sup>
Cathode reaction	$\frac{1}{2} O_2 + H_2O + 2e^- \rightarrow 2OH^-$	$\frac{1}{2} O_2 + 2H^+ + 2e^- \rightarrow H_2O$	$\frac{3}{2} O_2 + 6H^+ + 6e^- \rightarrow 3H_2O$	$\frac{1}{2} O_2 + 2H^+ + 2e^- \rightarrow H_2O$	$\frac{1}{2} O_2 + CO_2 + 2e^- \rightarrow CO_3^{2-}$	$\frac{1}{2} O_2 + 2e^- \rightarrow O^{2-}$
Anode reaction	$H_2 + 2OH^- \rightarrow 2H_2O + 2e^-$	$H_2 \rightarrow 2H^+ + 2e^-$	$CH_3OH + H_2O \rightarrow CO_2 + 6H^+ + 6e^-$	$H_2 \rightarrow 2H^+ + 2e^-$	$H_2 + CO_3^{2-} \rightarrow H_2O + CO_2 + 2e^-$	$H_2 + O^{2-} \rightarrow H_2O + 2e^-$
Realized power	Small plants 5 - 150 KW	Small plants 5- 250 KW	Small plants 5 KW	Small-medium sized plants 50 KW -11 MW	Small power plants 100 KW - 2 MW	Small power plants 100 - 250 KW
Efficiency	50-60%	50-60%	35 – 40%	55%	60-65%	55-65%
Applications	Space, military and energy storage systems, Traction applications	Transport, space, military and energy storage systems.	Transport	Heat and power for decentralized stationary power systems	Power generation	Power generation

### 1.2.1 Why DMFC? An Overview

Recent years have seen an increased interest in fuel cells for a range of applications including transport and small-scale static power. This activity has largely been directed at the use of hydrogen as the fuel. Hydrogen is the most promising fuel because of its maximum energy density and the maximum voltage that can be derived closer to the theoretical value (See Table 1.4). However, the use of hydrogen as fuel is always associated with the complexities regarding its appropriate generation, safe transportation, storage and handling. Alternatively, a liquid fuel can be used and reformed/oxidized to hydrogen *in situ*, which in turn adds to the cost of the system. Thus the competition between various organic fuels lies with size, weight, cost and efficiency of chemical reformers and the electrochemical activity and cost of electrode materials.

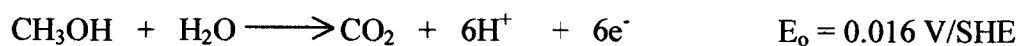
**Table 1.4:** Some common fuels and their corresponding maximum voltage and energy density [62]

Fuel	$E^{\circ}_{\text{theor}}$ (V)	$E^{\circ}_{\text{max}}$ (V)	Energy Density (kWh/kg)
Hydrogen	1.23	1.15	32.67
Methanol	1.21	0.98	6.13
Ammonia	1.17	0.62	5.52
Hydrazine	1.56	1.28	5.22
Formaldehyde	1.35	1.15	4.82
Carbon monoxide	1.33	1.22	2.04
Formic acid	1.48	1.14	1.72

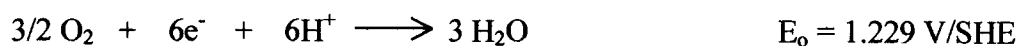


Therefore, electrochemists are challenged to use a fuel that is easily transportable and easily converted into energy from liquid state. Methanol is the favored fuel in terms of cost, efficiency, availability, chemical inertness at cathode and electrical yield per gram of fuel [63]. Methanol can be electrooxidised at a fuel cell anode either directly (DMFC) or indirectly (using reformer). The reformer required to accomplish this, however, lowers the practical power densities. As a result, there are strong incentives for developing fuel cells that directly oxidize methanol as a fuel in their anodic compartments. A typical design of DMFC is shown in Figure 1.5.

The Direct methanol fuel cell consists of an anode at which methanol is electrooxidised to carbon dioxide through the reaction [62];



And a cathode at which oxygen (usually as air) is reduced to form water or steam



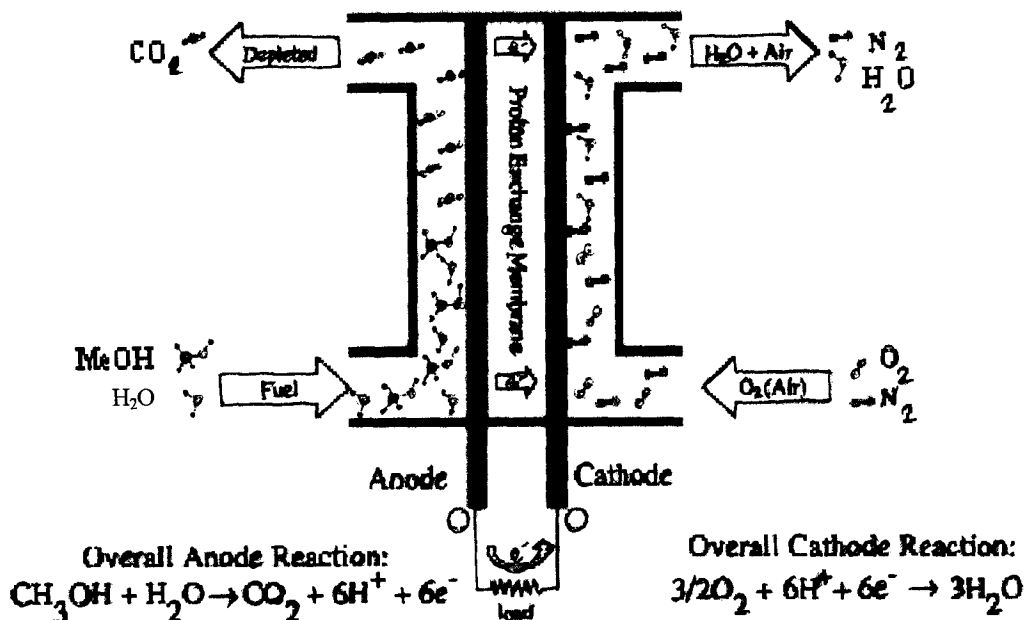
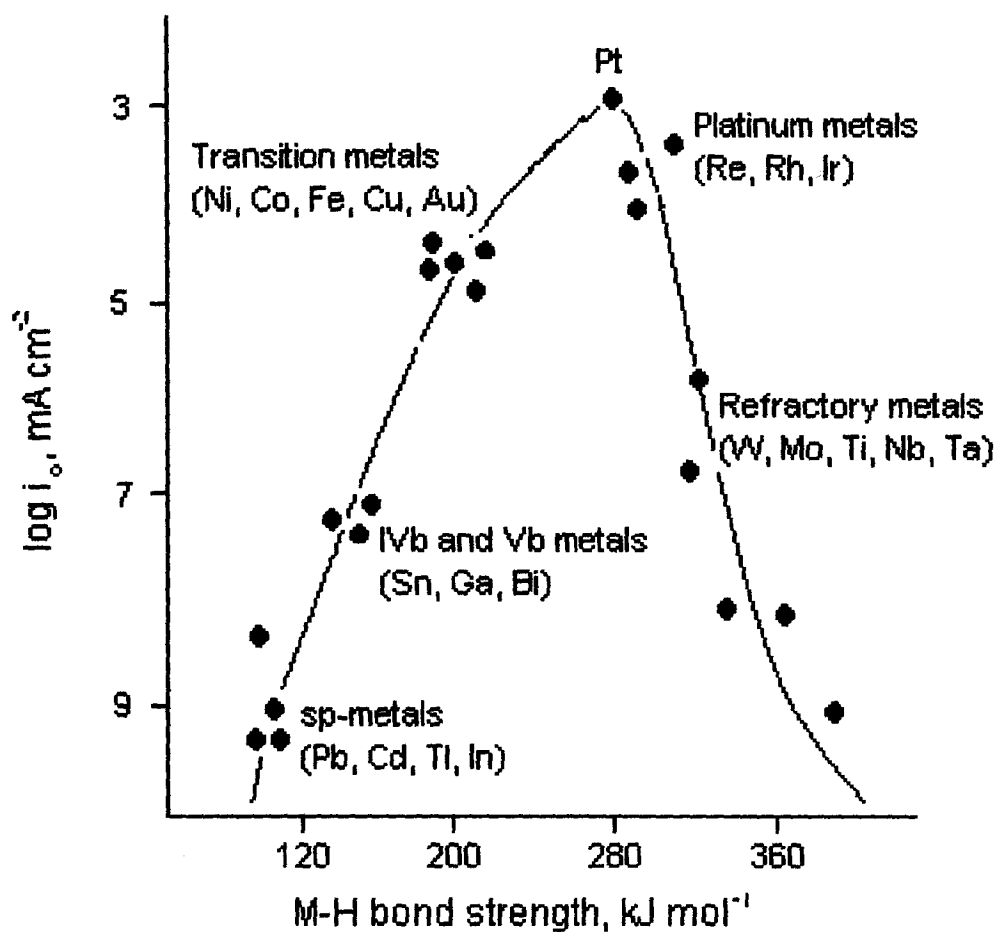


Figure 1.5: A representation of a Direct Methanol Fuel Cell (DMFC) [64]

### 1.2.2 Conventional electrocatalysts: A glimpse at the methanol oxidation mechanism

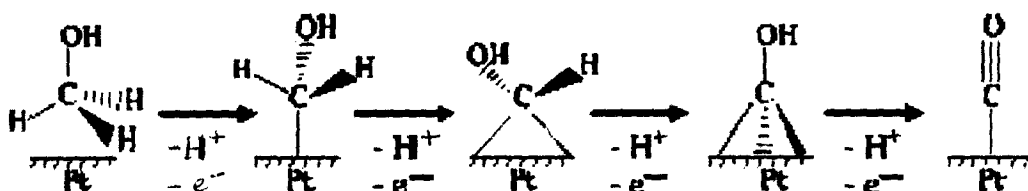
For many years hydrogen evolution reaction (HER) was mainly the only one where the effect of electrode material on the rate of hydrogen evolution was studied in detail. Platinum was found to be the only electrode material over which hydrogen evolves with minimum overpotential [62,63]. These results were then confirmed for oxidation of larger molecules like methanol, ethanol, etc [65-73]. This special activity of platinum can be explained based on the “volcano plot” of various metals, as can be seen in Figure 1.6. A similar plot is shown elsewhere [74,75]. The ascending part of the curve denotes increase of coverage of the reactants over various catalysts, relatively lower bonding energy of radicals to the surface resulting in a faster recombination between them and hence faster overall reaction, which reaches a maximum with platinum. On the descending side, further increase in substrate

coverage is no longer dominant since the coverage is already high and further increases are small; but invariably there seems to be increase in radical-substrate bond energy, which dominates and reaction rate decreases [75]. On platinum the rate-determining step (rds) is believed to be the water-discharge step. Thus, per site (in the volcano plot), the specific rate constant for discharge of water increases from left to right.



**Figure 1.6:** Volcano Plot for different metals active for HER [74]

Kinetics of methanol oxidation is complex. Of the very few metals that are able to adsorb methanol in acidic medium, platinum is an excellent catalyst for the oxidation of hydrogen (as discussed earlier) and the cleavage of C—H bonds in small molecules and have also shown practical activities and sufficient stability [66-74]. C—H bond cleavage over platinum catalyst takes place as shown in Scheme 1.2.

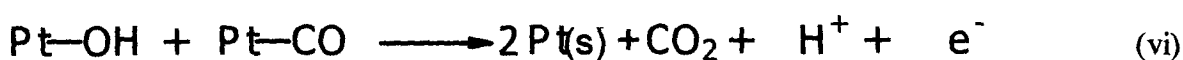
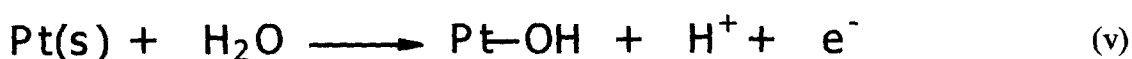
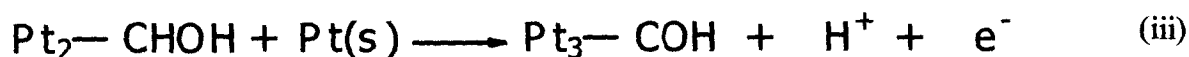
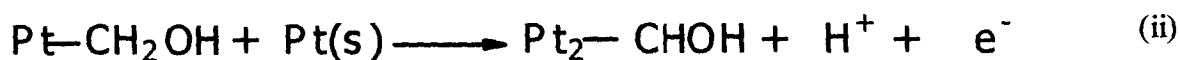
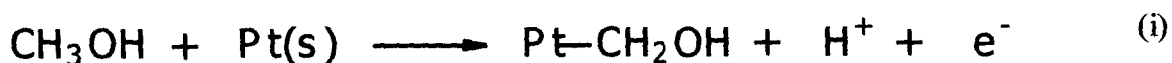


**Scheme 1.2:** Methanol oxidation over a platinum catalyst [76]

Whether oxidation of methanol follows the C—H bond scission or O—H bond scission has been a topic for debate. But recent Density Functional Theory (DFT) studies have proved the former path to be the prevalent mode of oxidation [77-80] although it seems to be a highly competitive one. Thus, during the methanol oxidation reaction, the following primary processes are believed to occur:

- The methanol and water molecules are first adsorbed on the catalyst solid surface at energetically favoured sites.
- The reaction goes through sequential proton stripping giving rise to a series of multiply bonded intermediates that eventually convert to linearly bonded CO.
- CO gets further oxidized to CO<sub>2</sub> either by attack of water from outside the CO islands or by the migration of CO from edges of islands to the active sites.

It is generally accepted that adsorption and subsequent reaction of methanol on platinum takes place by a 6-electron process, which involves the following steps [65] as shown in Scheme 1.3.



**Scheme 1.3:** A six-step methanol oxidation mechanism on conventional Pt catalysts [65]

Additional reactions have also been suggested which involve the formation of carboxylic acid intermediates and its subsequent oxidation to  $\text{CO}_2$ , although the rates of the processes and the dominant species on the surface of Pt is still not clearly known.

For reactions (i) – (iv), Pt is the best-known catalyst has been discussed [66]. However, OH formation at Pt (reaction v) begins slowly, at potentials above 0.45 – 0.5 V v/s RHE. Carbon monoxide and other methanolic residues that remain unoxidised at the surface of the Pt electrode cause a blockage of active sites (thus leading to poisoning of the catalyst) and impede further reaction at energetically desirable potentials.

*These kinds of problems are the center of interest in electro catalysis.*

### **1.2.3 Drawbacks**

There are some difficulties encountered in improving the efficiency of the DMFC, which are as follows:

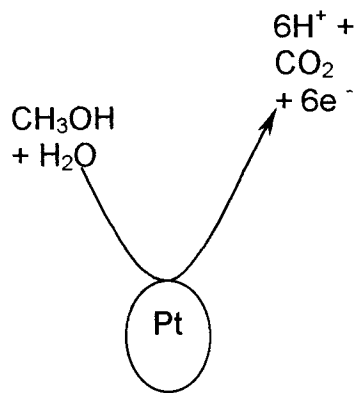
- Acid electrolytes must be used because carbonate formation is a serious problem in alkaline solutions, particularly at current densities regarded as commercially desirable.
- Acid electrolytes invariably cause problems of corrosion.
- The anode reaction is slow near the thermodynamic potential, with the catalysts that are currently used resulting in a large over potential.
- The catalysts currently used for the anode are all based on high platinum content which makes them cost ineffective.
- These catalysts are easily poisoned, both by impurities and more seriously by the products of the anodic reaction itself, the worst being CO.

### **1.2.4 Move towards other catalysts:**

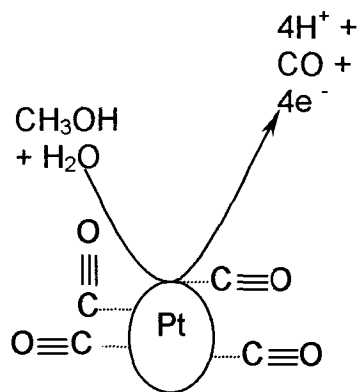
#### *(a) Promotion by Metal alloys:*

It is known that for practical fuel cell applications, Pt alone is not sufficiently active and a promoter that effectively provides oxygen in the active form is required to achieve facile oxidation of the chemisorbed CO on Pt. From this stemmed the idea of using catalyst combinations of Pt with other metals like Pt/Ru, Pt/Mo, Pt/Os, Pt/Sn, etc [65-68]. Although binary alloys of Pt with many other oxophilic elements have been studied, none is more active than the high surface area Pt-Ru catalyst [66]. Many investigators have tried to explain the promotion of methanol oxidation on platinum catalysts by Ru and some key findings are summarized as follows;

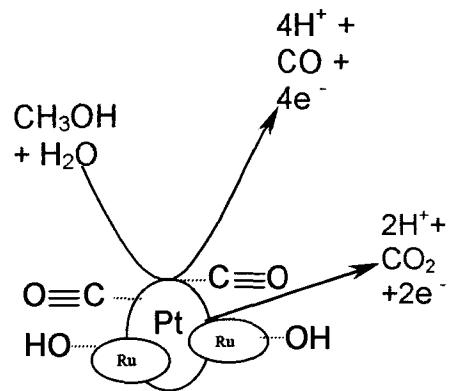
- The *bi-functional mechanism* [70] where the Ru metal atom is the oxophilic metal, which acts as a site for H<sub>2</sub>O adsorption. This model, suggests that effective catalysts should contain at least two kinds of surface elements, namely those that activate the C – H bond (for example Pt), and those that adsorb and activate water so that ‘OH’ groups are produced (for example Ru). The OH groups so formed are believed to help in the oxidation of the stubborn carboxylic species like CO to CO<sub>2</sub> thus releasing the active Pt site once again for further adsorption of methanol.



**Ideal reaction on Pt**



**CO poisoning reduces active area of catalyst**



**Ru catalyses the removal of CO**

**Figure 1.7: Ru assisting Pt in the oxidation of poisonous residues (CO)**



- According to the *electronic model* [70,71], CO poisoning of the active Pt sites is caused by the back bonding from Pt orbitals to the  $\pi^*$  orbital of CO as shown in Figure 1.8. In Pt/Ru binary alloys, there is reduction in the back bonding due to the interaction of the Ru orbitals with the Pt orbitals viz. electron transfer from Ru to Pt occurs resulting in reduction in local density of states, thus electron density on the  $2\pi^*$  orbital of adsorbed CO is reduced and hence CO becomes less strongly bonded. This results in a higher positive charge on the carbon and thereby makes it more susceptible to nucleophilic attack by water and hence assists the oxidation of CO to CO<sub>2</sub> at a lower potential.

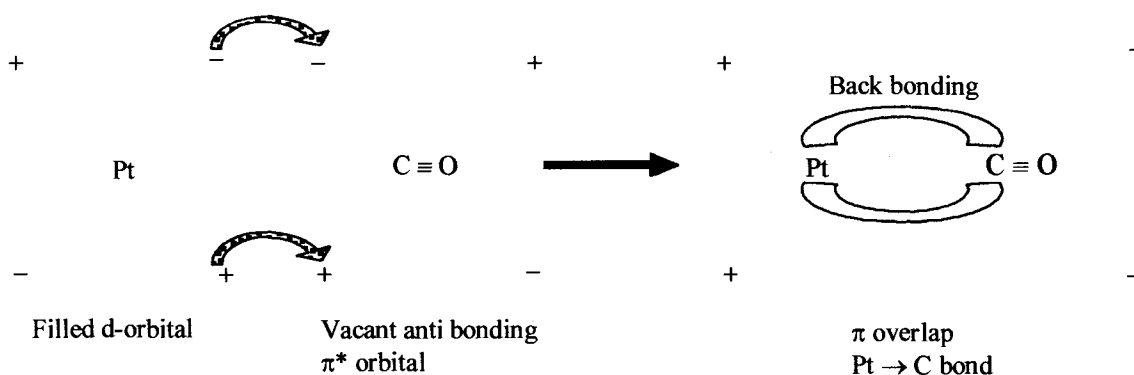


**Figure 1.8** Possible mechanism of back bonding from filled  $\pi$  orbital of Pt to vacant  $\pi^*$  orbital in CO

- A second role of Ru was identified to be that of increasing the coverage of Pt-Ru surface by oxy species. It was found that adsorbed oxygen containing species were formed on the secondary metal at potentials lower ( $\sim 250$  mV vs SHE) than that for Pt ( $> 450$  mV) [81]. This could also help some of the platinum atoms to be oxidized to Pt-O species. Detailed studies revealed that the presence of Ru enhanced the amount of Pt-O species [72,73]. Also in co-deposited Pt-Ru

particulate electrodes, Ru was present in the form of an oxyhydroxide rather than a well-defined RuO<sub>2</sub> species. During the course of the reaction the activity of the catalyst decreased which was attributed to transformation of the hydrous oxide (RuOH) to a more inactive anhydrous phase (RuO<sub>2</sub>) [82].

- According to Rolison *et al.* [83], Pt-Ru blacks are primarily made up of a mixture of RuO<sub>2</sub>, RuO<sub>x</sub>H<sub>y</sub>, Pt, PtO<sub>x</sub> and PtO<sub>x</sub>H<sub>y</sub>. *Hydrous ruthenium oxide is a mixed proton and electron conductor and inherently expresses Ru-OH speciation.* Ru-OH is a critical component of the bifunctional mechanism since it is an oxygen transfer species that oxidatively dissociates bound CO fragments from the Pt surface. The catalysts and membrane electrode assembly (MEA) should not be exposed or processed at temperatures > 423 K as such conditions deleteriously lower the proton conductivity of ruthenium hydroxide and thus affect the ability of the ruthenium component to dissociate water.

*(b) Transition metals as promoters:*

Promotion of platinum for more rapid methanol oxidation has been approached in a number of other ways involving the reduction in the amount of the noble metal:

- (i) A simple method for enhancing the oxidative activity was found to be by generating more Pt – O species on the Pt surface by incorporating another metal e.g. Pt<sub>3</sub>Cr and Pt<sub>3</sub>Fe and its subsequent dissolution leading to a highly reticulated and active surface [65]. The resulting high surface area and higher access to the electroactive species were believed to enhance the oxidation of methanol.
- (ii) Use of surface ad-atoms deposited by *under potential deposition* (upd) on the Pt surface was studied using metals like Au, Sn, Bi, etc. [84] though it was

found that under carefully controlled conditions, these metals inhibited methanol oxidation.

(iii) Alloying of platinum with certain metals is shown to form a surface oxide in the potential range for methanol oxidation. This surface oxide furnishes the necessary oxy species required for the further oxidation of the methanolic residues to CO<sub>2</sub>. Besides Pt-Ru, promoting effects have also been demonstrated for many metals including Ir, Re, Os, W and Sn [85]. In addition, Pt-Mo prepared by electro deposition has been shown to be highly active for methanol oxidation at low current densities, which also happens to be explained well by the bifunctional mechanism [86].

(iv) *Replacing Pt with other Noble metals:* Other noble metal catalysts such as Ir have been investigated [87] but are found to be less active than Pt. Amorphous metal alloys such as NiZr [88] were active, and the reason was believed to be due to the formation of a thick passivating oxyhydroxide film on the catalyst surface on which the methanol oxidation took place. In such catalysts Ni<sup>III</sup>OOH/Ni<sup>II</sup>(OH)<sub>2</sub> were believed to be the active components of the oxyhydroxide film of which NiOOH is the stable phase. The mixed valence Ni<sup>2+/3+</sup> components accounts for the high electronic conductivity of the surface layer [89,90]. These catalysts were found to be well protected from corrosion and stable in methanol oxidation conditions. Kawahima et al. [91] used alloys of NiZr and NiTi [89] with a small percentage of Pt and were found to be active for methanol oxidation.

(v) A valuable method of catalyst evaluation is combinatorial selection [92], which involves systematic preparation, processing and testing of large diversities of chemically and physically different material libraries in a high

throughput fashion. This technique enables the discovery of superior catalytic materials in a matter of hours or days as opposed to months and years taken using traditional methods. Array-based samples depending on the number of metal components are the most commonly used library platform in combinatorial studies [92]. Appropriate metal salt precursors are systematically constructed to form an array of various compositions over a single plate or electrode, which is then reduced to the active metals. This serves as the working electrode for further testing of substrate oxidation. A quaternary catalyst of optimum composition Pt-Ru-Os-Ir has been selected by this method, which showed higher activity than the conventional Pt-Ru catalyst [93]. Recently, sample gradients have been representing a particularly interesting format providing a highly dense composition spread that can be constructed and evaluated in a single sample [94].

### **1.2.5 Transition metal oxides as promising catalysts:**

#### *(a) Combination of Pt with a base metal oxide:*

Hammnet *et al.* [95] found Nb, Zr and Ta to promote Pt activation, particularly at higher currents. Later they also attempted to use  $ZrO_2$  [96] to promote Pt/Ru but were unsuccessful. Studies have also shown that hydrous  $WO_{3-x}$  acts as a promoter for Pt when electrodeposited on its surface [97] or by codepositing onto a carbon substrate [98]. These carbon supported Pt- $WO_{3-x}$  electrodes have been reported to give superior activity to methanol oxidation than Pt-C electrodes. In the case of W based catalysts, the mechanism involving a redox couple of W(IV) and W(V) has been suggested.

Lasch *et al.* [99] studied the electrooxidation of methanol using ternary alloys by introducing transition metal oxides such as  $\text{WO}_x$ ,  $\text{MoO}_3$  and  $\text{VO}_x$  to Pt-Ru catalysts where Pt-Ru particle sizes were  $\sim 3 - 5$  nm. In these metal oxide containing ternary catalysts, a lower polarization of methanol oxidation was observed and were capable of sustaining large current densities. However, above 750 mV/RHE, deactivation of the catalysts occurred which was attributed to the formation of a catalytically inactive surface oxide. The most prominent effect of catalytic activity was found to be that of Pt-Ru- $\text{VO}_x$  and methanol oxidation started at 360 mV/RHE, which was almost identical to Pt-Ru electrode (380 mV) the latter being slightly superior.

The influence of dispersing metal oxides like  $\text{Al}_2\text{O}_3$ ,  $\text{Cu}_2\text{O}$ ,  $\text{ZnO}$ ,  $\text{TiO}_2$ ,  $\text{Fe}_2\text{O}_3$ ,  $\text{SiO}_2$ ,  $\text{RuO}_2$  [100] was also studied with a commercial Pt-Ru catalyst for methanol oxidation in phosphoric acid (98%). At 150 °C, catalysts made by mixing with  $\text{Fe}_2\text{O}_3$  were identified as giving the best performance in terms of reduced polarization compared to Pt-Ru alone.

Samant and Fernandes [101] have reported the use of Ni and Fe modified manganese dioxide as methanol oxidation catalysts in sulphuric acid electrolyte. The Ni modified  $\text{MnO}_2$  catalyst, formed as a thin film (by thermal decomposition) onto a Platinum substrate exhibited significant activity for methanol oxidation (420 mV vs. SCE, at 100  $\text{mAcm}^{-2}$ ). The improved activity has been associated with the simultaneous proton-electron intercalation of the Ni-manganese electrode.

*(b) Incorporation of Pt directly into oxide structures:*

In addition to electrodeposition of Pt onto an oxide surface, incorporation of Pt directly onto oxide structures was also attempted on perovskite-based

oxides, such as  $\text{SrRu}_{0.5}\text{Pt}_{0.5}\text{O}_3$  [102] and  $\text{Dy}_x\text{Pt}_3\text{O}_4$  [103]. It is presumed that they undergo reductive decomposition through methanol adsorption to give fine platinum particles at the surface, which act as catalytic sites. However, there exists ambiguity about their long-term stability in acidic environments.

**Table 1.5:** Effect of catalyst promoters on methanol oxidation

Type of Promotion	Catalyst promoter	Comment	Ref.
Alloying and dissolution to produce highly reticulated surfaces.	Cr Fe Sn	Typically less than 100 mV lower potential than Pt.	65
Alloys	Ru Sn, Mo Os, Ir Ti, Re	Ru has the greatest effect. Sn, Mo, Os and Re are substantial promoters.	65-68
Metal oxides	Ru	Hydrous Ru oxide is the most active catalyst	83
Surface adatoms	Sn Bi	Improved activity to a small extent in few cases.	84
Base metal oxides	W Nb, Zr Ta	W oxide is a notable promoter. Small effect of other metal oxides	95-99

### 1.2.6 Supported Metal catalysts:

Dispersed micro/nano particles of noble metals supported on high surface area materials are of considerable interest to catalysis, in part due to their unique physical and chemical properties. The primary function of the support is to separate the individual particles physically in order to diminish the rate of agglomeration.

The choice of a suitable support is a factor, which affects the performance of supported catalysts. Interactions between the catalyst and the support have been identified to modify the intrinsic catalyst activity. In the studies of methanol oxidation, the supports so far employed for dispersing catalytic metal particulates are carbon and conducting polymers.

#### *(a) Polymer supports:*

Catalyst particles have been dispersed in conducting polymer matrices of polyaniline [104,105], polypyrrole [106,107], and poly-(3-methyl)thiophene [108]. These materials were evaluated for their activity towards methanol oxidation and although the initial activity was often promising, the performance in many cases rapidly deteriorated due to either poisoning of the electrode surface or destruction of the polymer at the high temperature used.

#### *(b) Carbon supports:*

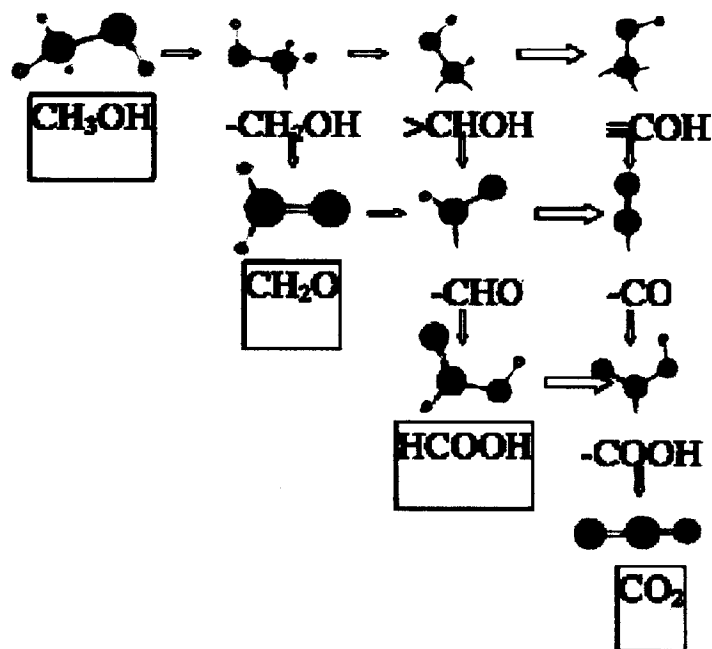
The current trend is to investigate newer support materials rather than using the conventional Vulcan XC carbon or acetylene black. Thus, Pt-Ru supported over highly oriented pyrolytic graphite (HOPG) or on mesocarbon microbeads have recently been investigated as catalysts for anodic oxidation of methanol and are reported to show lower polarization characteristics than with carbon black [109,110].

*(c) Zeolites:*

Zeolites are found to be efficient support materials when incorporated with metals like Pt, Ru, Pd, Au, etc [111,112]. The zeolite material contains acidic proton entities on its surface, which makes it more hydrophilic than carbon, and when used as a catalyst support in fuel cell electrodes, it results in lower resistance and less ohmic power losses than are found in electrodes that employ the use of carbon exclusively as the support material [111,113]. Further, these zeolites materials are known to contain an array of channels, which allow relatively high gas permeability [113,114]. The enhanced electrocatalytic activity is also attributed to the formation of CO clusters inside the zeolite cages, which facilitates its oxidation to CO<sub>2</sub> [112].

Thus, as can be seen, the mechanism of methanol oxidation has proved extremely difficult to elucidate, since the precise pathway is sensitive to many factors. These include: the morphology of the Pt surface, the nature of co-adsorbed anions/cations, temperature, methanol concentration, the presence of adventitious “impurities”, pH, and electrochemical polarization history. It is evident that a number of pathways can be followed (and a number of intermediates identified) in the oxidation of methanol, which can be represented as in Scheme 1.4.





**Scheme 1.4:** The different pathways (and a number of identified intermediates) in the oxidation of methanol. (Arrows represent electron production and molecules in boxes are stable) [115]

### 1.2.7 Objectives:

Thus the current trend is to

- ❖ Reduce catalyst cost for direct methanol fuel cells.
- ❖ Reduce noble metal catalyst loading to less than  $0.5 \text{ mgcm}^{-2}$ .
- ❖ Identify potential non-noble metal catalytic systems.

### 1.3 Summary:

- a. Octahedral molecular sieves are currently 'hot' materials, which can find use in various applications.
- b. The ability to adjust their pore sizes and activities make them great materials for separation and sorption applications.
- c. Fine-tuning the valence states of the active sites gives the ability to perform selective catalytic reactions and conductivity changes for sensors.
- d. Ion diffusion through the channels and pores opens up potential applications as battery materials.
- e. Fuel cells are currently gaining much attention in the area of energy/power generation.
- f. Various catalysts have been tried out so far with platinum and its alloys being the best.
- g. Thus the search is on for new materials, which will use lesser amount of expensive noble metals, but one which will not compromise on efficiency.
- h. This situation dictates the following requirements:
  - Presence of optimum sized pores in the electrode to diffuse the methanol and the electrolyte towards the reactive sites and to diffuse out carbon dioxide bubbles.
  - Electrode should remain porous for a long period of time to facilitate fuel transport to fuel- electrode-electrolyte interface (triple point).
  - Presence of as many catalytic sites as possible inside the pores is necessary since this is where methanol and electrolyte get adsorbed.
- i. Therefore, mass transport of carbon dioxide bubbles thus produced has to be quick if further reaction has to occur.

- j. This calls for a study of designing electrodes with specific structures using the catalytic material if one needs to develop high performance electrodes.
- k. Electrocatalysis studies are thus directed to establishing the nature of the species formed during adsorption, understanding the mechanism of the reaction, studying surface structural effects and invariably *a search for new catalysts*.

*The present investigation is thus aimed at synthesis of manganese OMS-2 and studying its applications in catalytic and electrocatalytic oxidations.*

*CHAPTER – II*

*SYNTHESIS OF OMS-2 USING ANION*

*TEMPLATE*

## 2.1 Introduction:

Microporous manganese oxides are prepared via a variety of routes [23-40]. Many of the materials with similar gross structural features nevertheless show a diversity of properties depending on the specific synthetic route. These differences can be attributed to variations in particle size and the type and amount of defects on the structures. For this reason small changes in synthetic parameters can result in materials with novel catalytic, electrochemical, and ion – exchange properties [10,11]. In chapter I the literature review laid an emphasis on recent preparations, including precipitation, ion-exchange/hydrothermal routes [23-30], sol – gel [31-33], microwave heating [10,33], high temperature solid-state routes [35-37], and electrochemical methods [38,39].

We recall that OMS-2 are  $MnO_x$  ( $x = 1.85 - 2.0$ ) materials with one-dimensional  $2 \times 2$ -type tunnels, built up with  $[MnO_6]$  octahedra with pore diameter of 4.6 Å. They are known to exhibit small particle sizes and large surface areas up to 250  $m^2/g$ , which make them outstanding materials for molecular sieving and catalysis. By altering the method of preparation, doping with suitable cations, etc. the properties of these materials like acidity, pore size, shape, etc. can be varied. Hence their synthetic strategies are of great importance. The various OMS-2 forms viz cryptomelane, hollandite and coronadite are known to be formed in the presence of  $K^+$ ,  $Ba^{2+}$  and  $Pb^{2+}$  respectively. They can be conveniently synthesized by (i) heat treatment of birnessite at 600 °C and (ii)  $KMnO_4$  oxidation of  $Mn(II)SO_4$  in acidic medium [23]. Synthesis of OMS-2 is also reported to form by disproportionation of  $Mn_2O_3$  in sulphuric acid medium without the specific use of any template [35]. It is also known to be synthesized electrochemically and effect of cations like  $Ca^{2+}$ ,  $Mg^{2+}$ ,  $Na^+$ ,  $K^+$ ,  $Cs^+$ , etc on the phase formation has been discussed [37].

Till date there are no reports in literature in the use of anion templates. In this study we report synthesis of OMS-2 by chlorate oxidation of Mn(II) salt precursor and show the important role of sulphate ions in the formation of OMS-2 type materials.

## **2.2 Synthesis of OMS-2**

### *2.2.1 By $KMnO_4$ oxidation*

Manganese oxide octahedral molecular sieves of the cryptomelane type have been synthesized by a reported method [23]. The synthesis involves  $KMnO_4$  oxidation of  $MnSO_4$  in nitric acid medium. Thus hot 0.037 M  $KMnO_4$  (23.56 g in 400 ml distilled-deionised water) was added dropwise with the help of a transfer funnel to hot 0.052 M  $MnSO_4$  solution (35.2 g in 120 ml) containing 12 ml of conc.  $HNO_3$ . The mixture was under constant agitation on a rotamantle and then refluxed for 24 hrs. The dark brown – black residue of manganese oxide was extracted in hot water after cooling to room temperature, filtered, washed till washings were neutral, then dried at 120 °C overnight, crushed, powdered and stored in a vacuum dessicator. The sample is labeled as S1.

### *2.2.2 By Chlorate oxidation*

A series of experiments were carried out in order to study the phase formation by using potassium perchlorate –  $KClO_3$  as oxidant. In this process molar quantities of the reactants and nitric acid used here were optimized to give maximum yield of the product with minimum usage of nitric acid. In a typical experiment, an aqueous solution of Mn (II) salt along with the required quantity of nitric acid was taken in a tall beaker and the temperature was controlled at  $98 \pm 2$  °C on a sand bath. After this,

the calculated quantity of  $\text{KClO}_3$  was added in a single installment followed by vigorous stirring for one hour. The precipitate was allowed to cool and was then filtered, washed with distilled deionised water till washings were neutral and then dried in an air oven at  $120\text{ }^\circ\text{C}$  for 24 hours, crushed, powdered and again dried at  $110\text{ }^\circ\text{C}$  and stored in a vacuum dessicator until further analysis.

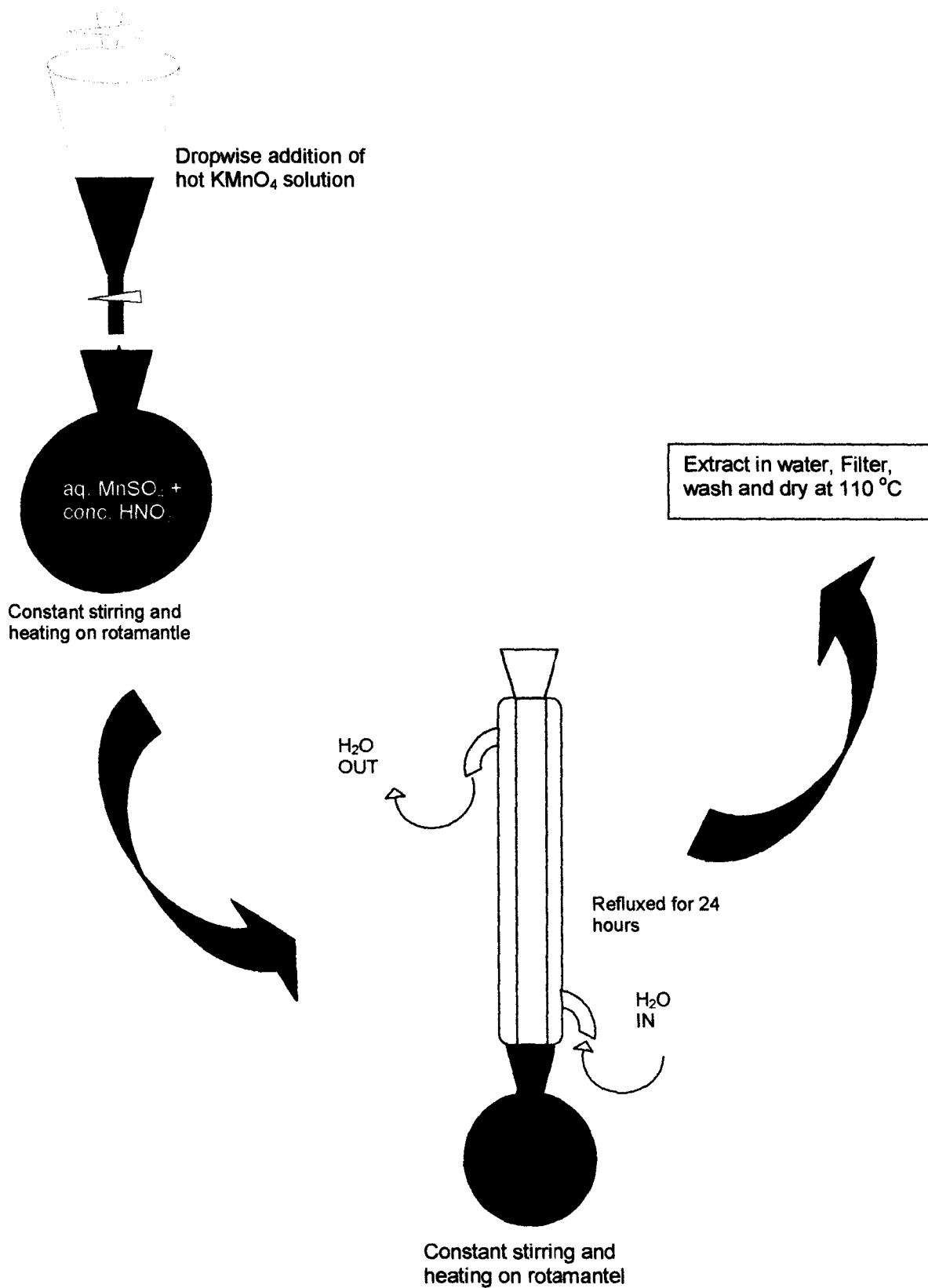


**Figure 2.1:** Scheme of the synthesis of OMS-2 by  $\text{KMnO}_4$  oxidation method



**Table 2.1:** Synthesis of OMS-2 by chlorate method

Code	Amounts of various reactants				% Yield of MnO <sub>2</sub>
	MnSO <sub>4</sub> .H <sub>2</sub> O (moles)	HNO <sub>3</sub> (ml)	OMS-2 (mg)	KClO <sub>3</sub> (moles)	
1	0.025	3	-	0.01	6
2	0.025	25	-	0.01	21
3	0.025	50	-	0.01	39
4	0.025	120	-	0.01	61
5	0.025	25	200	0.01	47
6	0.025	50	50	0.02	90
7	0.025	50	200	0.02	94
8	0.025	25	100	0.02	55
9	0.025	100	100	0.02	98
10	0.025	100	50	0.02	96
11	0.025	25	100	0.026	78
12	0.025	120	-	0.023	100
13	0.025	25	-	0.041	100
14	<b>0.025</b>	<b>25</b>	-	<b>0.033</b>	<b>100</b>
15	0.025	25	-	0.026	76
16	*Mn(NO <sub>3</sub> ) <sub>2</sub>	<b>25</b>	-	<b>0.033</b>	<b>68</b>
17	**Mn(NO <sub>3</sub> ) <sub>2</sub>	<b>25</b>	-	<b>0.033</b>	<b>62</b>
18	<b>0.025</b>	<b>25</b>	-	<b>0.033 moles of NaClO<sub>3</sub></b>	<b>79</b>

\*,\*\* = 0.025 moles of Mn(NO<sub>3</sub>)<sub>2</sub>

\*\* = Solid state reaction where all the reactants as their salt solutions were mixed together, evaporated to dryness on a water bath and then calcined at 200 °C.

As evident from Table 2.1, % yield of the final product increased with increase in amount of nitric acid. Further, OMS-2 was added to the reactants to test whether it may act like nucleating centers for the formation of the product, but did not affect the yield substantially. Subsequently, increase in amounts of nitric acid and the oxidant; perchlorate were optimized to obtain a satisfactory yield.

Optimum conditions were obtained with 0.025 moles of Mn(II) salt, 25 ml of nitric acid and 0.033 moles of oxidant. Thus this composition provided maximum yield of product with minimum amount of nitric acid as well as the oxidant. For convenience, the samples marked bold were further studied since they gave maximum yield, were prepared under similar conditions, and also contained same number of moles of two different Mn (II) salts. Sample 17 contains same reactants as sample 16 but the preparation was carried out via solid-state reaction. Thus the samples are designated with simpler codes and will henceforth be called as **S2** (14), **S3** (16), **S4** (17) and **S5** (18) as shown in Table 2.2.

**Table 2.2:** Simple codes for the synthesized samples

<b>Code as per Table 2.1</b>	<b>New Code</b>
S1 (not shown in table 2.1)	S1
14	S2
16	S3
17	S4
18	S5

## 2.3 Characterization of the samples

### 2.3.1 Powder X-ray Diffraction studies (XRD)

The crystal phases of the samples were monitored with the help of powder X-ray diffraction analysis carried out on a Shimadzu labX-100 diffractometer using Ni-filtered Cu-K $\alpha$  radiation ( $\lambda = 1.5406 \text{ \AA}$ ) with a step scan of 0.05 degrees/min. The data obtained was compared to JCPDS file 20-908 [116] for cryptomelane ( $\alpha$  – phase) and as reported by Koshiha *et al.* [117] for  $\gamma$  – phase.

The characteristic diffraction data for typical OMS-2 and nsutite ( $\gamma$ -MnO<sub>2</sub>) manganese oxides is given in Tables 2.3 and 2.4 respectively.

**Table 2.3:** Characteristic X-Ray diffraction data of OMS-2

JCPDS 20-908 [116]	
d	I/I <sub>0</sub>
6.9	90
4.9	80
3.1	80
2.39	100
2.25	60
1.80	40
1.63	60
1.54	60
1.35	50

**Table 2.4:** Characteristic X-Ray diffraction data of  $\gamma$ -MnO<sub>2</sub>

Ref. [117]	
<i>d</i>	<i>I/I<sub>o</sub></i>
4.10	100
2.43	100
2.13	80
1.64	80
1.40	60

**Table 2.5:** Typical X-ray powder diffraction pattern of the samples

S1		S2		S3		S4		S5	
<i>d</i>	<i>I/I<sub>o</sub></i>	<i>d</i>	<i>I/I<sub>o</sub></i>	<i>d</i>	<i>I/I<sub>o</sub></i>	<i>d</i>	<i>I/I<sub>o</sub></i>	<i>d</i>	<i>I/I<sub>o</sub></i>
6.91	59	-	-	-	-	-	-	6.80	40
-	-	-	-	4.07	83	4.15	43	-	-
4.84	72	4.81	26	-	-	-	-	4.85	27
3.08	87	3.10	90	3.07	15	-	-	3.08	37
2.38	100	2.39	100	2.40	100	2.43	100	2.39	100
2.14	36	2.14	40	2.11	49	2.13	52	2.14	42
1.91	15	1.91	-	-	-	-	-	2.00	11
1.83	40	1.82	40	1.83	11	-	-	1.81	20
1.63	33	1.63	41	1.62	51	1.64	73	1.62	20
1.52	39	1.53	52	-	-	-	-	1.52	25
-	-	-	-	1.39	34	1.40	54	-	-

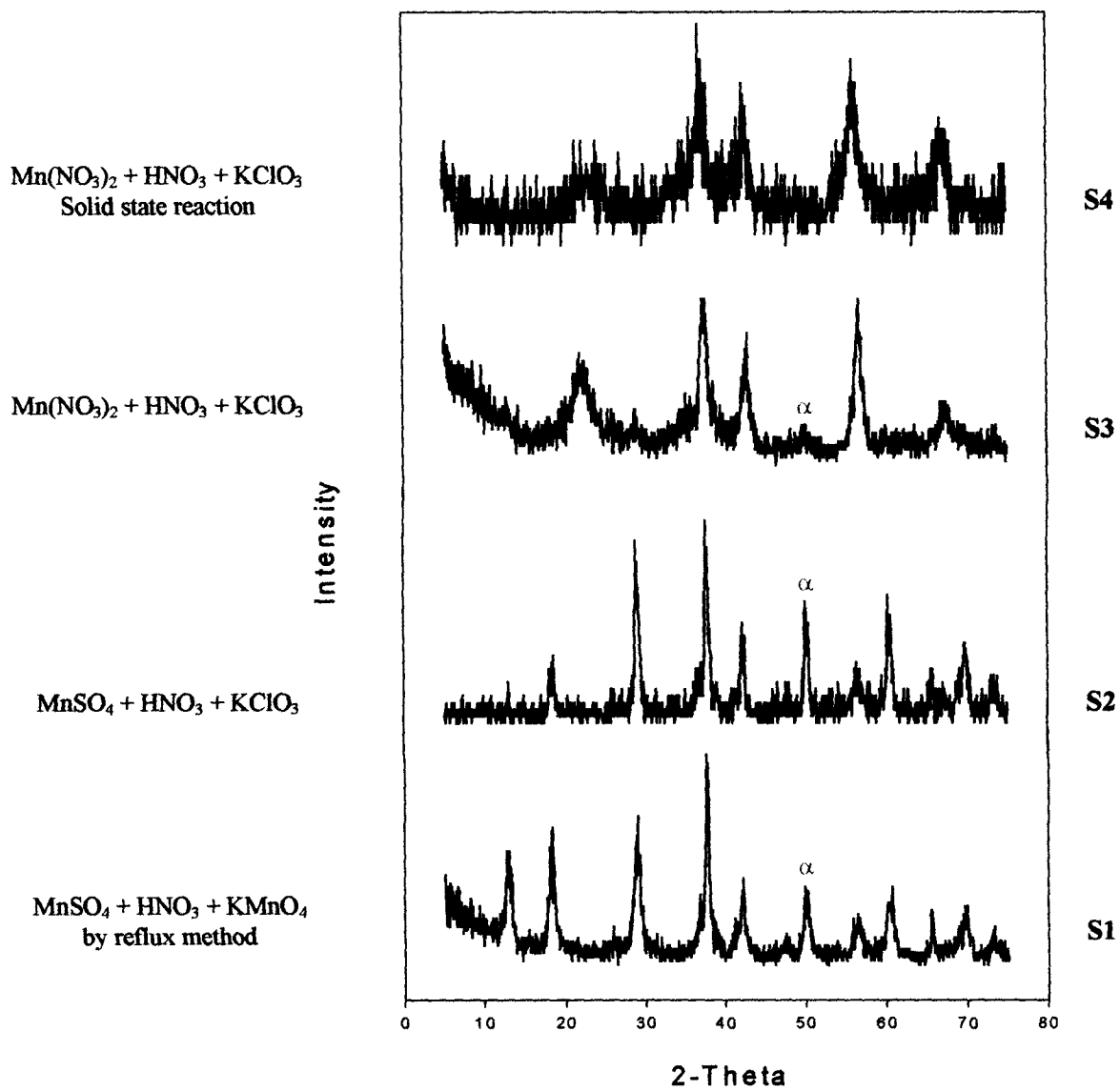


**Figure 2.2:** XRD profiles of; (a) S1, (b) S2, (c) S3 and (d) S4

Use of  $\text{KClO}_3$  to prepare active manganese oxides has been reported more than a century ago [118]. While many workers of that time observed various forms of the oxides, Cole *et al.* [119] and subsequently Desai [120,121] reported formation of  $\alpha$  – phase under various conditions. It can be seen from the XRD profiles shown in Figure 2.2, that sample S1 and S2 have identical XRD profiles. This confirms that OMS-2 can also be obtained by chlorate method. The samples show the characteristic peak of cryptomelane or OMS-2 ( $\alpha$ - $\text{MnO}_2$ ) seen at  $d \sim 1.80 \text{ \AA}$  ( $2\theta \sim 50^\circ$ ). The  $\text{K}^+$  ion is believed to be the template responsible for formation of (2 $\times$ 2) tunnels of OMS-2 [23,118-121]. The sample S3 was prepared in a similar manner as that of S2, but using Mn(II)nitrate in place of Mn(II)sulphate. As can be seen in the figure, its XRD pattern has become significantly diffuse, similar to that of nsutite or  $\gamma$ - $\text{MnO}_2$  [121-123]. The nsutite peak at  $d \sim 4.1 \text{ \AA}$  was formed at a significant intensity of 83%. At the same time, the characteristic peak of cryptomelane at  $d \sim 1.80 \text{ \AA}$  is greatly reduced in intensity for S3. Thus S3 can be called as an OMS-2/nsutite mixed phase. In a similarly prepared sample S4, even the residual OMS-2 peak that could be seen at  $2\theta \sim 50^\circ$  has vanished, and the pattern is akin to the nsutite phase. In order to further confirm that  $\text{SO}_4^{2-}$  ion is essential for OMS-2 formation rather than  $\text{K}^+$  ion, synthesis of another sample S5 was subsequently carried out in a similar manner as S2, the only difference being that, an equivalent amount of  $\text{NaClO}_3$  was used as oxidizing agent in place of  $\text{KClO}_3$ . In both cases,  $\text{MnSO}_4$  concentration was same. Once again XRD pattern revealed that OMS-2 was formed. Thus, among the Mn(II) salt precursors,  $\text{Mn(II)NO}_3$  seemed to favour nsutite formation while  $\text{Mn(II)SO}_4$  favoured cryptomelane or OMS-2 formation under similar experimental conditions. Thus one can conclude that OMS-2 can be formed irrespective of whether the cation is  $\text{K}^+$  or  $\text{Na}^+$  ion, but in either case,  $\text{SO}_4^{2-}$  ion is essential. This confirms the crucial role of the

$\text{SO}_4^{2-}$  ion in formation of OMS-2 phase, even when the precipitation was carried out in the presence of  $\text{K}^+$  or  $\text{Na}^+$  ions.

### 2.3.2 *Infrared Spectroscopy (IR):*

Each of the manganese oxides were ground with KBr and then pressed into thin wafers/pellets using a hydraulic press. These wafers were then loaded on a Shimadzu DR-8031 FTIR spectrometer and the spectra of the samples were recorded in the range  $400\text{-}4000\text{ cm}^{-1}$ . Whether the manganese dioxide is OMS-2 type or nsutite can also be detected by IR spectroscopy (Figure 2.3), wherein OMS-2 samples show characteristic absorption at around  $700\text{ cm}^{-1}$  [121]. Such an absorption is prominent in the OMS-2 samples S1, S2 and S5. In the nsutite sample S4, however, this absorption has almost disappeared, while it appears as a shoulder in the OMS-2/nsutite mixed phase sample, S3.

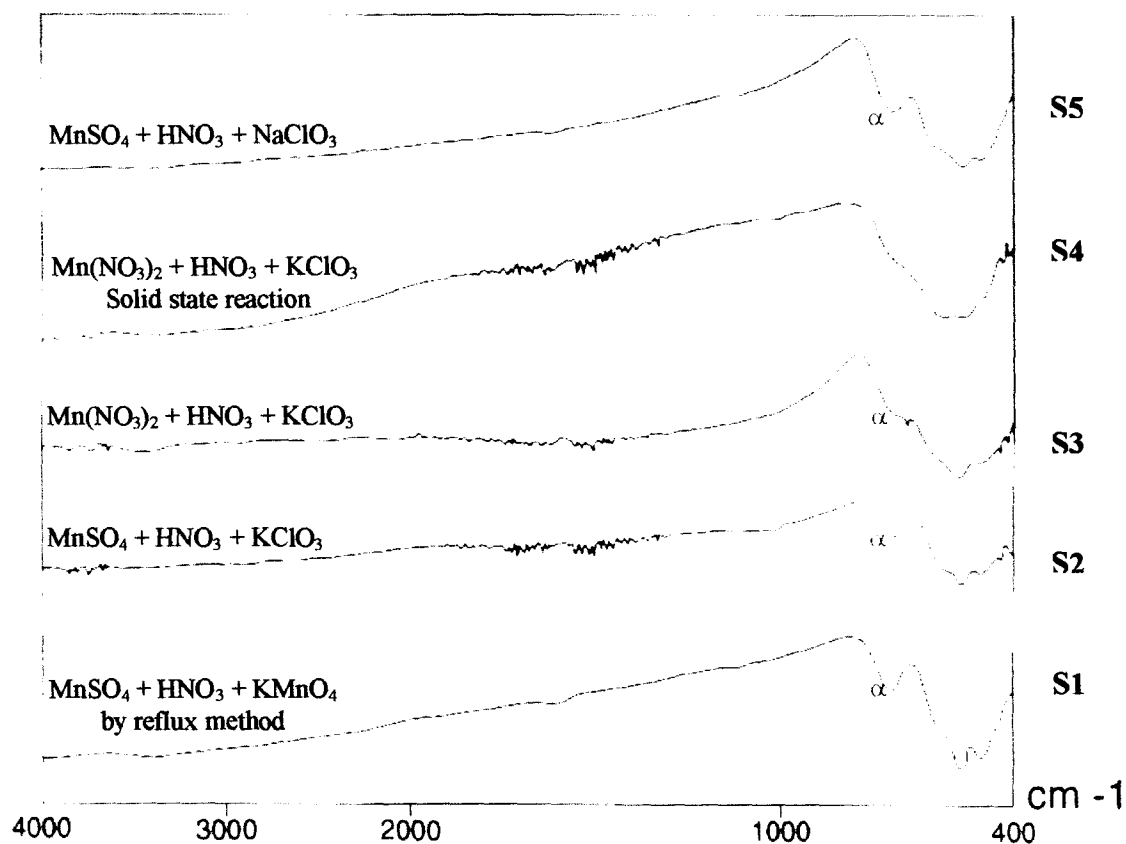


**Figure 2.3:** Infrared spectra of the synthesized manganese oxides

### 2.3.3 Chemical analysis (Average Oxidation State)

The amount of manganese in the material was estimated as % Mn as described elsewhere [35]. A typical analysis procedure involved, heating a weighed quantity of the oxide in concentrated hydrochloric acid on a sand bath covering the beaker with a watch glass for around 10 minutes till it dissolved. The clear solution was then cooled and diluted to a known volume with deionised-distilled water, followed by a complexometric titration using standard EDTA method with Eriochrome black – T as the indicator.

Experiments involving redox titrations of the manganese oxide samples first using ferrous ammonium sulphate to reduce manganese to  $Mn^{+2}$  and then back-titrating the excess  $Fe^{2+}$  with standard  $KMnO_4$  solution gave the amount of  $MnO_2$  in the sample i.e. Mn in +4 state [35] (%  $MnO_2$ ).



The average oxidation state of manganese in the manganese dioxides was calculated using the relation [35,60,124]:

$$N = \{ [F(\text{Mn}) / F(\text{MnO}_2)] \times [\% \text{ MnO}_2 / \% \text{ Mn}] + 1 \} \times 2$$

where N = Oxidation number of Mn

$$F(\text{Mn}) = \text{Atomic weight of Mn} = 54.938$$

$$F(\text{MnO}_2) = \text{Formula weight of MnO}_2 = 86.938$$

$$\% \text{ MnO}_2 = \text{weight content of MnO}_2 \text{ in the sample}$$

$$\% \text{ Mn} = \text{weight content of Mn in the sample}$$

The results thus obtained are presented in Table 2.6. These results show that the average oxidation state of Mn in the manganese oxides synthesized vary between 3.63 – 3.91. These values are in agreement with those reported in the literature [23]. Thus Mn is not only present as Mn<sup>4+</sup> but also has some amount of Mn in lower oxidation states, which results in the lowering of the average oxidation state. These sub-stoichiometric oxides were found to have good activity for many reactions, as will be discussed in subsequent chapters. Pyrolusite (a form of manganese oxide) on the other hand usually shows almost stoichiometric (near 100 %) MnO<sub>2</sub>. This results in the oxidation state of manganese being +4.

#### 2.3.4 Chemical activity studies

This method is used for the evaluation of the relative activity of the manganese dioxides. The activity of manganese dioxides is found to be greatly dependent on the method of preparation. The active manganese dioxides are shown to have the following general formula:



so it appears that the acidic 'OH' groups result from the MnOOH groups forming the solid-state solution with manganese dioxide, according to Brenet *et al.* [124]. The

MnOOH groups imply the presence of manganese in +3 state. The Mn – O bond lengths in various dioxides is known to influence chemical reactivity. The method takes advantage of the fact that acidic OH groups are present in all active dioxides. It is the H<sup>+</sup> ions from these groups that are being exchanged. In order to understand the reactivity of the samples, the H<sup>+</sup> ion exchange capacity was determined in DMF medium [121]. The reaction involves liberation of iodine from KI after the exchange of H<sup>+</sup> from MnOOH groups by K<sup>+</sup> ions. In a typical experiment, 200 mg of each of the samples was weighed accurately into a beaker containing 20 ml of DMF solution containing 10 % KI (10 g KI in 10 ml water and 90 ml DMF). The sample was stirred continuously on a magnetic stirrer for exactly 10 minutes after which the mixture was filtered under vacuum with the washings transferred quantitatively into a conical flask.

The iodine thus liberated was estimated by titrating with 0.03 M Na<sub>2</sub>S<sub>2</sub>O<sub>3</sub> solution using starch as the indicator. The volume of the thiosulphate consumed is considered to give a fair measure of the relative activity of the manganese dioxides. Table 2.6 gives the H<sup>+</sup> ion exchange capacity of the samples expressed as volumes of thiosulphate consumed,  $V_{S_2O_3^{2-}}$ . This implies that the samples are active compounds. The H<sup>+</sup> ion exchange capacity is directly related to the presence of acidic ‘OH’ groups attached to Mn<sup>3+</sup> in the host Mn (IV) oxide lattice [37,38,121,124]. It is known from literature that the stoichiometric Mn(IV) oxide (pyrolusite) has no exchangeable protons or active hydroxyl (OH) groups. It is thus catalytically and electrochemically inactive, and shows no evolution of I<sub>2</sub> in the ion exchange experiment [121,125]. Hence the synthetic pyrolusite MnO<sub>2</sub> is used as a reference sample in this investigation.

**Table 2.6:** Synthesis of manganese oxides in relation to its crystal phase and H<sup>+</sup> ion exchange capacity

Sample	Reagents	Chemical Analysis		Oxidation state 'x'	Crystal phase	V <sub>S<sub>2</sub>O<sub>3</sub><sup>2-</sup></sub> (ml)
		%MnO <sub>2</sub>	%Mn			
S1	MnSO <sub>4</sub> + HNO <sub>3</sub> + KMnO <sub>4</sub>	86	61.81	3.76	OMS-2	3.4
S2	MnSO <sub>4</sub> + HNO <sub>3</sub> + KClO <sub>3</sub>	81.51	63.18	3.63	OMS-2	1.3
S3	Mn(NO <sub>3</sub> ) <sub>2</sub> + HNO <sub>3</sub> + KClO <sub>3</sub>	92.38	63.18	3.85	OMS-2/ nsutite	1.8
S4	Mn(NO <sub>3</sub> ) <sub>2</sub> + HNO <sub>3</sub> + KClO <sub>3</sub> *	83.42	61.81	3.69	Nsutite	3.3
S5	MnSO <sub>4</sub> + HNO <sub>3</sub> + NaClO <sub>3</sub>	91.48	60.43	3.91	OMS-2	5.8

All the precipitation reactions were aqueous and carried out at ~ 100°C.

\*S.S.R. – solid-state reaction – the salt solutions were mixed together, evaporated to dryness on a water bath and then calcined at 200°C.

### 2.3.5: Effect of SO<sub>4</sub><sup>2-</sup> on manganese oxide formation with Mn(II) nitrate precursor

That sulphate ion leads to the formation of OMS-2 or α-phase is also confirmed by thermal decomposition studies of Mn(II) nitrate. It is well known that Mn(II) nitrate gives pure pyrolusite or β-phase. When decomposition was carried out in presence of K<sub>2</sub>SO<sub>4</sub> or Na<sub>2</sub>SO<sub>4</sub>, distinct α-characteristic peaks appear in the XRD pattern as shown in Figure 2.4.

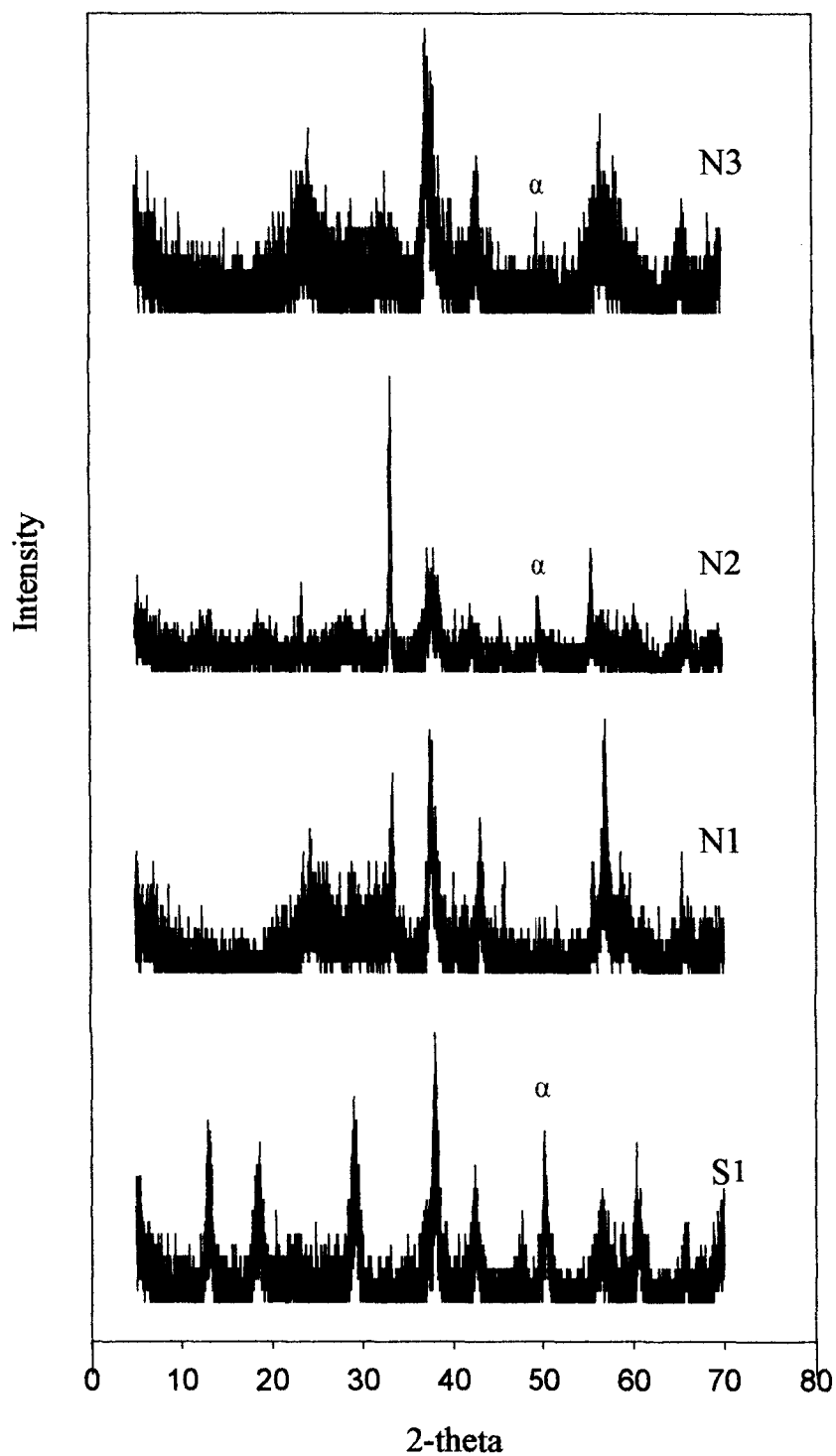


**Figure 2.4:** XRD profiles of OMS-2 by reflux method (S1); Mn(II) nitrate decomposed at 200 °C (N1); Mn(II) salt +  $K_2SO_4$  in 1:1 ratio (N2); Mn(II) salt +  $Na_2SO_4$  in ratio 1:1 (N3)

## 2.4 Conclusions:

- This is the first report, which shows the formation of OMS-2 in the presence of  $\text{SO}_4^{2-}$  ion without the need for  $\text{K}^+$ ,  $\text{Pb}^{2+}$  or  $\text{Ba}^{2+}$  ions.
- Although pH has been considered as a factor which controls the OMS-2 phase formation [23], it cannot be a determining factor in this case since the synthesis is carried out in a strongly acidic medium.
- Thus, under the present conditions, the investigation confirms that
  - (i)  $\text{SO}_4^{2-}$  ion has a crucial role in OMS-2 phase formation,
  - (ii) OMS-2 could be synthesized without the presence of  $\text{K}^+$  ion,
  - (iii) OMS-2 could be formed in a facile manner by use of chlorate as oxidizing agent in place of permanganate and
  - (iv) OMS-2 samples could be successfully characterized both by IR and XRD techniques.

*CHAPTER – III*

*OXIDATION OF BENZYL ALCOHOL*

### 3.1 Introduction

Catalytic partial oxidation of alcohols to produce aldehydes or ketones is an industrially important process and a fundamental reaction in organic synthesis. Carbonyl compounds such as ketones and aldehydes are the precursors for many drugs, vitamins and fragrances and are also important intermediates for many complex syntheses [126,127]. Most of these reactions, however, use toxic, corrosive, and expensive oxidants, stringent conditions such as high temperature or pressure, and strong mineral acids [128,129]. Alcohol oxidation is traditionally carried out in liquid phase by stoichiometric oxidants such as toxic and expensive chromium (VI), which produces a lot of heavy metal waste, thus posing environmental problems [126-127]. Hence replacing them with heterogeneous catalytic oxidation using clean and atom-efficient oxidants such as molecular oxygen is a definite need, as well as an important goal of the “green chemistry” concept.

Despite the increasing demand for more efficient catalytic processes, few efficient catalytic oxidations have been reported for the oxidation of alcohols to carbonyl compounds. However, there have been a few interesting reports which employ aerobic oxidation of alcohols that use copper [130,131], palladium [132] and ruthenium compounds [133,134]. Aerobic oxidation of alcohols using Pd and Pt/C has also been reported but it is limited to water-soluble alcohols [135]. In industrial chemistry, heterogeneous catalyst systems have some advantages over homogeneous systems, such as easy recyclability and separability, however heterogeneous catalyst systems often lack good conversion and selectivity. Therefore an important challenge is to develop active and selective heterogeneous systems for this type of reaction.

Benzyl alcohol and its derivatives find extensive use in perfume industry. However benzyl alcohol gives different oxidation products over various catalysts,

both homogenous and heterogeneous. Various catalytic systems have been investigated both for liquid phase and vapour phase oxidation of benzyl alcohol. Viswanathan *et al.* [136-139] have investigated vapour phase oxidation of benzyl alcohol, both in presence and absence of molecular oxygen over perovskite oxides. They observed formation of benzaldehyde and toluene in absence of oxygen, while in presence of oxygen; some benzoic acid and benzyl benzoate were also detected. Up to 50-60% catalytic activity at  $\sim 400^{\circ}\text{C}$  has been reported with high selectivity to benzaldehyde. Catalytic activity was found to be inversely proportional to the M—O bond length. Bond strength and role of lattice oxygen have been explained on the basis of Langmuir-Hinshelwood mechanism. Similar results were also obtained over copper chromite catalyst [140]. Pillai *et al.* [141] have also studied selective photocatalytic oxidation of benzyl alcohol to benzaldehyde using immobilized  $\text{TiO}_2$  films as catalyst and have reported 35% conversion and  $> 95\%$  selectivity.

Increased catalytic activity for oxidation of benzyl alcohol has been recently reported over ruthenium oxo complex phase transfer catalysts with oxychloride ( $\text{OCl}$ ) as co-oxidant [142,143] or  $\text{H}_2\text{O}_2$  [144] and over Pd (II)-hydrotalcite using molecular oxygen [145]. Ebitani *et al.* [146] report over 90% conversion over ruthenium-based heterogeneous catalyst system, Ru-Mn-Fe-Cu-O, also using molecular oxygen as oxidant and water instead of organic solvent and surfactants in an attempt towards a greener process.

Mixed metal oxides are widely used as catalysts for partial or total oxidation of various substrates [147], electrode materials for electrochemical and electrocatalytic applications [148] and as solid-state chemical sensors for reductive gases [149] the properties of which are usually dominated by their capability and propensity of cycling between different valence states of relevant cations and mobility



of lattice oxygen ions. These factors are determined intrinsically by the binding situation between the local metal and oxygen atoms, viz. the M—O bond. Knowledge about the behaviour of different M—O bonding in various applications is very informative. In oxidative catalysis, it is generally accepted that surface O<sup>-</sup> or O<sup>2-</sup> is responsible for the total oxidation of hydrocarbons [150]; however, lattice oxygen ions are much more selective in partial oxidation reaction [151]. In view of the presence of several inequivalent M—O bonds in a mixed metal oxide, the M—O bonds have considerable variation in strength, leading to catalytic selectivity.

The present investigation reports liquid phase oxidation of benzyl alcohol using air over pure and various cation-doped OMS-2 catalysts. Suib *et al.* have developed simple synthetic procedures to obtain OMS materials and studied their various properties and applications [23,32-34,40-59]. It is well known that the efficiency of oxidation of benzyl alcohol depends on the crystal phase of manganese dioxide used. The oxidation of benzylic alcohols with manganese dioxides generally stops at the carbonyl stage but further oxidation can occur in hot aqueous solutions or in neutral media.

On the basis of isotope exchange studies using  $\alpha, \alpha$ -dideuteriobenzyl alcohol, Suib *et al.* [23] have shown that the rate determining step during catalytic oxidation of benzyl alcohol over active manganese dioxide catalysts, is due to C—H bond cleavage. They suggested on the basis of <sup>18</sup>O<sub>2</sub> isotope labeling experiments that the catalytic activity of OMS materials should be inversely related to Mn—O bond strengths. They further observed that the active OMS-2 material exchanged <sup>16</sup>O of the lattice with <sup>18</sup>O more easily.

### 3.2 Effect of Al on catalytic activity of OMS-2

#### 3.2.1 Catalyst Synthesis:

The synthesis of sample (S1) has already been discussed in the previous section 2.2.1 by the  $\text{KMnO}_4$  oxidation of  $\text{MnSO}_4$  in nitric acid medium. Henceforth it will be called as S. The Al-doped OMS-2 (sample SA) was prepared by adding 0.015 M  $\text{Al}_2(\text{SO}_4)_3 \cdot 16\text{H}_2\text{O}$  initially, before the dropwise addition of  $\text{KMnO}_4$  during the synthesis of OMS-2 such that the amount of final Al in the manganese oxide was around 2.8 %.

In order to arrive at a correlation of the activities of the OMS-2 compounds, a standard pyrolusite sample (sample P) was synthesized by thermal decomposition of Mn (II) nitrate solution at 180 °C in an evaporating dish. The mass was allowed to cool to room temperature and extracted with deionised-distilled water, filtered, washed, powdered and dried in the oven at 110 °C.

#### 3.2.2 Characterization

##### (a) X-ray diffraction analysis:

The Al-doped OMS-2 shows a similar XRD pattern as the pure undoped sample as can be seen in Figure 3.1. There were no significant changes in the XRD peak positions suggesting similar phases. Also no additional peaks have appeared, indicating that the aluminium centers are well dispersed and that a separate segregated alumina phase is absent. However there seems to be a slight narrowing of the peak widths. This indicates a small increase in particle size and the presence of small structural distortions, which could be due to the minimal difference in size between  $\text{Mn}^{4+}$  (67 pm) and  $\text{Al}^{3+}$  (67.5 pm) ions [152].

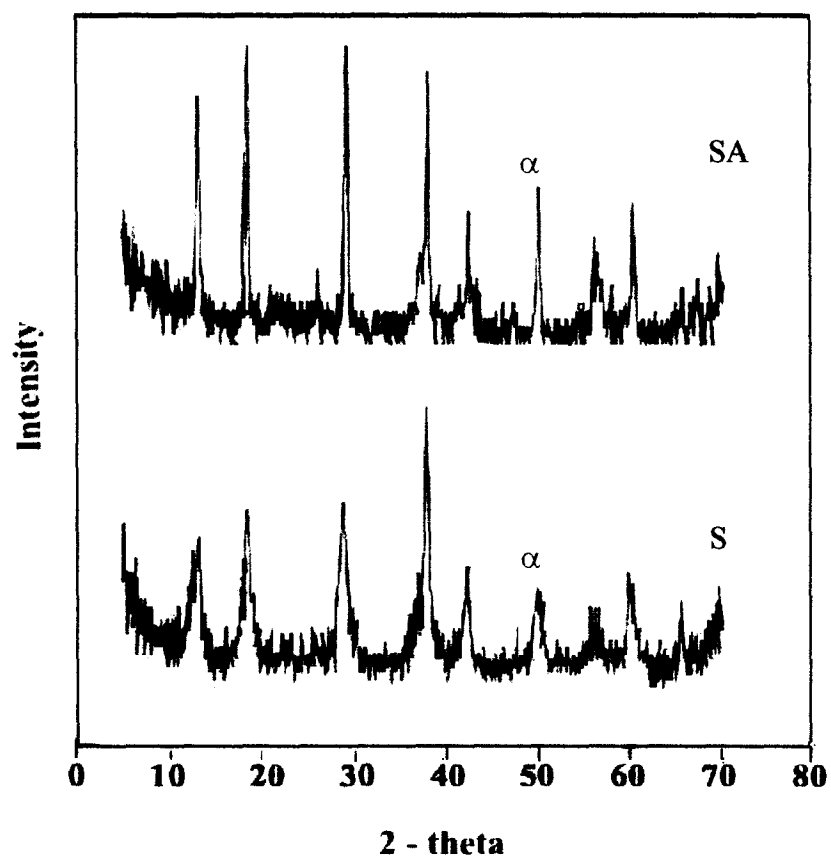


**Figure 3.1:** XRD profiles of pure OMS-2 sample, S and Al<sup>3+</sup> containing OMS-2 sample, SA

**Table 3.1:** X-Ray diffraction data of the OMS-2 catalysts

S		SA		JCPDS 20-908	
d	I/I <sub>0</sub>	d	I/I <sub>0</sub>	d	I/I <sub>0</sub>
6.7786	84	6.5057	49	6.9	90
4.8572	68	4.7163	48	4.9	80
3.1186	94	3.0406	78	3.1	80
2.3811	100	2.3482	100	2.39	100
2.1373	39	2.1206	44	2.25	60
1.8227	35	1.8025	40	1.80	40
1.6274	35	1.6209	49	1.63	60
1.5406	45	1.5234	56	1.54	60
1.4210	-	1.4134	25	1.35	50
a = b = 9.7584 Å c = 2.8463 Å		a = b = 9.5683 Å c = 2.9176 Å		a = b = 9.84 Å c = 2.86 Å	

The  $d$  and  $I/I_0$  and the lattice parameters calculated on the basis of a tetragonal unit cell are given in Table 3.1. These are in agreement with the literature values and also compare well with JCPDS file 20-908 [116] for cryptomelane  $\text{KMn}_8\text{O}_{16}$ . The peak at  $d \sim 1.80 \text{ \AA}$ , which is a characteristic of cryptomelane OMS-2, is seen to have a slightly higher relative intensity in Al-OMS-2 ( $I/I_0 = 40 \%$ ) than in pure OMS-2 ( $I/I_0 \sim 35 \%$ ). It is also seen from Table 3.1 that the lattice parameter ‘ $c$ ’ for the  $\text{Al}^{3+}$  doped sample is significantly higher ( $\sim 2.91 \text{ \AA}$ ) as compared to the other cryptomelane sample (S) having an average value of  $\sim 2.85 \text{ \AA}$ . This suggests enhanced Mn—Mn internuclear distance along the  $c$  direction, implying slight lattice dilation following  $\text{Al}^{3+}$  doping. It could probably be due to lattice substitution of  $\text{Al}^{3+}$  in place of  $\text{Mn}^{4+}$ , their ionic radii in octahedral environments being 67.5 pm and 67.0 pm respectively [152].

(b) Infra-red analysis:

The FTIR profile of OMS-2 shows the characteristic band at  $\sim 700 \text{ cm}^{-1}$  as can be seen in Figure 3.2. This once again proves that the Al-doped sample is of the OMS-2 type. Such an absorption is generally not seen in case of pyrolusite and nsutite forms of manganese oxides [125] and is also evident in the figure in case of the synthesized pyrolusite. A strong absorption band in the range  $3200\text{--}3600 \text{ cm}^{-1}$  and another at  $1620 \text{ cm}^{-1}$  are normally due to the OH stretching and OH bending modes of vibration respectively. Such bands are seen in case of the  $\alpha\text{-MnO}_2$  compounds but absent in sample P as it does not have any structural water or MnOOH groups. It has been shown earlier [124] that Mn(IV) oxides can be represented by the general formula as:



where 'n' is a measure of the degree of oxidation of Mn in the sample and 'm' is the number of neutral water molecules in the crystal lattice. Thus depending on the amount of MnOOH in the sample, strength of the OH absorption bands will vary.

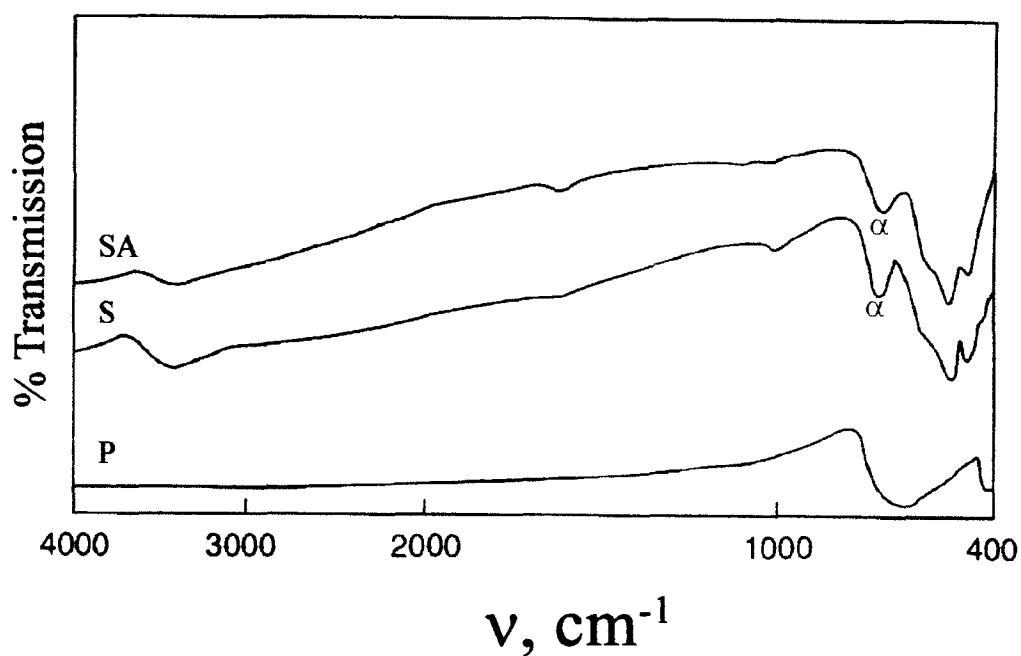


**Figure 3.2:** Infra-Red profiles of stoichiometric manganese dioxide (Pyrolusite), P; pure OMS-2 sample, S and Al<sup>3+</sup> - doped OMS-2, SA

*(c) Field Emission Scanning Electron Microscopy (FESEM):*

The pure OMS-2 sample was analyzed by the FESEM technique on a Hitachi FESEM, S-900 instrument, at a voltage of 10 kV. The sample was heated at 120 °C prior to scanning and then coated with platinum for 6 seconds to prevent charging and to protect the material from thermal damage by the electron beam. The morphology of the sample is as seen in Figure 3.3.

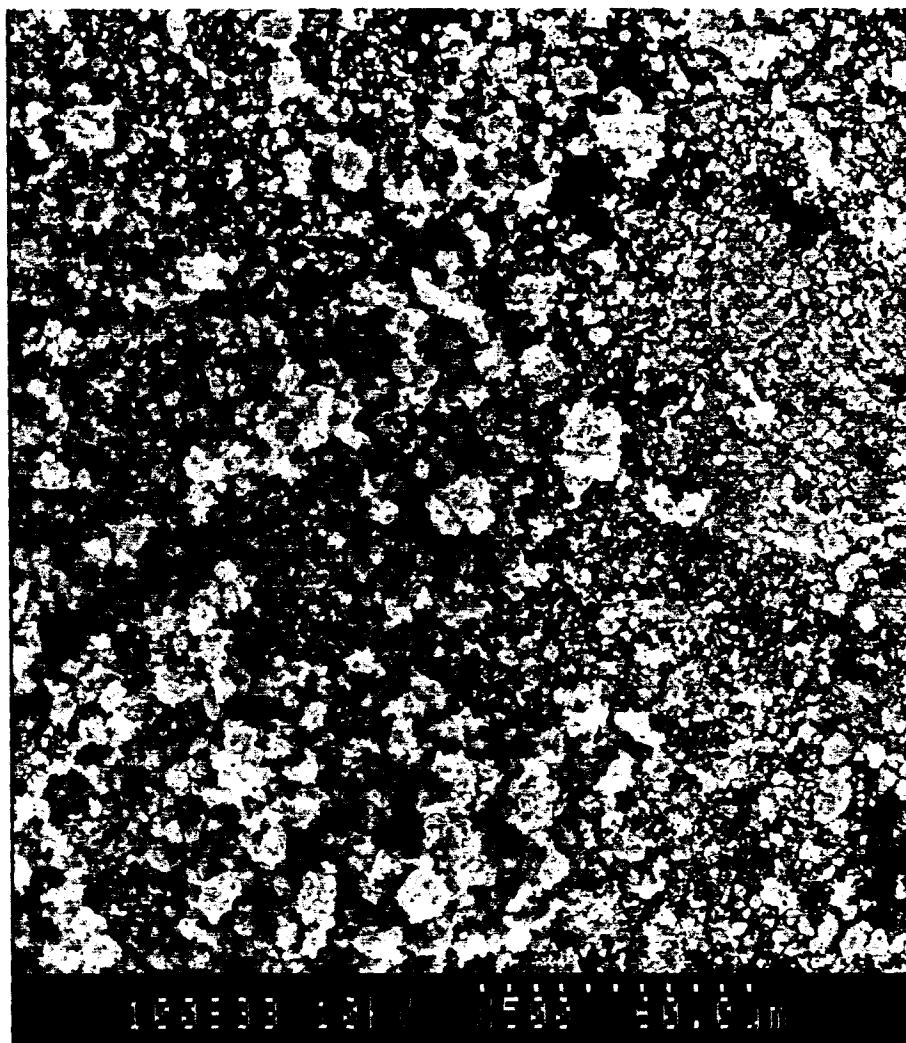


**Figure 3.3:** FESEM micrograph of pure OMS-2 (S) sample

*(d) Surface area measurements:*

Surface areas of the samples were determined by Nitrogen adsorption/desorption at  $-196\text{ }^{\circ}\text{C}$  attained by using liquid nitrogen. The instrument used for the purpose was a SMART SORB 91 surface area analyzer. All samples were pre-dried in the oven at  $120\text{ }^{\circ}\text{C}$  for 1 hour and then flushed with Nitrogen for another hour. The surface area was calculated using the BET method from the adsorption and desorption curves obtained. The  $\alpha\text{-MnO}_2$  samples (doped as well as undoped) showed high surface area and compared well with literature [23]. The doping of the OMS-2

material also showed an increase in surface area, which could be due to the substitution of Al, which has a different ionic size compared to that of Mn. On the contrary, the synthesized pyrolusite material showed comparatively lesser surface area as expected.

**Table 3.2:** BET surface areas of the samples

Catalyst	BET (m <sup>2</sup> /g)
S	77
SA	84.2
P	7

### 3.2.3 Oxidation of benzyl alcohol

The reaction was carried out as per a procedure given in literature [153]. It was a typical batch reaction process, using a round bottom flask for the process and an oil bath for supplying the required amount of heat for gentle refluxing. The reaction conditions employed were as follows:

Weight of catalyst	= 0.5 g
Temperature of catalyst activation	= 120 °C, 1 h
Amount of Benzyl alcohol	= 1 mmol
Volume of n-Hexane	= 10 ml
Time of refluxing	= 1 hr

The reaction mixture was then cooled and centrifuged, the supernatant was collected in a clean hard glass test tube and the solvent was evaporated on a water-bath. The reaction product being higher boiling liquid remained behind and was then



analyzed on Chemito 8610 Gas Chromatograph instrument using an SE 30 column and a flame ionization detector (FID).

**Table 3.3:** % Conversion of Benzyl alcohol over the various catalysts

Sample code	% Conversion
S	43
SA	58
P	2

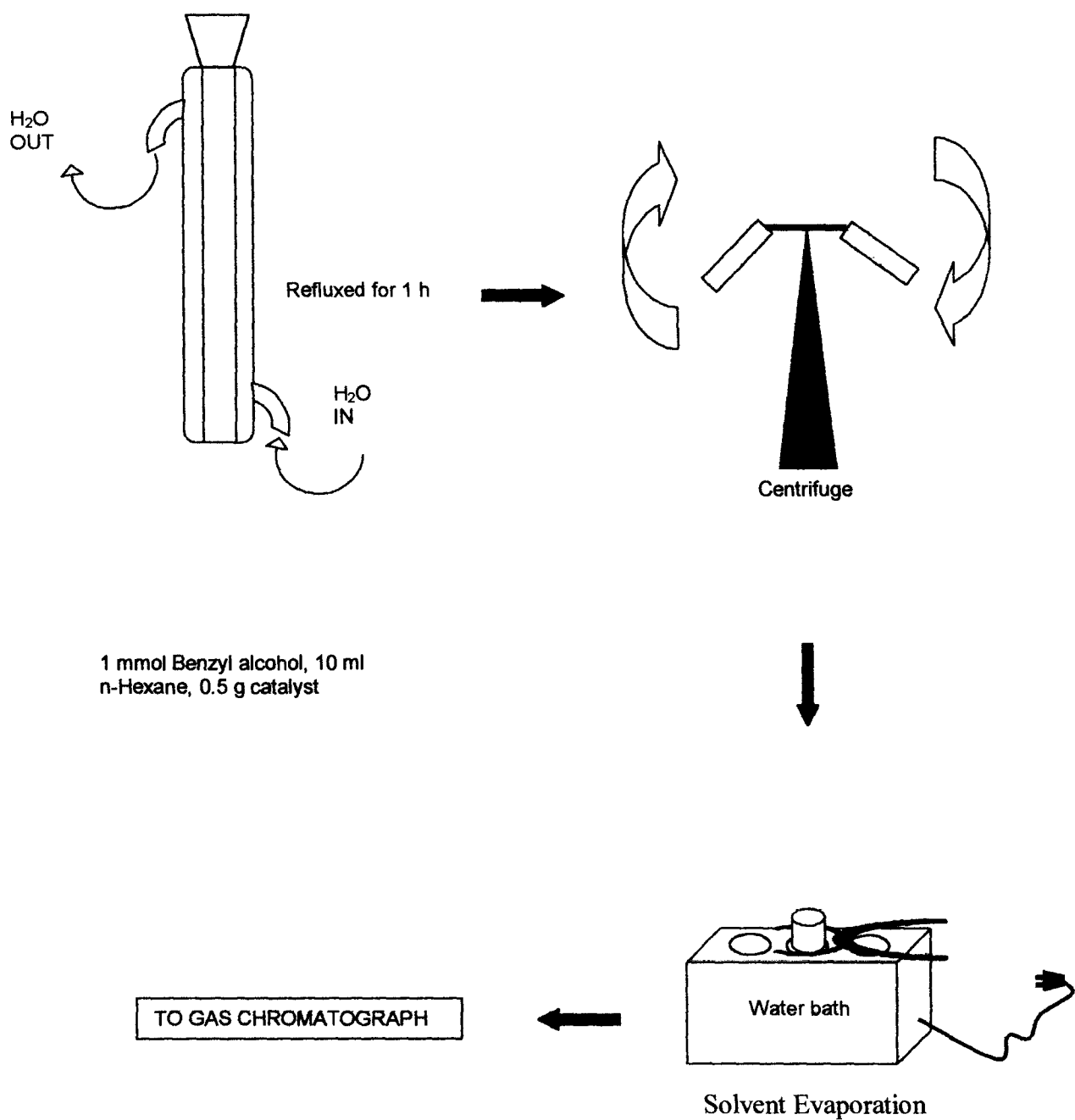


**Figure 3.4:** Scheme for the oxidation of Benzyl alcohol

### 3.2.4 Thermal analysis

It is known that oxidation of benzyl alcohol follows Mars-van-Krevelen mechanism which involves participation of lattice oxygen during oxidation of volatile organic compounds [154-156]. In such a case, one could hypothesize the higher catalytic activity to be associated with the extent of participation of lattice oxygen. In order to confirm this hypothesis, thermogravimetric (TG/DSC) studies were carried out in air. 10 mg of the sample was loaded in a small clean and dry alumina crucible having a lid with an opening, which serves as an outlet for the evolved gases. The NETZCH STA 409 PC TG/DSC instrument was used for the purpose. The analysis was carried out at a heating rate of  $10\text{ }^{\circ}\text{C min}^{-1}$  within a temperature range of 30 – 1200  $^{\circ}\text{C}$ .

As can be inferred from the Figure 3.5, the OMS-2 compounds show a clear weight loss of about 4% up to around 150  $^{\circ}\text{C}$ , which is due to loss of structural water and some physisorbed water.

Mn (IV) oxides are known to lose

- (i) Bound water and some physisorbed oxygen up to 300 $^{\circ}\text{C}$  [41] and thereafter
- (ii) Chemisorbed oxygen and some lattice oxygen up to the temperature of about 500 $^{\circ}\text{C}$ .
- (iii) The oxygen loss beyond 500 $^{\circ}\text{C}$  till the decomposition temperature is more reflective of only lattice oxygen loss [41, 125,156].
- (iv) At around 600 $^{\circ}\text{C}$ , thermal decomposition of the type  $\text{MnO}_2 \rightarrow \text{Mn}_2\text{O}_3$  occurs [41].

In the present case, this decomposition occurs at  $\sim 600^{\circ}\text{C}$ . Table 3.4 gives various TG weight losses in the temperature range from 120-570 $^{\circ}\text{C}$ ; since beyond this the OMS-2 structure is not stable. The weight loss between 500-570 $^{\circ}\text{C}$  is purely lattice

oxygen loss. The catalytically active Al-OMS-2 sample shows greater oxygen loss in all the three temperature intervals. Therefore, the catalytic activity can be directly related to the rate of oxygen evolution as evident from the TG analysis. We therefore propose the mechanism of oxidation of benzyl alcohol, involving anion vacancy generation through loss of lattice oxygen.

**Table 3.4:** Percent weight losses of the samples in three different temperature intervals

Catalyst	Thermal analysis		
	% O <sub>2</sub> loss		
	120-300 (°C)	300-500 (°C)	500-570 (°C)
S	4.45	3.69	2.04
SA	6.15	5.44	2.8
P	2.8	3.29	1.2

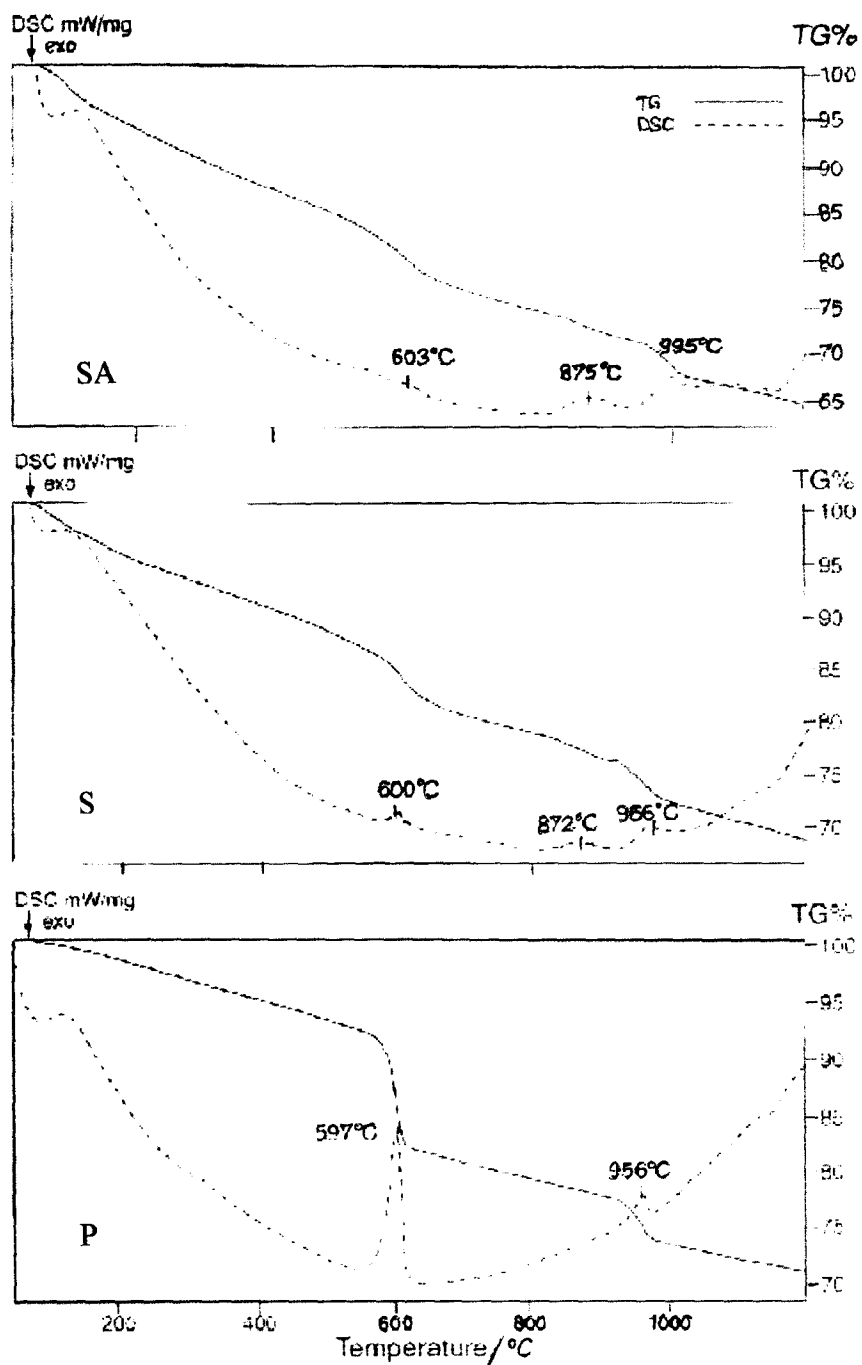


**Figure 3.5:** TG/DSC profiles of stoichiometric manganese dioxide (Pyrolusite), P; pure OMS-2 sample, S and Al<sup>3+</sup> - doped OMS-2, SA

### 3.2.5 $H^+$ ion exchange capacity:

Catalytic activity studies carried out in the form of  $H^+$  ion exchange capacity in DMF medium expressed as volumes of thiosulphate consumed,  $V. S_2O_3^{2-}$  revealed that ion exchange capacity increases with increase in catalytic activity. The  $H^+$  ion exchange capacity depends on the presence of acidic 'OH' groups attached to  $Mn^{3+}$  in the host Mn (IV) oxide lattice. The lattice dilation associated with the lengthening of Mn—O bond may have enhanced the proton exchangeability of the dioxides. The mobile proton of the MnOOH group could then hop on to the neighbouring  $Mn^{4+}$  sites to generate new  $Mn^{3+}$  centers;  $H^+ + MnO_2 \rightleftharpoons MnOOH$ . The catalytic activity may therefore, be directly related to the presence of active  $Mn^{4+}/Mn^{3+}$  redox couple, which may be responsible for the acid centers in the catalysts.

### 3.2.6 Temperature Programmed Desorption (TPD) studies

Manganese oxides are known to be solid oxides having Brønsted and/or Lewis acidity [154]. The nature and strength of acid sites can be probed by adsorption of ammonia followed by its temperature programmed desorption. Typical TPD measurements were carried out in a continuous flow vertical muffle furnace using ammonia as the probe molecule for estimation of acidity of the catalysts. 0.5 g of the catalyst was packed in the center of a glass column using glass wool as a bed. On either side of the catalyst, the tube was filled with ceramic beads, which helped in pre-heating the column. The catalysts were activated at 120 °C for about 1 hour with constant flow of nitrogen. The catalyst was allowed to cool to room temperature and then ammonia vapours were allowed to pass over the catalyst bed for 45 minutes at a flow rate of 50 ml/min. Using a temperature controller, the sample was heated at a rate of 5 degrees per minute. This caused desorption of the adsorbed ammonia, which was collected in a known volume of 0.03 M HCl and back titrated against standard

NaOH using phenolphthalein indicator. Thus the amount of desorbed gas was quantitatively estimated at various temperatures, which gave a fair measure of the acidity and is expressed in millimoles per gram. Figure 3.6 shows the typical TPD profiles of the samples.

Suib *et al.* [154] in fact suggested presence of such strong Lewis acid centers in such materials. It is also seen from Table 3.5 and the TPD profiles in Figure 3.6, that the  $\text{Al}^{3+}$ -doped sample has higher concentration of acidic centers, which are also stronger than in the undoped sample as well as in the pyrolusite.

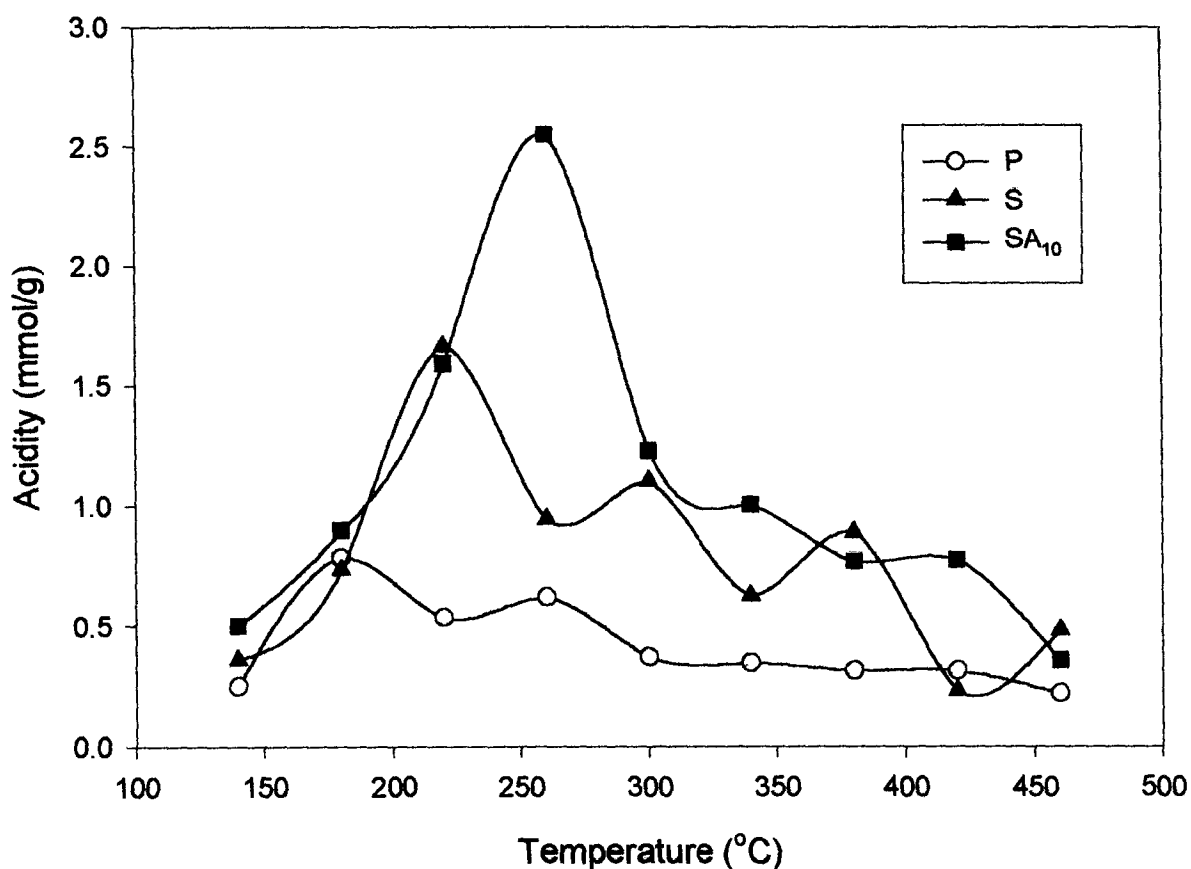


**Figure 3.6:** TPD profiles of stoichiometric manganese dioxide (Pyrolusite), P; pure OMS-2 sample, S and  $\text{Al}^{3+}$ -doped OMS-2, SA

### 3.2.7 Chemical analysis

Chemical analysis of the OMS-2 samples revealed that the chemical composition was  $\text{MnO}_{1.86}$  corresponding to average oxidation state of manganese 3.72. These values are close to the values reported by DeGuzman *et al.* for materials obtained using different precursors [23]. In comparison, the pyrolusite sample prepared by thermal decomposition of Mn (II) nitrate showed stoichiometric composition of  $\text{MnO}_2$  wherein the oxidation state of manganese is +4.

Table 3.5 gives catalytic activity of the samples in relation to their other physico-chemical characteristics, viz, surface area,  $\text{O}_2$  loss by TG, acidity levels and volumes of thiosulphate (as a measure of  $\text{H}^+$  ion exchange capacity of the OMS-2). The catalytic activity is expressed in terms of % conversion of benzyl alcohol to benzaldehyde. Al-OMS-2 shows significantly higher conversion (~58 %) as compared to pure OMS-2 (~ 43 %). In comparison, the stoichiometric pyrolusite sample is practically inactive for the reaction.

**Table 3.5:** Catalytic activity of the Mn(IV) oxides in relation to their physicochemical characteristics

Catalyst	(1-x) in $\text{MnO}_{(1-x)}$	Crystal phase	Thermal analysis					Total Acidity (mmolg <sup>-1</sup> )	V $\text{S}_2\text{O}_3^{2-}$ (ml)	% Conversion of benzyl alcohol
			BET (m <sup>2</sup> /g)	% $\text{O}_2$ loss 120-300 (°C)	300-500 (°C)	500-570 (°C)	Decomp. Temp. (°C)			
S	1.86	Cryptomelane (OMS-2)	77	4.45	3.69	2.04	600	1.66	3.3	43
SA	1.86	Cryptomelane (OMS-2)	84.2	6.15	5.44	2.8	600	2.55	5.9	58
P	2	Pyrolusite	7	2.8	3.29	1.2	597	0.78	0	2



### 3.3 Effect of Fe<sup>3+</sup> and Ti<sup>4+</sup> on catalytic activity of OMS-2

#### 3.3.1 Catalyst synthesis:

The cation doped manganese oxide samples were prepared by permanganate oxidation of Mn(II) sulphate in nitric acid medium. Three different Fe<sup>3+</sup> doped manganese oxides were thus prepared by dissolving calculated quantities of Fe (III) nitrate (AR grade, Loba Chemie, India) in the acidified Mn(II) sulphate solution followed by treatment with KMnO<sub>4</sub> and reflux. The resultant samples are labeled as Sf1 (0.5 % Fe), Sf2 (5 % Fe) and Sf3 (15 % Fe) respectively.

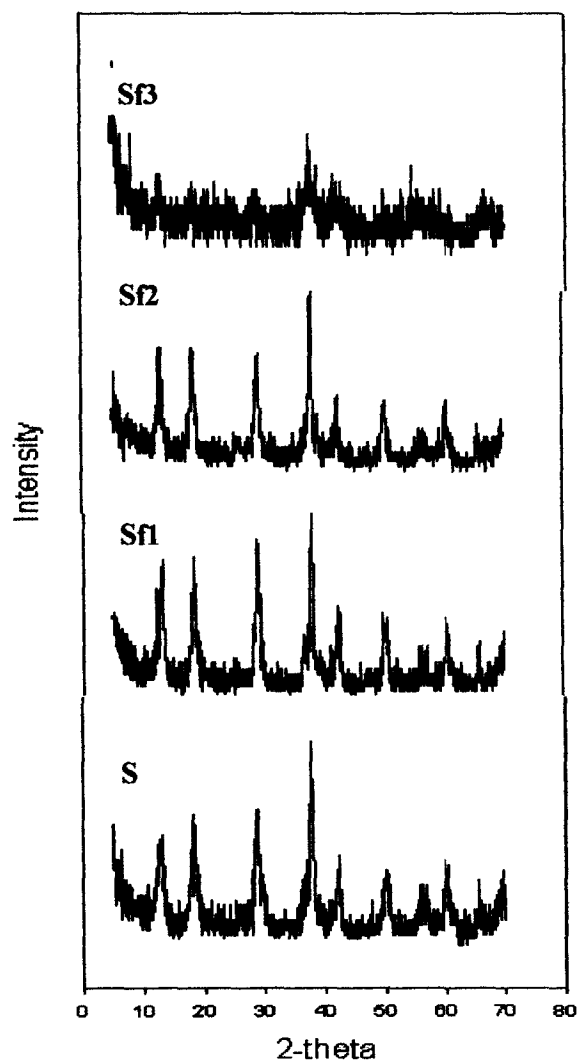
Similarly, three different samples of Ti<sup>4+</sup> modified OMS-2 were also synthesized using appropriate quantities of violet coloured 15% TiCl<sub>3</sub> solution in HCl (AR grade, Loba Chemie, India). Thus, the samples obtained were; ST5 (5% Ti), ST10 (10% Ti) and ST20 (20% Ti).

#### 3.3.2 Catalyst characterization

Figure 3.7 illustrates the relative XRD patterns of the Fe modified manganese oxides and the XRD data  $d$  and  $I/I_0$ , Table 3.6, conforms to the JCPDS 20 – 908 file [116]. Thus the synthesized samples were confirmed to have formed the OMS-2 phase. Modifying the sample with Fe did not affect the phase formation, though the XRD pattern of the OMS-2 containing higher amount of Fe (Sf3) seemed more or less diffuse which could be due to the structural distortion and loss of crystallinity induced following the excess substitution of Fe into the structure. However, no extra peaks related to Fe<sub>2</sub>O<sub>3</sub> were observed, therefore ruling out the possibility of such a separate phase in the samples.

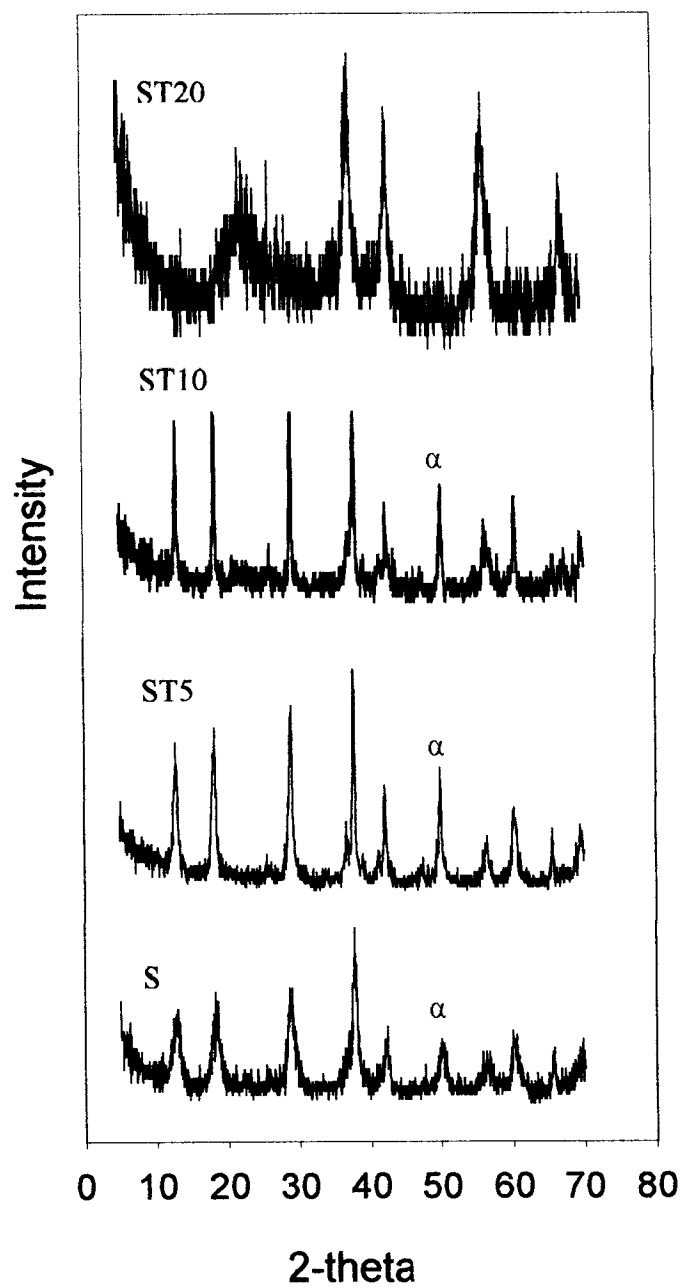
**Table 3.6:** X-ray diffraction data of Fe OMS-2 samples

S		Sf1		Sf2		Sf3	
d	I/I <sub>0</sub>	d	I/I <sub>0</sub>	d	I/I <sub>0</sub>	d	I/I <sub>0</sub>
6.91	59	6.76	90	6.76	90	6.92	45
4.84	72	4.83	70	4.91	72	4.81	28
3.08	87	3.11	95	3.08	78	3.04	43
2.38	100	2.39	100	2.37	100	2.39	100
2.14	36	2.12	40	2.15	60	2.15	50
1.91	15	1.91	12	1.93	10	1.81	34
1.83	40	1.83	31	1.83	44	1.67	32
1.63	33	1.54	28	1.63	24	-	-
1.52	39	1.43	14	1.54	56	1.40	32
a = b = 9.75 Å c = 2.85 Å		a = b = 9.75 Å c = 2.89 Å		a = b = 9.62 Å c = 2.91 Å		a = b = 9.89 Å c = 2.75 Å	



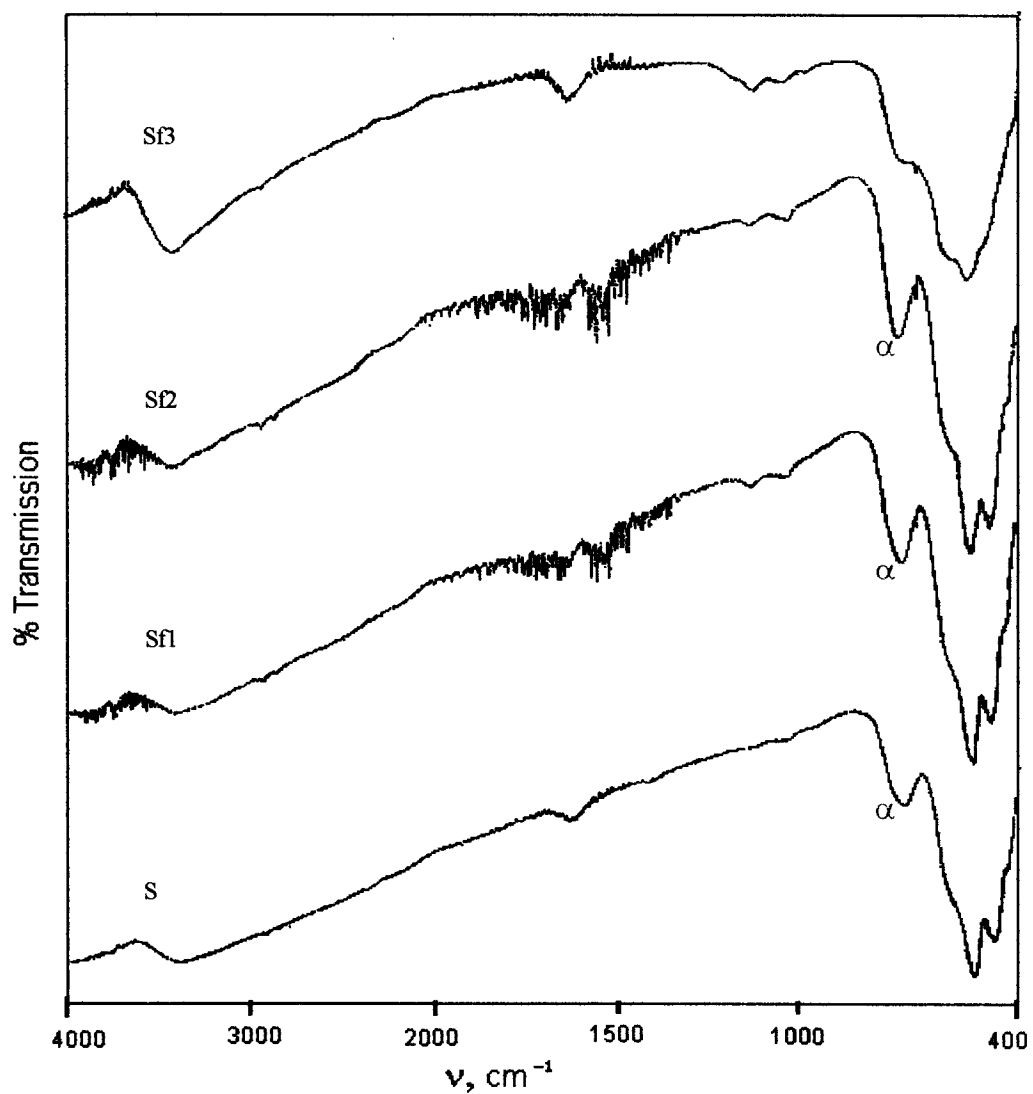
**Figure 3.7:** XRD profiles of pure OMS-2, S; 0.5% Fe modified catalyst, Sf1; 5% Fe modified catalyst, Sf2 and 15% Fe modified catalyst, Sf3

Figure 3.8 shows XRD pattern of  $Ti^{4+}$  modified OMS-2 catalysts. As can be seen in the profile, modifying OMS-2 with Ti was a success upto a certain limit with no separate titania phase seen. After about 10 % Ti, the material seemed to show signs of saturation. The sample with highest amount of Ti no longer shows the OMS-2 pattern. Instead it has been converted to the rutile phase. Once again cationic size plays an important role in deciding the formation of the OMS-2 phase.



**Figure 3.8:** XRD profiles of pure OMS-2, S; 5% Ti modified catalyst, ST5; 10% Ti modified catalyst, ST10 and 20% Ti modified catalyst, ST20

IR spectroscopy (See Figure 3.9) supported the data as the characteristic OMS-2 absorption was clearly seen at  $700\text{ cm}^{-1}$  in case of pure OMS-2 (S) and the two other samples containing lower amounts of Fe viz. Sf1 (0.5% Fe) and Sf2 (5% Fe), while it disappears in the case of Sf3 (15% Fe).



**Figure 3.9:** Infra-red profiles of pure OMS-2, S; 0.5% Fe modified catalyst, Sf1; 5% Fe modified catalyst, Sf2 and 15% Fe modified catalyst, Sf3

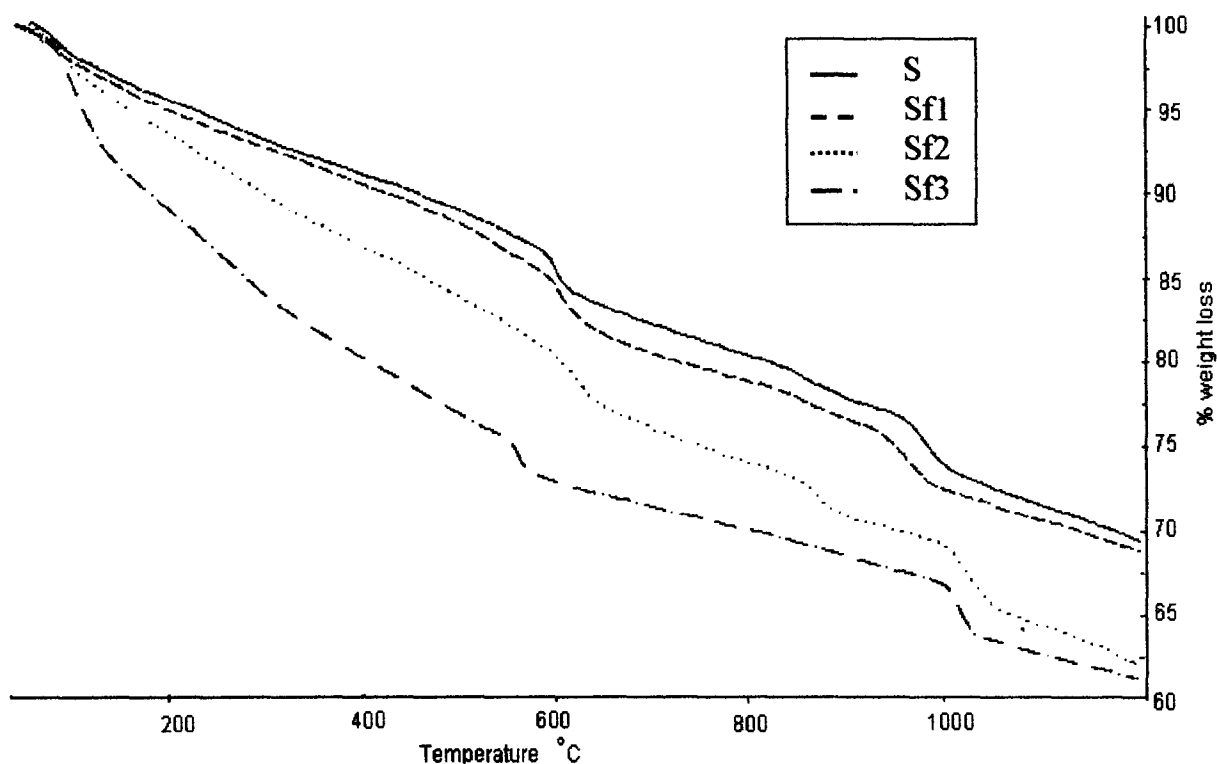


**Figure 3.10:** Thermogravimetric patterns of the various Fe modified catalysts

Table 3.7 gives various TG weight losses of Fe modified OMS-2 catalysts in the temperature range from 120 – 570 °C since beyond this the OMS-2 structure will not be stable.

**Table 3.7:** Thermogravimetric weight losses of Fe<sup>3+</sup> modified manganese oxides

Code	Thermal analysis		
	% Wt. loss		
	120-300 (°C)	300-500 (°C)	500-570 (°C)
S	4.45	3.69	2.04
Sf1	4.56	4.05	2.1
Sf2	5.16	4.68	2.9
Sf3	9.52	6.91	3.25

The TG studies carried out on the samples showed that in all the temperature intervals, weight loss in each of the samples increases with the increase in the amount of Fe in the samples (Figure 3.10). Therefore the sample containing highest amount of Fe shows higher loss as compared to the others in the series. Corresponding increase in conversion of benzyl alcohol to benzaldehyde was seen down the series with increasing amounts of Fe content in the samples. This could be due to the substitution of larger sized  $\text{Fe}^{3+}$  ion ( $\text{Fe}^{3+}$  ionic radius in octahedral environments is 69 pm which is larger in comparison to 67 pm for Mn in similar environments [152]) in place of Mn in the lattice structure thus causing structural distortion leading to the increase in Mn—O bond length. This increased bond length also implies lesser bond strength, which in turn facilitates the loss of oxygen during the catalytic oxidation process. Thus the higher catalytic activity could be correlated with the ease of oxygen loss from the lattice during the oxidation process.

Table 3.8 gives catalytic activity of the samples in relation to the various physico-chemical characteristics. Catalytic activity is expressed in terms of % conversion of benzyl alcohol to benzaldehyde. It is seen that all the samples are active for the oxidation of benzyl alcohol. Although the samples showed increase in activity with increasing amount of Ti, the effect was not as pronounced as in the case of Fe modified OMS-2.

Besides, active manganese dioxides are known to have Mn in lower oxidation states viz. +3 and +2 states in small quantities besides the  $\text{Mn}^{+4}$  [35]. These results could be confirmed by  $\text{H}^+$  ion exchange experiments in aprotic medium, given as volumes of thiosulphate in Table 3.8. The  $\text{H}^+$  ion exchange capacity is directly related to the presence of acidic 'OH' groups attached to  $\text{Mn}^{3+}$  in the host Mn (IV) oxide lattice [141,142]. These results showed increase in titre values, which correspond to



higher number of active hydroxyls in the samples modified with Fe. This shows the presence of  $Mn^{+3}/Mn^{+4}$  redox couple. Similar is the case with Ti modified samples.

**Table 3.8:** Physico-chemical characteristics of various metal cation modified manganese oxides

Code	% MnO <sub>2</sub>	%Mn	Crystal phase	Thermal analysis			BET (m <sup>2</sup> /g)	V S <sub>2</sub> O <sub>3</sub> <sup>2-</sup> (ml)	% Conversion
				% O <sub>2</sub> loss					
				120-300 (°C)	300-500 (°C)	500-570 (°C)			
S	86	61.81	OMS-2	4.45	3.69	2.04	77	3.3	43
Sf1	80.9	62.9	OMS-2	4.56	4.05	2.1	73	5.7	45
Sf2	71.2	60.4	OMS-2	5.16	4.68	2.9	81	6.2	49
Sf3	68.1	46.7	-	9.52	6.91	3.25	186	9.5	70
ST5	78.4	57.7	OMS-2	2.97	2.7	1.00	69	6.2	38
ST10	75	54.9	OMS-2	5.36	5.42	2.41	78	6.3	48
ST20	68.6	49.5	Nsutite	6.18	5.89	3.14	150	6.5	53

Thus from thermogravimetric data (% weight loss studies) and the % conversion of benzyl alcohol to benzaldehyde, we could arrive at a conclusion that the higher the weight loss higher was the conversion. This confirms the theories put forth [133] that the oxidation ability of the catalyst depends on lattice oxygen participation. Thus a correlation was observed between the TG weight losses (in the temperature interval 300 – 570 °C) and catalytic activity of the samples, which is illustrated in Figure 3.11. An almost straight line is observed for the given set of Fe modified catalysts with a positive slope implying, improved catalytic activity depends on ease of loss of oxygen.

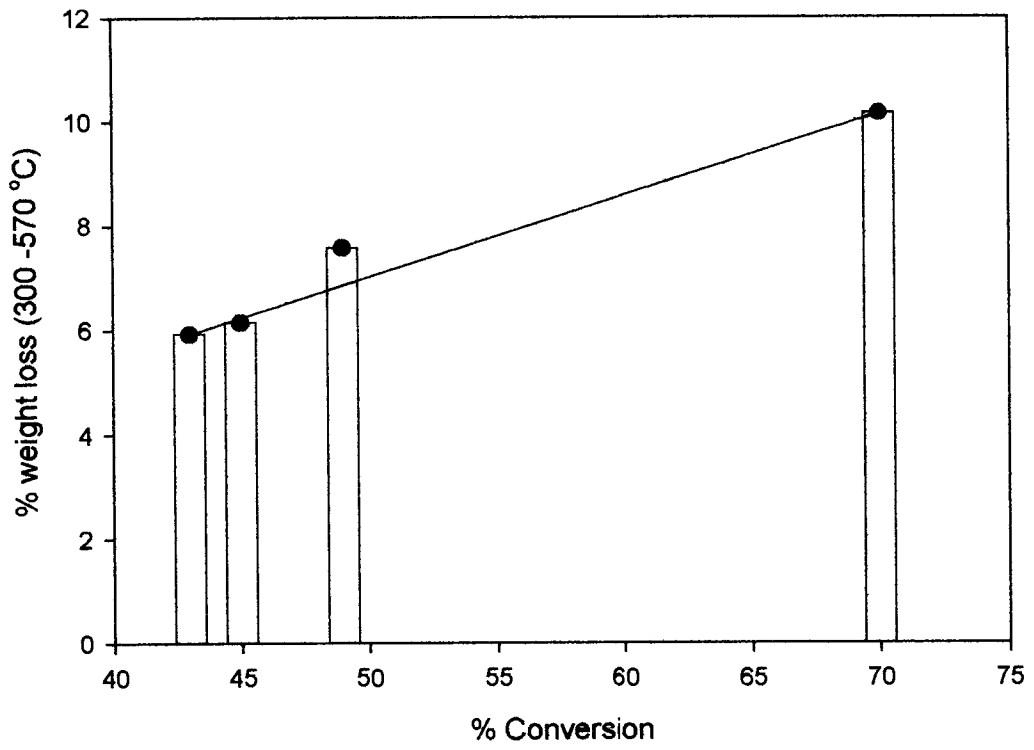
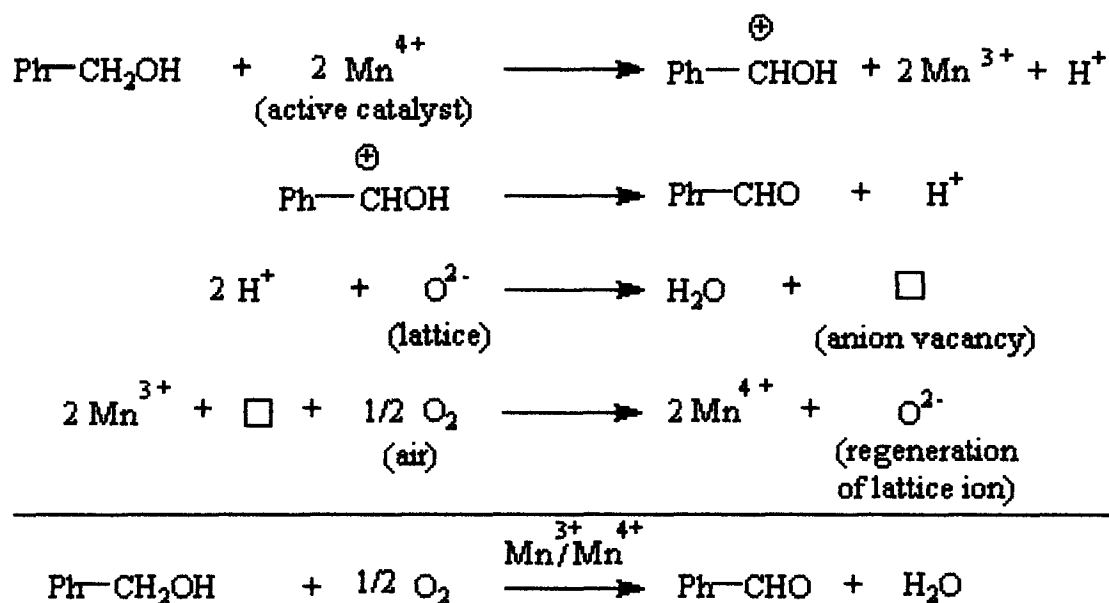


**Figure 3.11:** Correlation plot of % weight loss for the temperature interval 300-570 °C v/s % Conversion

Therefore the oxidation of benzyl alcohol could be facilitated due to (i) participation of lattice oxygen and (ii) presence of  $Mn^{3+}/Mn^{4+}$  redox couple in agreement with earlier reports [154].

Based on all these results a mechanism has been proposed for the oxidation of benzyl alcohol over the OMS-2 catalysts. Hence the catalytic oxidation of benzyl alcohol may be mediated by: (i) lattice oxygen and (ii)  $Mn^{4+}/Mn^{3+}$  redox couple, as shown in Scheme 3.1.



**Scheme 3.1:** Mechanism of benzyl alcohol oxidation via lattice oxygen vacancy in OMS-2 catalysts

### 3.4 Conclusions:

- ✓ The OMS-2 catalysts show good activity towards the oxidation of Benzyl alcohol.
- ✓ Modifying OMS-2 with Aluminium resulted in
  - Lattice dilation, which is associated with the lengthening of the Mn—O bond, which in turn enhanced the proton exchangeability of the dioxides.
  - The proton exchangeability is a measure of amount of acidic protons, which indirectly show the presence of active  $\text{Mn}^{4+}/\text{Mn}^{3+}$  redox couple.
- ✓ Adding transition metal cations (Fe and Ti) has resulted in improved catalytic activity thus showing increasing % conversion with increase in transition metal content in the samples. The effect with  $\text{Fe}^{3+}$  was found to be more as compared to that by  $\text{Ti}^{4+}$ .
- ✓ Corresponding increase in chemical reactivity and % weight loss in the three temperature intervals, with metal content is seen.
- ✓ The higher activity is associated with the extent of participation of lattice oxygen.
- ✓ The oxidation involves anion generation; thus a mechanism has been proposed through the loss of lattice oxygen.

*CHAPTER – IV*

*ELECTROCHEMICAL REDUCTION*

*STUDIES*

#### 4.1 Introduction:

Manganese oxide compounds occur in numerous phases of widely variable structures [9,10,157,158] that are enabled by the ability of their building unit,  $[\text{MnO}_6]$  or  $[\text{Mn}(\text{O},\text{OH})_6]$  octahedra to form infinite layers and three – dimensional structures. These structures usually contain relatively freely accessible tunnels and/or interlayer spaces of various sizes, that both can serve as a suitable space for ion insertion.  $\alpha$ - and  $\gamma$ - $\text{MnO}_2$  compounds are favourable candidates with one dimensional tunnel structures. As discussed earlier, the structure of  $\alpha$ - $\text{MnO}_2$  or nsutite is made up of double chains of edge – sharing octahedra, which then share corners to form  $2\times 2$  and  $1\times 1$  channels, the former of which are of suitable size for the insertion/extraction of  $\text{Li}^+$ . The structure of  $\gamma$ - $\text{MnO}_2$  is more complex than that of  $\alpha$ - $\text{MnO}_2$ , which consists of a random intergrowth of ramsdellite ( $2\times 1$  channels) and pyrolusite ( $1\times 1$  channels) structures [159] as shown in Figure 4.1

Several new findings have recently refreshed the interest in electrochemistry of manganese oxides: the development of secondary cells with EMD [160], proposals to employ Bi-doped birnessite in secondary cells [161] and perovskite  $\text{CaMnO}_3$  in primary cells [162], and attempts to utilize practically the reversible insertion of  $\text{Li}^+$  (aq) into spinel – type Mn oxides [158,163-168]. Compared to vanadium-based oxides, manganese dioxides are advantageous because of their lower cost, lower toxicity and higher average voltage [38]. Rossouw *et al.* [169] obtained a discharge capacity of 210 mAh/g of  $\text{Li}/\alpha$ -  $\text{MnO}_2$ , when discharged at  $0.2 \text{ mAcm}^{-2}$  to a cut off voltage of 2.0 V. While Dai *et al.* [29] report Li ion-exchanged  $\alpha$ -  $\text{MnO}_2$  showing a discharge capacity of 200 mAh/g for the second discharge. Hill and coworkers [39] have studied Li-insertion behaviour of  $\alpha$ - and  $\gamma$ - $\text{MnO}_2$  and have found that  $\alpha$ - $\text{MnO}_2$  shows a very stable capacity of 145 mAh/g.

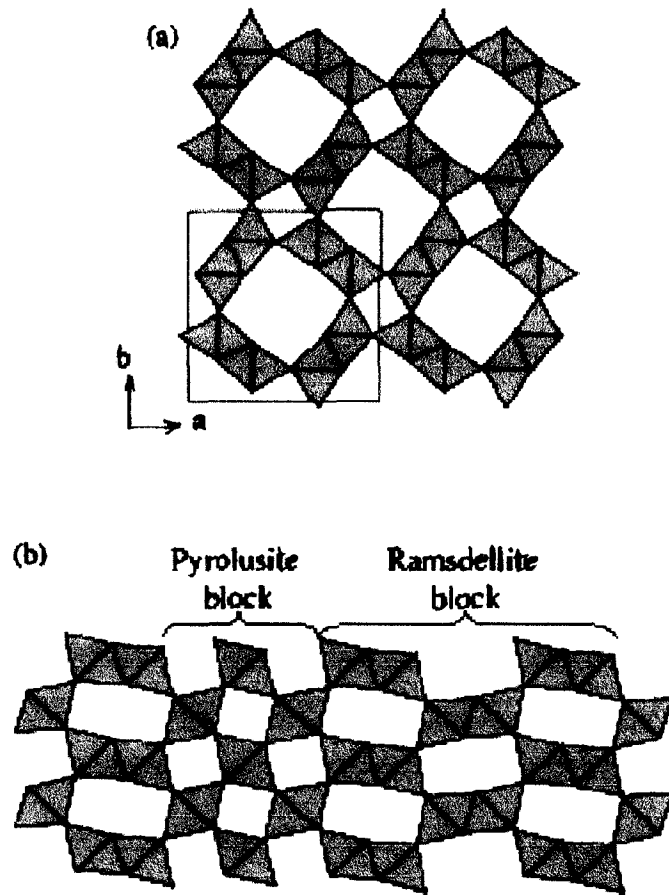


**Figure 4.1** Structures of (a)  $\alpha$ -  $\text{MnO}_2$  (OMS-2) and (b)  $\gamma$ - $\text{MnO}_2$  (nsutite) showing intergrowth of pyrolusite and ramsdellite [39]

What exactly is meant by the activity of manganese dioxide is not very clear and has intrigued many workers in the field of the dry cell technology for quite some time now. The sample, which gives maximum energy over a longer period of time with as high a cell voltage as possible can be considered the most active sample. The experimental techniques and data evaluation have hence been focused on such properties like cell voltage, depth of discharge and cycle number. Individual Mn oxide phases are commonly evaluated with a particular respect to their practical application [60,157]. Many physical and chemical properties such as electrical conductivity, porosity,  $\text{MnO}_2$  content, surface electrode potential, pore size, particle shape and size,

etc. have been measured and discussed in terms of dry cell performance. Yet exactly what combination of any of these factors will render a given sample of  $\text{MnO}_2$  most active is difficult to determine a priori. It has, however, been shown that the differences in electrochemical reactivity of the dioxides can be easily recognized by discharging them in 9M KOH solution. Since this method has also the added advantage of supposedly being independent of cell fabrication factors [170] it has been adopted in this study, though slightly modified as carried out by Fernandes *et al.* [60].

## 4.2 Experimental

### 4.2.1 Catalyst synthesis

The synthesis of OMS-2 and a pyrolusite manganese oxide sample (P) and its characterization is described earlier in Chapters 2 and 3. Three  $\text{Li}^+$  modified samples were synthesized using  $\text{LiNO}_3$  at the initial stage before addition of hot  $\text{KMnO}_4$ . These samples were labeled as 0.5 % Li-S, 1 % Li-S and 2 % Li-S containing 0.5, 1 and 2 % of Li in each sample.

### 4.2.2 Electrochemical reduction studies (Cell preparation):

As mentioned earlier, the method adopted for the construction of the electrochemical cell was similar to that used by Fernandes *et al.* [53], which itself was a modified Kozawa's method. The cell consisted of a threaded plastic cap (height 11 mm and inner diameter 24 mm) with a hole in the side, small enough for a silver wire to pass through. The end of the wire inside the cap is coiled to fit well and extends long enough outside for necessary external connections.

The cathode mixture (working electrode) was prepared with well-dried samples of 100 mg manganese oxide and 900 mg conducting graphite, which were



intimately mixed to form a homogenous mixture on a cyclo mixer. This was moistened using 10 drops of 9 M KOH and the resulting paste was poured carefully into the cap and firmly secured at the bottom of the assembly over the coiled silver wire current collector as illustrated in Figure 4.2. Above the cathode mix was placed a separator cloth and perforated plastic disc. Next a hollow cylindrical plastic container (inner diameter 22 mm and height 55 mm) threaded at one end was fitted to the cap containing the cathode mix and this assembly was pressed by applying a pressure of approximately  $100 \text{ kgcm}^{-2}$  using a hydraulic press. After 10 min of applying the pressure, the sides were sealed to avoid leaking of electrolyte. The cell was then filled to occupy ~ 80% of the volume of the plastic vessel with 9 M KOH.

Two zinc sheets ( $100 \text{ mm} \times 6 \text{ mm} \times 1 \text{ mm}$ ), one of which serves as counter electrode and the other as reference electrode, were inserted into the electrolyte approximately maintained at 3 mm above the porous disc and left as such for equilibration for about 15 min. The cell was connected as shown in the Figure 4.3 and the potential of the manganese oxide was measured with respect to the zinc reference electrode.

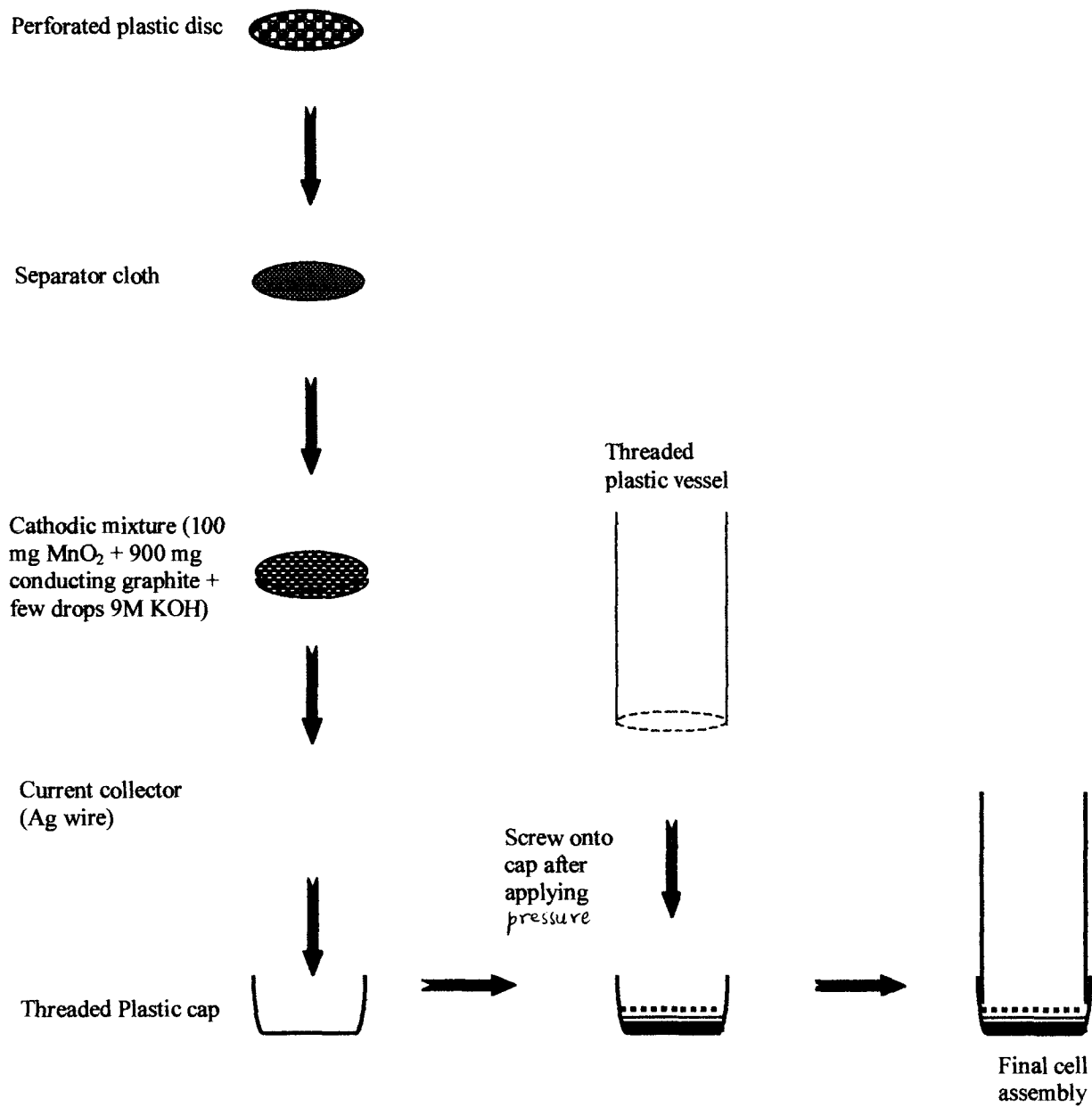


**Figure 4.2:** Scheme for the preparation of a manganese dioxide electrochemical cell

All the tests were carried out at a room temperature of 28 °C. The initial voltage of the cell called as open circuit potential, OCP was first determined, and then the cell was discharged continuously at a current of 1 mA. The closed circuit potential, CCP were recorded every 1-hour for 5 hours. The cell was then allowed a rest period of 15 hours to recuperate and the OCP was determined again at the end of it. The cell discharge was continued henceforth for 8 hours per day till a cut off CCP of 1.0 V.

All the intrinsic polarization values ( $\eta = \text{OCP} - \text{CCP}$ ) are measured after a rest period of 15 hours. While there are many ways of expressing the activity of a manganese dioxide sample, in this study the main parameters considered are (i) OCV at 5 mAh discharge, (ii) polarization at 5 mAh discharge and (iii) discharge duration at 1.0 V cut-off. The discharge characteristics so determined are presented in Table 4.1.

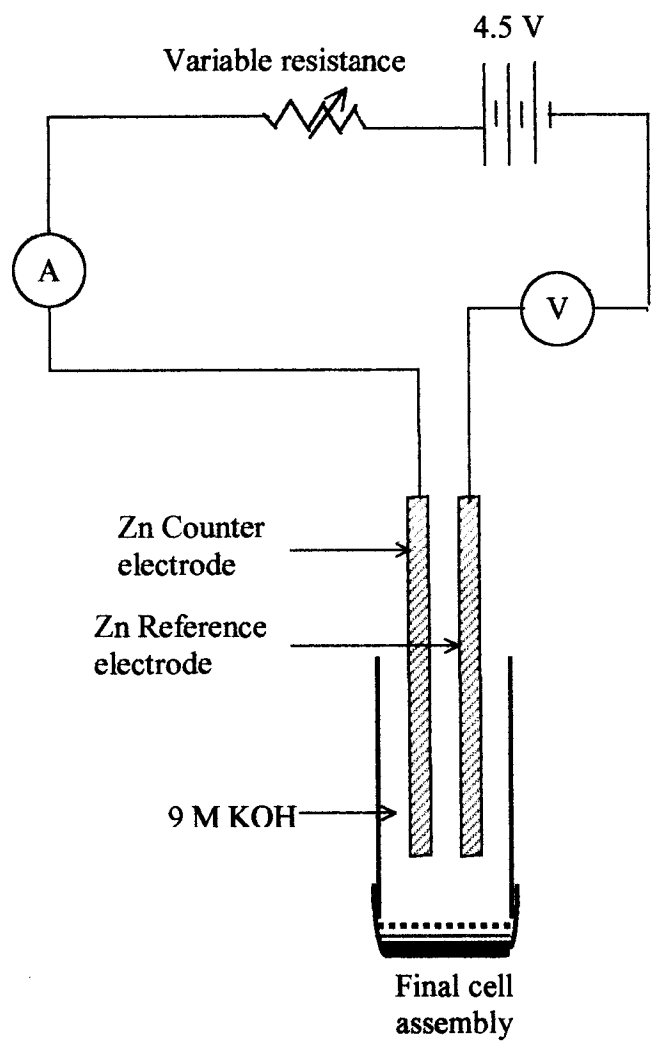
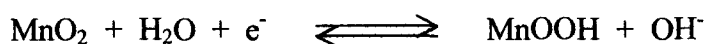


**Figure 4.3:** Experimental circuit diagram for the electrochemical reduction of manganese oxides

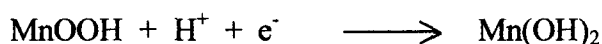
### 4.3 Results and discussion:

It is known that manganese dioxide is an insertion electrode and undergoes proton-electron insertion in two steps [171-173]. It initially undergoes one electron homogenous phase reduction in alkaline medium. The reduction in this region has been called the electron-proton mechanism. During reduction, electrons from the conductor are inserted into the  $\text{MnO}_2$  structure, causing reduction of  $\text{Mn}^{4+}$  to  $\text{Mn}^{3+}$  ions. At the same time, water molecules are decomposed at the  $\text{MnO}_2$ /electrolyte interface, resulting in  $\text{H}^+$  ions being inserted into the  $\text{MnO}_2$  structure. This process can be represented by the general reduction reaction:



wherein  $\text{MnO}_2$  and  $\text{MnOOH}$  coexist. It was found that a separate chemical phase was not formed rather a solid solution of  $\text{MnO}_2$  and  $\text{MnOOH}$  distributed throughout the structure [171]. Such a situation arises because protons and electrons are able to move through the structure by “hopping” from site to site, and this continues provided the lattice parameters allow it. The electrode potential at this stage is characteristic of a homogeneous phase reduction, in support of the electron-proton mechanism.

This is then followed by heterogeneous phase reduction of  $\text{MnOOH}$  to  $\text{Mn}(\text{OH})_2$ . The reduction mechanism in this region has been called the dissolution-precipitation mechanism and is dependent on the relative solubilities of  $\text{Mn}^{3+}$  and  $\text{Mn}^{2+}$  in the electrolyte. Thus  $\text{MnOOH}$  in the electrode undergoes dissolution, releasing  $\text{Mn}^{3+}$  ions into the electrolyte, which are then reduced to soluble  $\text{Mn}^{2+}$  on the surface of the conductor. The electrode potential during this stage remains constant, which is typical of a heterogeneous phase reduction.



These steps are now found to be not as simple as shown here and known to consist of as many as three steps in the homogeneous stage [173]. After the rest period, some partial reversibility in the structure occurs which accounts for the slight increase in the open circuit potential.

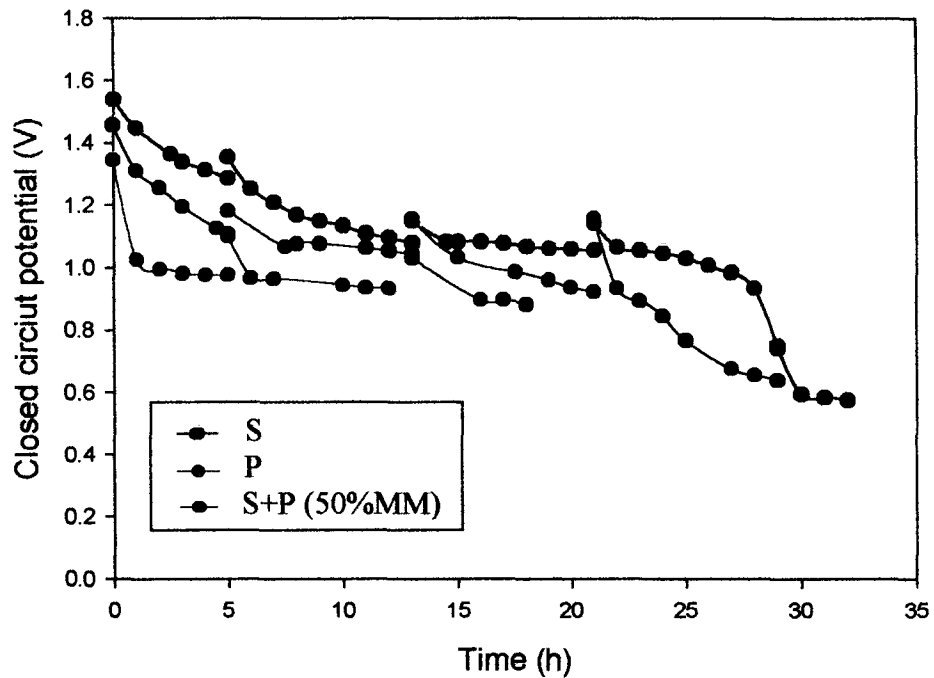


**Figure 4.4:** Discharge curves of the various MnO<sub>2</sub> samples in 9 M KOH

**Table 4.1:** Discharge characteristics of the various manganese oxides in 9 M KOH solution

Sample	OCP (V)		CCP (V) 5 mAh	Polarisation (mV)			Discharge time at 1.0 V cut off (h)	Usable energy (J)
	OCP (V) initial	OCP (V) 5 mAh		5 mAh	13 mAh	21 mAh		
S	1.550	1.360	1.288	7.2	8	9	26	13.05
P	1.371	1.190	0.980	21	10.4	-	1	0.791
P + S	1.463	1.185	1.110	7.5	11.2	23.5	17.5	8.33
S (50 mg)	1.470	1.156	1.111	4.5	-	-	12	4.85

It is evident from Figure 4.4 that P has its homogenous phase reduction restricted to a very narrow phase breadth compared to that of OMS-2. A similar observation was made by Fernandes *et al.* [60]. The discharge characteristics of the samples are presented in Table 4.1. That OMS-2 sample (S) is superior over the pyrolusite sample (P) or  $\beta$ -MnO<sub>2</sub>, is clearly seen wherein, P was stable for hardly an hour while OMS-2 was stable up to 26 hours at a cut off potential of 1.0 V. The usable energy has been calculated by integrating the area under each curve.

It is well known that nsutite or  $\gamma$ -MnO<sub>2</sub> shows superior discharge characteristics as compared to other manganese oxides. Here the pyrolusite (1×1) – ramsdellite (2×1) intergrowth is expected to favour the proton-electron insertion. In the present case, further investigation was carried out to see the effect on discharge behaviour when (2×1) manganese oxide is replaced by (2×2) or OMS-2. Hence, a 50 % mixture of pyrolusite and OMS-2 were obtained by mixing equal quantities (50 mg + 50 mg) of the two powders. As seen in Figure 4.4, this combination showed that the discharge time at 1.0 V cut off of the composite mixture improved to 17.5 hours. In comparison, when just 50 mg of OMS-2 was investigated, it was stable up to 12 hours at the same cut off potential as evident in Figure 4.5. Thus, a synergistic interaction is believed to occur between the OMS-2 and pyrolusite phases leading to improved electrochemical performance.

Further investigations were also carried out to study the effect of Li<sup>+</sup> insertion on nsutite and OMS-2 samples in alkaline medium. Thus, as evident in Figure 4.6, OMS-2 (15 h at 1.0 V cut off) gave more stable discharge characteristics as compared to a synthetic nsutite (9 h at 1.0 V cut off) prepared in this work.

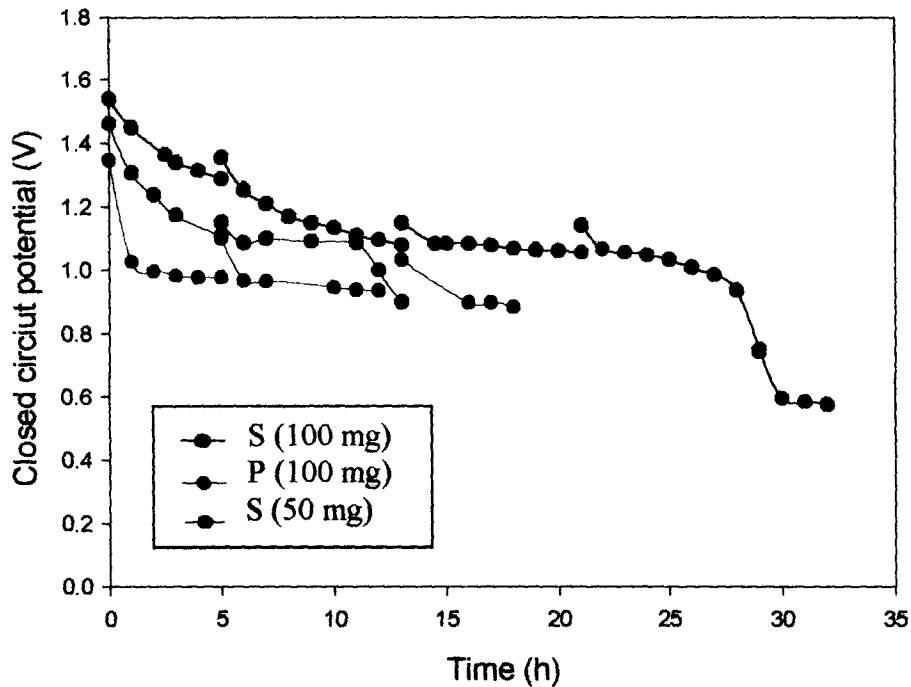


**Figure 4.5:** Discharge curves comparing half the amount of OMS-2 (50 mg) in 9 M KOH

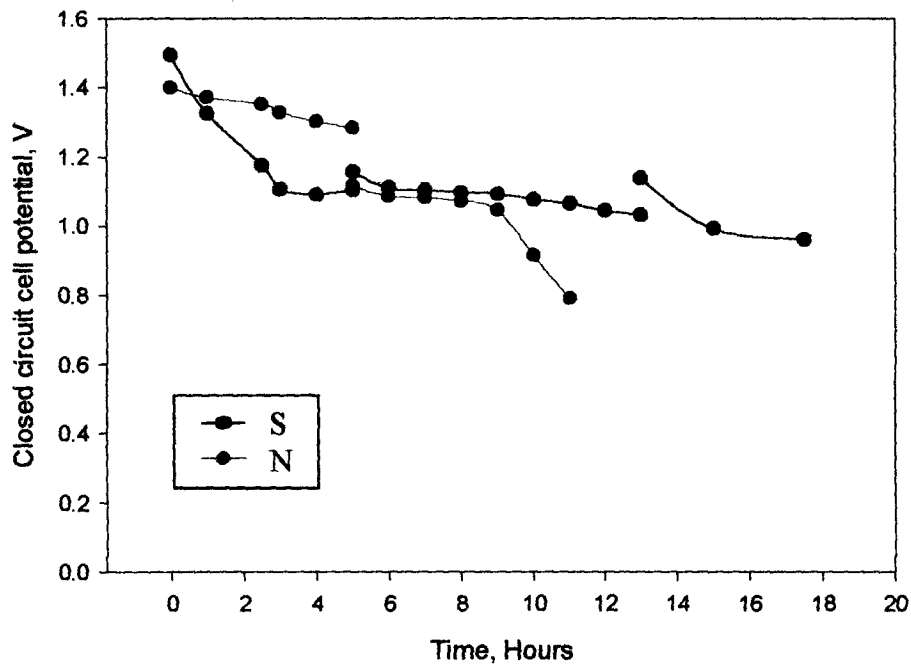


**Figure 4.6:** Discharge curves of the nsutite and OMS-2 samples during Li<sup>+</sup> insertion in alkaline medium



#### **4.4 Conclusions:**

Thus,

- OMS-2 shows superior discharge characteristics compared to pyrolusite.
- A synergistic interaction is believed to occur between OMS-2 and pyrolusite resulting in improved discharge characteristics.
- OMS-2 showed better characteristics in  $\text{Li}^+$  insertion studies in alkaline medium as compared to a nsutite sample prepared in this work.

*CHAPTER – V*

*ELECTROCATALYTIC OXIDATION OF*

*METHANOL*

## 5.1 Introduction:

The interest in alternative power sources has increased considerably in recent years especially due to the depletion of fossil fuels and the growing concern for environmental problems derived from their use. In this context, fuel cells are the subject of much research effort because of the potential for stationary and transportation applications and more recently in portable systems [174].

Today, a fuel cell that operates with hydrogen as fuel is capable of delivering high power densities. However, hydrogen presents several problems of production, storage and distribution and the research for alternative, more convenient fuels is of much interest. Due to the possibility of its complete oxidation to CO<sub>2</sub>, liquid methanol is currently the best alternative for hydrogen and its oxidation produces 6 electrons [65]. Thus there is much work dealing with the oxidation of methanol, involving research ranging from the study of the kinetics and the mechanism of methanol electro oxidation to the development of new catalysts for practical systems.

Platinum is presently the best electrocatalyst for methanol oxidation involving the processes like adsorption and several stages of dehydrogenation, leading to the formation of strongly adsorbed CO [66-84]. Various authors discuss the mechanism and the critical pathways related to the oxidation of the strongly adsorbed CO [66,68,69,82]. In the DMFC it is imperative to oxidize CO at lower potentials than on pure Pt (0.75 V vs. RHE), and for this purpose Pt can be alloyed with other metals like Ru [66,70], Mo [99], Os [85] and W [85,95-99], which form oxygenated species at lower potentials than Pt.

The present investigation reports possible use of supported Manganese Octahedral Molecular Sieves (OMS-2) for the electrooxidation of methanol. This is the first report in the use of octahedral molecular sieves in fuel cell studies. The effect

of combining these materials with a commercially available 5%Ru-Carbon sample has been studied with respect to the oxidation of methanol. The activity of the OMS-2 materials has been studied with respect to other forms of manganese oxides like pyrolusite and nsutite. The OMS-2 materials were found to show a synergistic interaction with the 5% Ru-C as well as the pyrolusite materials thus enhancing their electrochemical activities effectively. The OMS-2 materials not only proved to be cost effective but electrochemically very active too.

## **5.2 Effect of 5% Ru-C support:**

### *5.2.1 Catalyst synthesis*

The synthesis of the active  $\text{MnO}_x$  samples (OMS-2) has been discussed in the earlier chapters.

S: (same as S1 in Chapter II) synthesized by oxidation of  $\text{MnSO}_4 \cdot \text{H}_2\text{O}$  with  $\text{KMnO}_4$  in acidic medium as described earlier.

S/Ru-C: carbon-supported sample has been synthesized by taking appropriate quantities of the salts and in-situ generation of the phase on the support material such that OMS-2 phase/5% Ru-C is in ratio 1:1.

P: a pyrolusite manganese oxide as described in Chapters III and IV was synthesized by the thermal decomposition of  $\text{Mn(II)NO}_3$  at 200 °C.

IC8: An International Common sample, (nsutite form) supplied by Electrochemical Society, Cleveland, Ohio, U.S.A. has also been used in this study.

### *5.2.2 Catalyst characterization:*

The catalysts were characterized by various chemical methods to determine average oxidation state, catalytic activity by  $\text{H}^+$  ion exchange and instrumental

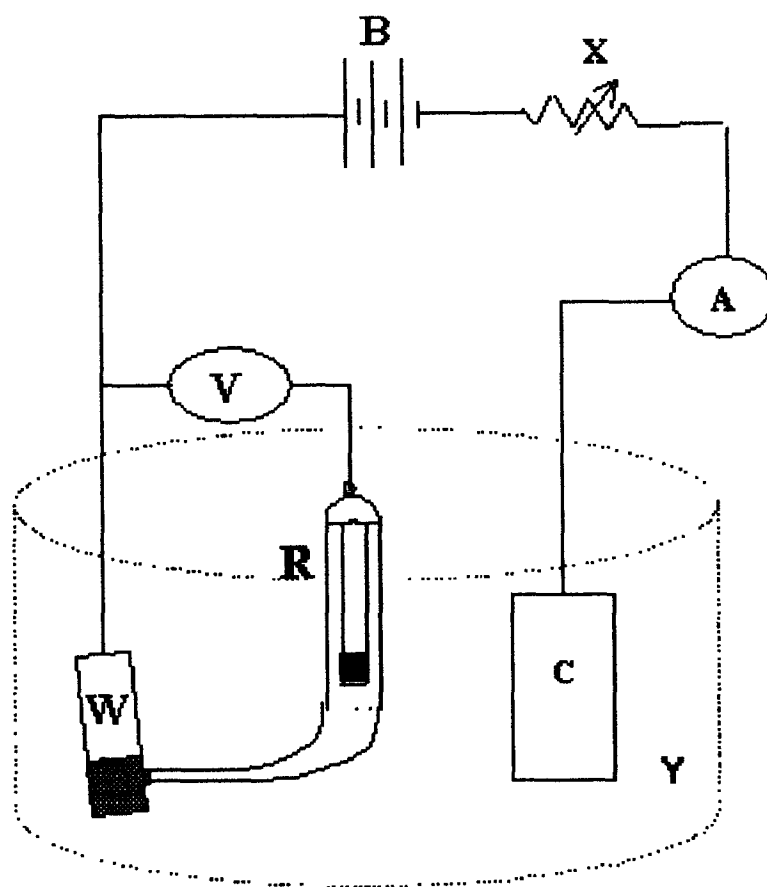
methods of analysis like XRD, IR, TG and BET surface area. Results are presented in Table 5.1. Also electrochemical characterization of the samples was carried out by cyclic voltammetry studies (CV).

### *5.2.3 Electrode preparation:*

The electrodes were made in a simple fashion as follows: 50 mg of sample and 5mg conducting graphite per 10 mg of sample were taken along with 3 ml isopropyl alcohol in a mortar and pestle and mixed well for about 5 minutes. Manganese oxides are known to be semiconductors and so the conducting graphite was used to make the samples more conducting. Next, 3 drops of Nafion® (15% solution in isopropyl alcohol) solution were added and mixed to make a homogenous mixture for about 5 minutes till most of the solvent evaporated. The ink thus formed was applied to obtain a manganese oxide catalyst loading of 10 mg over 1 cm<sup>2</sup> active surface area on a 3×1 cm Toray carbon paper. This strip was then dried in an oven at 120 °C for 1 hour and then used in the polarization studies by suspending with the help of Platinum wire for electrical contact.

### *5.2.4 Electrocatalytic activity studies:*

In the present investigation, electrochemical measurements were carried out in a cell containing 25 ml each of 2.5 mol dm<sup>-3</sup> H<sub>2</sub>SO<sub>4</sub> and 1 mol dm<sup>-3</sup> CH<sub>3</sub>OH with the specially fabricated electrode described earlier as the working electrode. Platinum foil was used as counter electrode, while saturated calomel electrode (SCE) was the reference electrode. The experimental set up is as shown in Figure 5.1. The electrocatalytic activity is evaluated from the resulting Tafel plots.



**B** – Battery or DC source

**X** – Variable Resistance

**A** – milliAmmeter

**V** – milliVoltmeter/Potentiometer

**W** – Working electrode

**R** – Reference Electrode (SCE with luggin capillary)

**C** – Counter Electrode (Pt foil)

**Y** – Cell containing 2.5M  $\text{H}_2\text{SO}_4$  + 1M MeOH

**Figure 5.1:** Experimental set-up to study Tafel Relationship

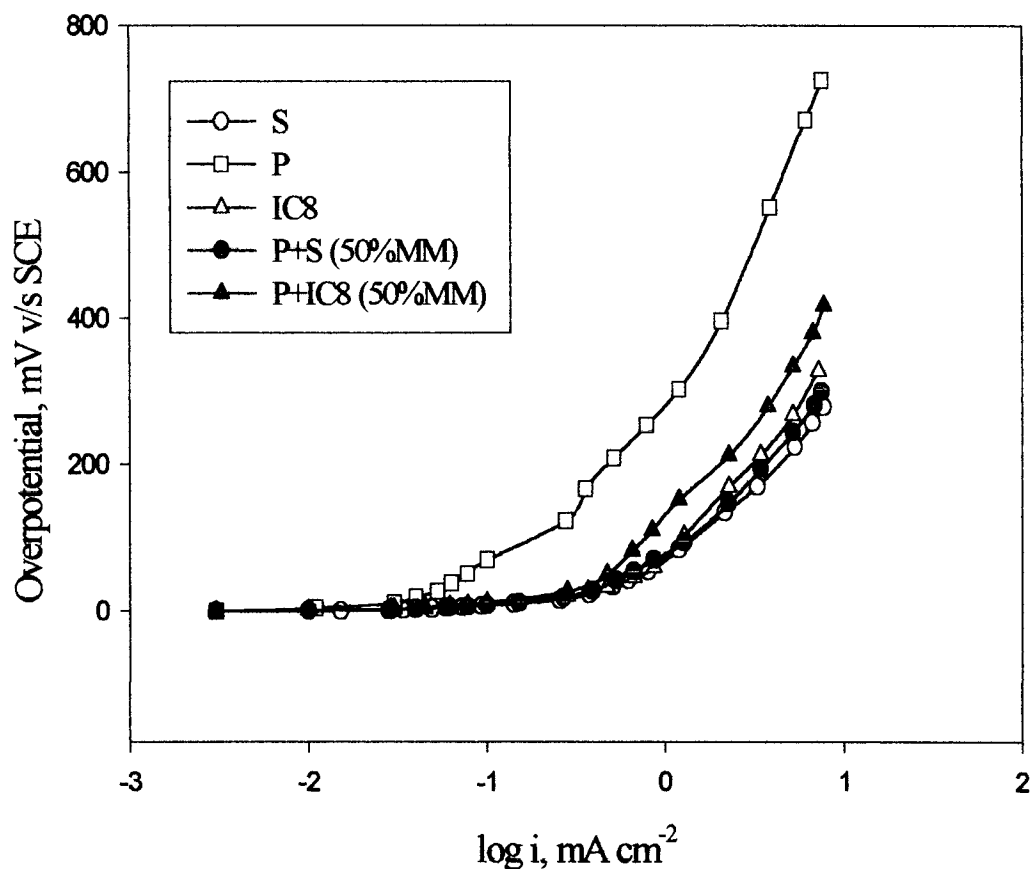


**Figure 5.2:** Tafel plots to study effect of pyrolusite (P) on OMS-2 (S) and nsutite (IC8)

### 5.3 Results and Discussion:

Table 5.1 gives activity of the samples in relation to their other physico-chemical characteristics, viz, surface area, O<sub>2</sub> loss by TG and volumes of thiosulphate (as a measure of H<sup>+</sup> ion exchange capacity of the OMS-2). The electrocatalytic activity of the samples is expressed in terms of  $i_{150}$ , (current produced at an overpotential of 150 mV) calculated from the Tafel Plots (Figures 5.2 and 5.3). These values are given in Table 5.2.

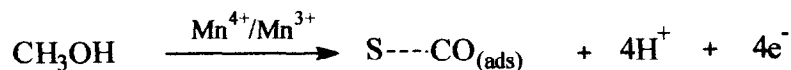
**Table 5.1:** Chemical reactivity of the Mn(IV) oxides in relation to their physicochemical characteristics

Catalyst	'x' in MnO <sub>x</sub>	Crystal phase	BET (m <sup>2</sup> /g)	Thermal analysis			Decomp. Temp. (°C)	V <sub>S<sub>2</sub>O<sub>3</sub><sup>2-</sup></sub> (ml)
				% O <sub>2</sub> loss				
				120-300 (°C)	300-500 (°C)	500-570 (°C)		
S	1.86	Cryptomelane (OMS-2)	77	4.45	3.69	2.04	600	3.3
P	2	Pyrolusite	7	2.8	3.29	1.2	597	0

It is seen from Table 5.1, that the OMS-2 sample S produced a large current of 3.2 mA cm<sup>-2</sup>. In comparison, the corresponding current shown by the pyrolusite sample P is negligible. The poor activity of P is due to its stoichiometric nature and absence of any acidic OH groups. The high activity of S could be due to presence of labile oxygen and acidic OH groups as discussed in Chapter 3.

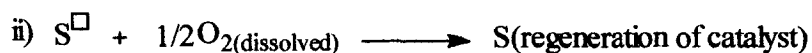
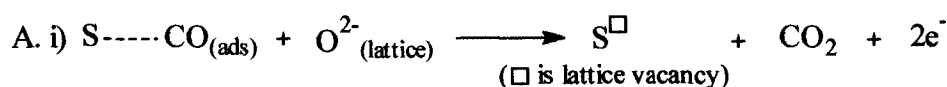
It is evident from Table 5.1 that the H<sup>+</sup> ion exchange capacity expressed as volumes of thiosulphate consumed, V<sub>S<sub>2</sub>O<sub>3</sub><sup>2-</sup></sub> increases with increase in catalytic activity. The activity may therefore, be directly related to the presence of active Mn<sup>4+</sup>/Mn<sup>3+</sup> redox couple, which may be responsible for the acid centers in the catalysts as evident in the TPD data in Chapter 3. Suib et al. [154] have in fact suggested presence of such strong Lewis acid centers. Hence the electrocatalytic oxidation of methanol may be mediated by: (i) lattice oxygen and (ii) Mn<sup>4+</sup>/Mn<sup>3+</sup> redox couple. It is believed that the Mn<sup>4+</sup>/Mn<sup>3+</sup> redox couple catalyzes methanol dehydrogenation by the evolution of protons and electrons followed by oxidation of





**Scheme 5.1:** Formation of adsorbed CO as a result of incomplete oxidation of methanol over OMS-2 (S) catalyst

the residual CO type species by lattice oxygen. The resulting anion vacancy would be healed by absorption of dissolved oxygen into the OMS-2 lattice. Thus the above discussion can be understood clearly from the following scheme of steps.



**Scheme 5.2:** Methanol oxidation over OMS-2 catalyst by lattice oxygen participation followed by its regeneration

Further, the investigation carried out on the International sample, IC8 also resulted in high currents although the OMS-2 sample was still superior. To understand the effect of pyrolusite, mechanical mixtures of pyrolusite/nsutite were prepared in a 1:1 ratio and activity tests were carried out. As can be seen from Table 5.2, the pyrolusite/IC8 mixture did not increase the activity in terms of the current produced. On the other hand, the current produced by the pyrolusite/OMS-2 mixture produced almost the same current as the pure OMS-2 (~ 3.0 mA cm<sup>-2</sup>). This showed that even though pyrolusite was by itself inactive, it gave the same result with OMS-2 with 50% reduction in the OMS-2 quantity in the final electrode mixture. Thus, pyrolusite produced synergistic interaction with OMS-2 material and not the nsutite material.

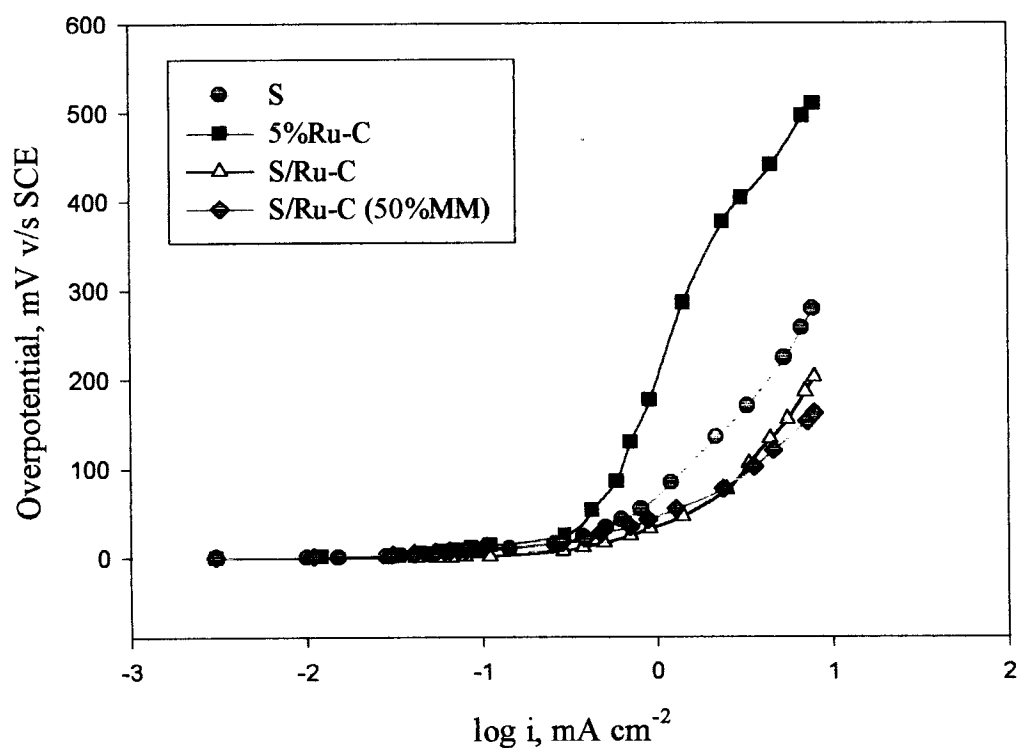


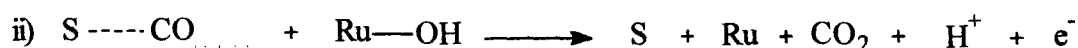
**Figure 5.3:** Tafel plots to study effect of Ru-C support on OMS-2 (S)

**Table 5.2:** Electrocatalytic activity of the various samples investigated expressed in terms of current produced at an arbitrarily chosen overpotential of 150 mV

Sample	S	P	IC8	P/S	P/IC8	5%Ru-C	S/Ru-C	S/Ru-C (50% MM)*
$i_{150}$ (mA cm <sup>-2</sup> )	3.2	0.3	2	2.8	1.2	0.75	5.6	7.2

50% MM\*: Mechanical mixture containing 50% OMS-2 compound.

It is well known that Ru in Pt–Ru alloy catalysts greatly enhances the electrocatalytic activity of Pt. In order to study the effects of Ru on OMS-2, further investigations were carried out with a commercially available 5% Ru-C sample (supplied by Arora Matthey Co. Ltd., Calcutta, India). Activity tests were carried out by synthesizing 50% OMS-2 on 5% Ru-C as described in section 2.1 and also by preparing electrodes by 1:1 mechanical mixing of separately prepared OMS-2 with 5% Ru-C. These results are also presented in Table 5.2. It is seen that the commercial 5% Ru-C used in the present investigation showed much lower activity compared to MnO<sub>x</sub> materials OMS-2 or IC8. The current on 5% Ru-C was only 0.75 mA cm<sup>-2</sup>. On the other hand OMS-2/Ru-C electrodes gave large increase in currents. The electrode prepared from 1:1 mechanical mixture produced a synergistic interaction with the value of current 7.2 mA cm<sup>-2</sup>, and was a superior combination even to the OMS-2/Ru-C *in situ* prepared sample.



**Scheme 5.3:** Methanol oxidation over S/Ru-C catalyst

It could be due to the fact that the hydroxylated Ru surface causes rapid oxidation of S---CO species. It is also believed that Ru could provide nucleating centers for CO clustering within the octahedral sieve framework of OMS-2 as in case of zeolite structures [112], causing facile oxidation of CO to CO<sub>2</sub>.

#### 5.4 Conclusions:

1. Manganese octahedral molecular sieves have been found to be active for methanol electrooxidation for the first time.
2. The high activity of the manganese oxide was associated with presence of  $\text{Mn}^{4+}/\text{Mn}^{3+}$  redox couple. The extent of participation of lattice oxygen played an important role in methanol oxidation reaction.
3. Pyrolusite in combination with manganese octahedral molecular sieves gave a higher current (more than twice) than the current produced by a combination of pyrolusite with the international sample (IC8), thus suggesting that it produced a synergistic interaction with OMS-2 thus improving its activity towards MOR.
4. In case of OMS-2 materials in combination with 5% Ru-C (whether *in situ* generated phase on the Ru-C or 1:1 mechanical mixture), Ru enhances oxidation of CO to  $\text{CO}_2$  significantly.

### 5.5 Effect of temperature:

The catalysts were also tested for methanol oxidation at higher temperature (60 °C). It is well known that kinetics of oxidation of methanol is improved with rise in temperature, which is confirmed by comparing Tables 5.2 and 5.3.

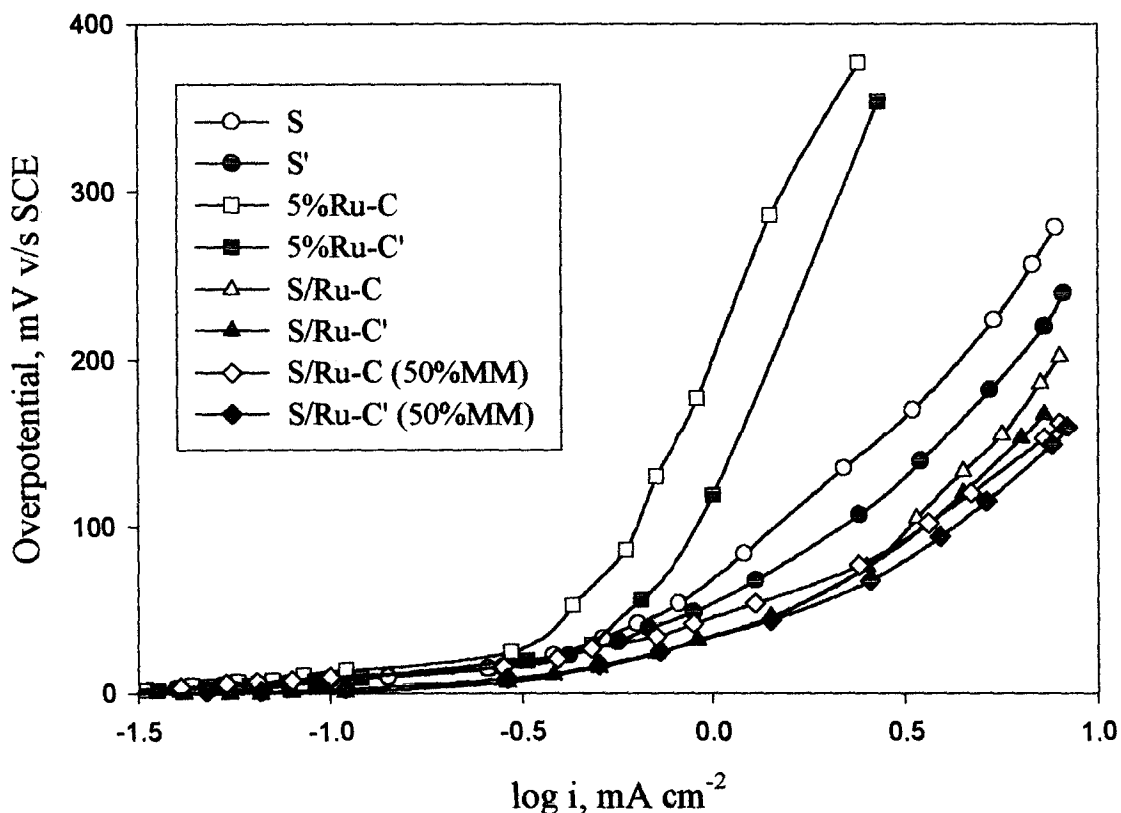


**Figure 5.4:** Tafel plots to study effect of elevated temperature on S/Ru-C composite electrocatalyst (white legends are at room temperature, while red legends are at 60 °C)

**Table 5.3:** Electrocatalytic activity at 60 °C of the samples investigated expressed in terms of current produced at an arbitrarily chosen overpotential of 150 mV

Sample	S	P	IC8	P/S	P/IC8	5%Ru-C	S/Ru-C	S/Ru-C (50% MM)*
$i_{150}$ (mA cm <sup>-2</sup> )	3.98	1.2	5.0	3.98	2.0	1.5	6.0	7.6

50% MM\*: Mechanical mixture containing 50% OMS-2 compound.

### 5.6 Effect of amount of OMS-2 on activity of RuC:

Since OMS-2 showed improved activity when combined with 5% Ru-C, it was necessary to study this effect. Hence three different mixtures of OMS-2 (S) and 5% Ru-C were taken in 1:3, 1:1 and 3:1 proportions corresponding to 25, 50 and 75% mixtures respectively. Electrocatalytic studies revealed that increase in amount of OMS-2 in Ru-C improved the activity of the sample from a value of  $3.98 \text{ mA cm}^{-2}$  for 25 % mixture to  $10 \text{ mA cm}^{-2}$  for the 75 % mixture. This proves that OMS-2 has some synergistic interactions with the Ru-C, which helps in facile oxidation of methanol. The current-potential profiles of the samples are shown in Figure 5.5 and current densities as shown in Table 5.4.

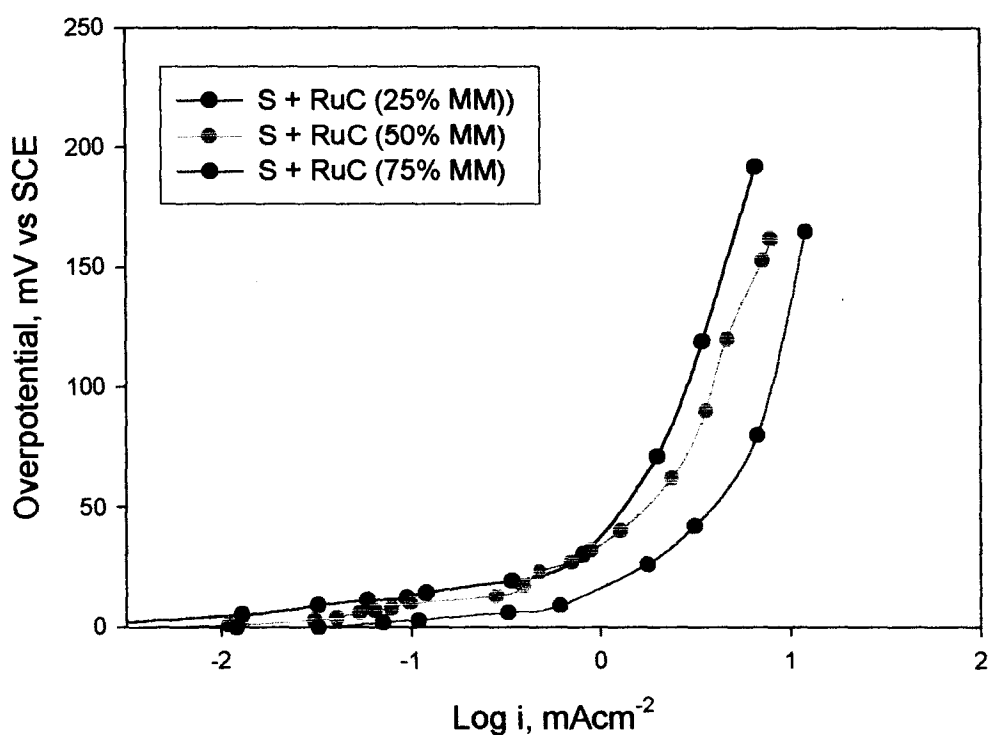


**Figure 5.5:** Tafel plots to study effect of amount of the OMS-2 phase (S) on Ru-C

**Table 5.4:** Electrocatalytic activity of the various samples investigated expressed in terms of current produced at an arbitrarily chosen overpotential of 150 mV

Sample	S	RuC	S + RuC (25% MM)	S + RuC (50% MM)	S + RuC (75% MM)
$i_{150}$ (mA cm <sup>-2</sup> )	3.2	0.75	3.98	7.2	10

### 5.7 Effect of hydrogen reduction on activity of 50% mixture of 5% Ru-C

#### supported OMS-2:

Many fuel cell systems use reformers to facilitate complete oxidation of the fuel. Thus along with the fuel feed, the reformat also contains considerable amount of hydrogen. In such a case it was but necessary to study the effect of hydrogen especially on OMS-2. Thus, equal quantities of 5% Ru-C and OMS-2 (S) were first ground together using mortar and pestle, then mixed well again till homogeneous in a cyclo mixer and the final mixture was divided into three equal portions and each was subjected to reduction in the presence of flowing hydrogen at a controlled flow rate of  $\sim 50 \text{ ml min}^{-1}$  at three different temperatures; 40, 60 and 80 °C in a horizontal muffle furnace for one hour. These samples are thus labeled as SR40, SR60 and SR80 respectively. Table 5.5 gives  $i_{150}$  for each of the treated samples.

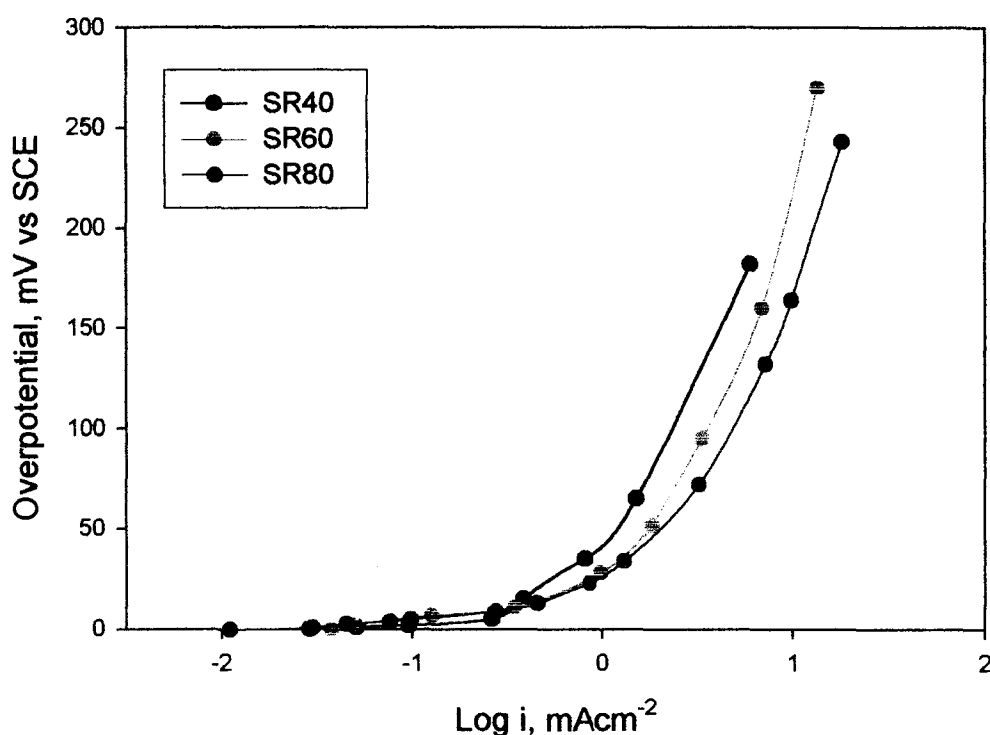


Figure 5.6: Tafel plots to study effect of reduction on S/RuC



**Table 5.5:** Electrocatalytic activity of the various hydrogen treated samples investigated expressed in terms of current produced at an arbitrarily chosen overpotential of 150 mV

Sample	S	RuC	SR40	SR60	SR80
$i_{150}$ (mA cm <sup>-2</sup> )	3.2	0.75	5.6	7.1	8.9

It was interesting to note that the current density improved with the treatment. This could be due to the activation of the hydroxylated Ru surface. Any RuO<sub>2</sub> formed due to air oxidation could have been reduced to Ru(OH)<sub>2</sub> or RuOH species, which are supposed to be the active species which helps in electrooxidation of methanol in case of Pt-Ru catalysts [70,82,83].

## **5.8 Effect of reduction on activity of OMS-2**

In the fuel cell, the catalyst has to thrive under various conditions, especially with hydrogen present as well. This reducing environment provided by the fuel can be a possible strain on the structure of the manganese oxide material. To study the effect on the OMS-2 in such reducing atmospheres, or in general to understand the reducibility, the following experiments were carried out.

### ***5.8.1 Sample treatment:***

The OMS-2 sample (S) synthesized by reflux method was divided into roughly six equal portions and each was subjected to different treatment. One portion was heated at 300 °C in a high temperature furnace for 1 hour. This sample was cooled and stored away in a dessicator and labeled as **S300**. Similarly, another portion was heated at 550 °C for one hour in the furnace (**S550**). The third portion of the sample was heated at 120 °C (**SH120**) in a horizontal muffle furnace with continuous flow of hydrogen gas at a controlled flow rate of approximately 50 ml per minute for 1 hour. The fourth portion was treated in the same manner as sample SH120 but at a temperature of 300 °C also for 1 hour (**SH300**). The fifth portion was treated with 0.1 M NaBH<sub>4</sub> solution with constant stirring for one hour followed by filtering, washing with hot water till neutral and drying in oven at 120 °C (**SBH**). The remaining sample was retained as blank sample (S) in order to compare the effects of the various treatment procedures carried out on the same.

The various reduction treatment procedures carried out over the samples are given in Table 5.6 along with the sample codes.

**Table 5.6:** Samples treated in various ways and their corresponding codes

<b>Sample code</b>	<b>Treatment</b>
S	As such OMS-2 sample
S300	Heated at 300 °C, 1h
S550	Heated at 550 °C, 1h
SH120	Heated at 120 °C with H <sub>2</sub> , 1h
SH300	Heated at 300 °C with H <sub>2</sub> , 1h
SBH	Treated with 0.1 M NaBH <sub>4</sub> drop wise, 1h

**5.8.2 Sample characterization:**

(a) Chemical analysis:

The chemical methods described earlier to determine average oxidation state and chemical reactivity by H<sup>+</sup> ion exchange was carried out. Table 5.7 gives the average oxidation state, catalytic activity in terms of volumes of thiosulphate and BET surface areas of the samples after the treatment.

**Table 5.7:** Activity of OMS-2 after different treatment procedures

Sample code	'x' in $\text{MnO}_{(1+x)}$	Chemical Analysis		Mn average oxidation state	$\text{V}_{\text{S}_2\text{O}_3^{2-}}$ (ml)
		% $\text{MnO}_2$	% Mn		
S	0.879	86.00	61.8	3.76	3.4
S300	0.876	85.14	61.4	3.75	2.8
S550	0.857	83.78	61.8	3.71	1.8
SH120	0.873	84.85	61.4	3.75	3.1
SH300	0.176	19.47	70.0	2.35	0.0
SBH	0.852	81.51	60.4	3.70	1.4

The average oxidation state of Mn for all the manganese oxide materials is affected by the treatment procedures carried out on the samples. The values have decreased from 3.76 for S to 3.71 for S550. This confirms the results by TG studies in the Chapter 3, which suggests loss of lattice oxygen at this temperature causing gradual reduction. While in case of S300, the average oxidation state shows no significant change, suggesting the structure is still stable and not much lattice oxygen is lost at this temperature, though the change in volumes of thiosulphate from 3.4 ml in S to 2.8 ml in S300 and 1.8 for S550 suggest considerable loss of surface hydroxyl groups and hence decrease in chemical reactivity.

Reduction treatment also showed interesting results. Thus SH120 showed almost no change or negligible change in average oxidation state while its activity showed a very small decrease from 3.4 ml (S) to 3.1 ml (SH120). The small loss in activity could have been attributed to dehydration (or removal of surface hydroxyl groups) caused by the reducing conditions of hydrogen. While, under the same hydrogen atmosphere but at a higher temperature of 300 °C, a drastic change was seen

to have occurred in the material. The sample obtained after the treatment was light brown in colour and looked fluffy. The weight of the sample decreased greatly (by about 50 %). Chemical analysis revealed that changes had indeed occurred, as the average oxidation state dropped to the lowest value of 2.35 suggesting that most of the Mn present in this sample is  $Mn^{2+}$  and probably some amount of  $Mn^{3+}$ . Thus thermal decomposition of the type  $MnO_2 \rightarrow Mn_2O_3$  or even  $Mn_3O_4$  has most likely occurred. The sample also showed absolutely no activity (zero ml of thiosulphate, i.e. no iodine was liberated by the sample), which suggests total removal of surface OH groups by the dehydration process. Thus a kind of limiting conditions has been optimized by this study, wherein the OMS-2 material is shown to be stable up to a temperature of 120 °C under reducing atmosphere of hydrogen and could be useful as electrocatalytic material under fuel cell conditions at elevated temperatures of 120 °C without any significant changes in electrocatalytic activity. The results have been supported well by instrumental methods like XRD data for phase determination.

Treating the OMS-2 sample with 0.1 M  $NaBH_4$  as reducing agent for 1 hour has also been studied and the AOS of Mn showed to drop to a value of 3.7, while the volume of thiosulphate to measure  $H^+$  ion exchange activity dropped to 1.4 ml. This procedure clearly seems not to be the best reducing agent if used to reduce some dopant metal salts to its corresponding metal, as it destroys most of the active surface hydroxyl groups on the OMS-2 surface.

(b) Instrumental analysis:

The catalysts were characterized by the instrumental methods of analysis like XRD, IR and BET surface area for phase determination and to observe the effects of the treatment.

(i) X-ray diffraction:

The XRD patterns of the samples are shown in Figure 5.7. The  $d$  and  $I/I_0$  values of the samples are given in Table 5.8.

The X-ray Diffractograms of samples S, S300 and S550 seem to be almost identical which proves that the structure is stable up to a temperature of about 550 °C. Sample S550 however shows appearance of three extra peaks (shown by asterisks in Figure 5.7), which are low in intensity. This probably marks the onset of structural changes occurring due to thermal decomposition of the type  $\text{MnO}_2 \rightarrow \text{Mn}_2\text{O}_3$  owing to the loss of lattice oxygen.

Treatment of OMS-2 with hydrogen at 120 °C (SH120) showed no changes in diffractogram. However for sample treated at 300 °C (SH300) a totally different pattern was observed due to formation of lower oxide of manganese, which showed absolutely no activity towards  $\text{H}^+$  ion exchange. The narrow peak widths in the diffractograms indicate larger particle size, which might have occurred due to sintering of the oxide particles.

Similarly no changes in XRD pattern of sample SBH were observed, suggesting that the OMS-2 structure was intact, though its chemical analyses showed that the properties had been permanently altered due to loss of hydroxyl groups. See Table 5.7.

**Table 5.8:** Typical X-ray powder diffraction data of the samples

S		S300		S550		SH120		SH300		SBH	
d	I/I <sub>0</sub>	d	I/I <sub>0</sub>	d	I/I <sub>0</sub>	d	I/I <sub>0</sub>	d	I/I <sub>0</sub>	d	I/I <sub>0</sub>
6.91	59	7.01	59	6.88	55	6.91	50	7.01	19	6.93	57
4.84	72	4.82	72	4.91	60	4.88	65	4.91	6	4.93	75
-	-	-	-	3.83	10	-	-	3.51	7	-	-
3.08	87	3.10	87	3.08	85	3.10	83	3.08	4	3.10	90
-	-	-	-	2.70	37	-	-	2.87	3	-	-
2.38	100	2.38	100	2.39	100	2.39	100	2.76	9	2.39	100
2.14	36	2.14	36	2.15	32	2.14	35	2.56	67	2.15	30
1.91	15	1.91	15	1.92	10	1.94	15	2.47	13	1.93	12
1.83	40	1.82	40	1.83	50	1.82	55	2.40	5	1.82	55
1.63	33	1.63	33	1.63	25	1.63	35	2.35	3	1.63	30
-	-	-	-	1.61	10	-	-	2.22	100	-	-
1.52	39	1.53	39	1.53	35	1.53	45	2.11	4	1.54	40
1.42	20	1.42	19	1.42	19	1.42	17	2.03	3	1.43	17
								1.79	2		
								1.57	48		
								1.54	5		
								1.47	2		
								1.42	1		
								1.33	17		
								1.28	14		

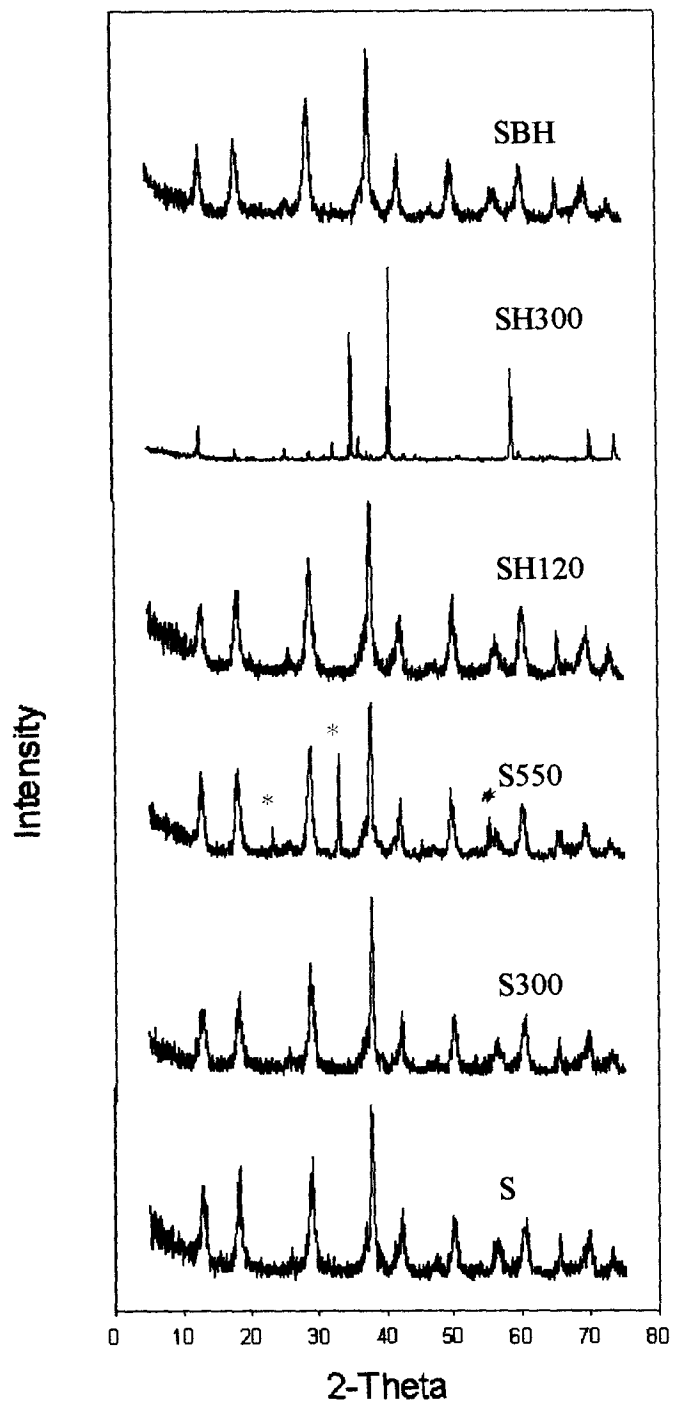


**Figure 5.7:** X-ray diffractograms of the various treated samples; pure OMS-2, **S**; **S** heated at 300 °C, **S300**; **S** heated at 550 °C, **S550** (\* indicates extra peaks); heating at 120 °C with flow of H<sub>2</sub>, **SH120**; heating at 300 °C with flow of H<sub>2</sub>, **SH300** and reduction with NaBH<sub>4</sub>, **SBH**



(ii) Infra-red analysis:

Figure 5.8 also confirms the disappearance of the OMS-2 characteristic peak at  $700\text{ cm}^{-1}$  in the sample SH300 thus, proving that structural distortion has occurred.

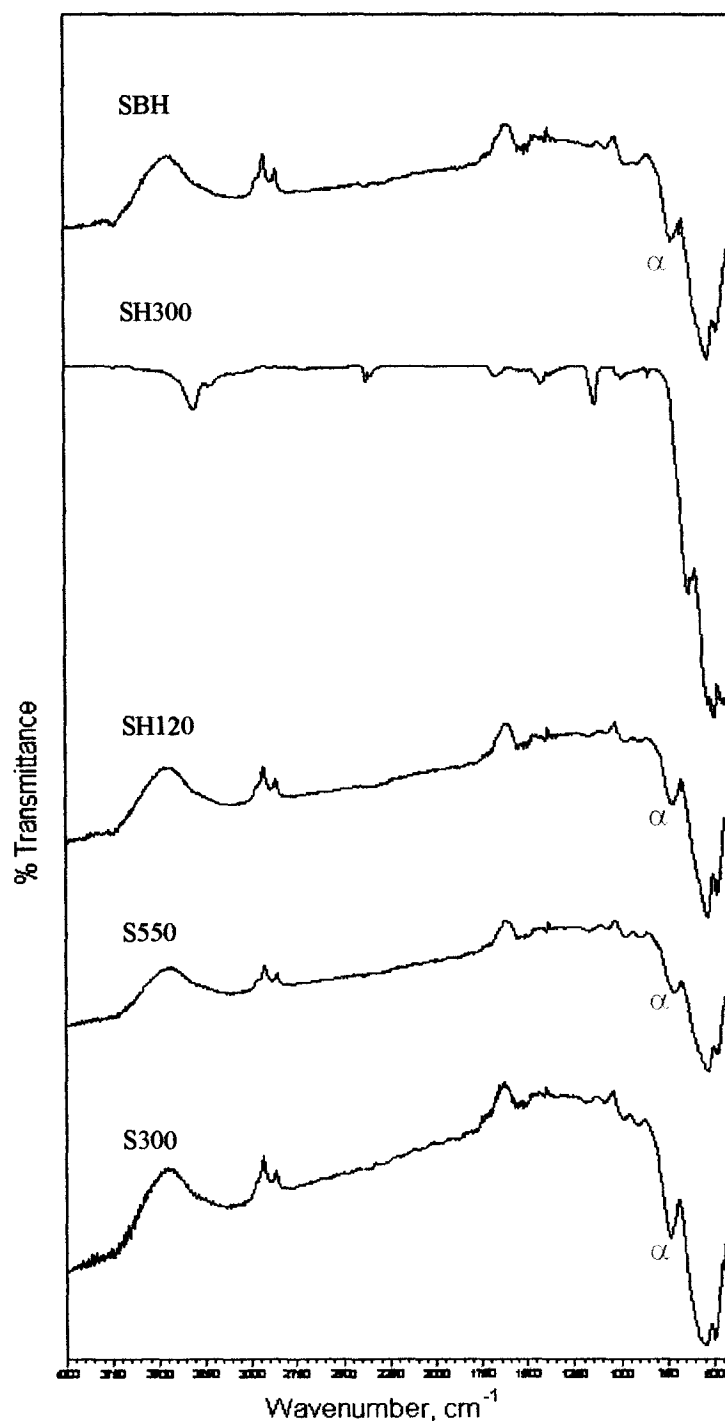


**Figure 5.8:** Infra-red spectra of the treated samples; S300, S550, SH120, SH300 and SBH

(iii) BET surface area analysis:

The surface areas of the samples are as shown in Table 5.9. The samples show progressive decrease in BET surface areas with the increase in temperature of the heat treatment. The sample SH300 showed a remarkable decrease in surface area from 83  $\text{m}^2\text{g}^{-1}$  to 2  $\text{m}^2\text{g}^{-1}$  also confirming that structure change and possible sintering had occurred thus reducing the surface area drastically. SBH however showed negligible or almost no changes in surface area.

Subsequent studies of such kind were carried out and helped us to arrive at a conclusion that the OMS-2 structure could withstand the reduction under hydrogen atmosphere up to about 225 °C though the activity kept decreasing gradually with corresponding increase in temperature. The sample at 120 °C showed the highest activity, after which it progressively decreased.

**Table 5.9:** BET surface areas of the treated samples

Sample code	Treatment	BET ( $\text{m}^2/\text{g}$ )
S	As such OMS-2 sample	83
S300	Heated at 300 °C, 1h	78
S550	Heated at 550 °C, 1h	68
SH120	Heated at 120 °C with $\text{H}_2$ , 1h	83
SH300	Heated at 300 °C with $\text{H}_2$ , 1h	2
SBH	Stirred with 0.1 M $\text{NaBH}_4$ drop wise, 1h	82

## 5.9 Cyclic Voltammetry studies on some OMS-2 catalysts

### 5.9.1 Cyclic Voltammetry Experiment:

A few selected samples were characterized by cyclic voltammetry. A 5% Pt supported on Norit Rox carbon (Pt-NR) was taken as reference for comparison with other materials tested in this work. Methanol oxidation over the different catalysts was studied in a simple three-electrode thermostated cell with platinum foil as counter electrode and saturated calomel electrode (SCE) as reference electrode. 2.5 M H<sub>2</sub>SO<sub>4</sub> and 1 M CH<sub>3</sub>OH were taken in equal quantities in the cell. The working electrode suspended with a platinum wire was lowered into the reaction mixture through one neck of the cell the reference electrode through another and the counter electrode through the third. A computerized potentiostat PGSTAT 10, AUTOLAB software GPES (General Purpose Electrochemical System, ECO CHEMIE Ltd., The Netherlands) was used for the measurements. The electrode was allowed to equilibrate with the surroundings for ~ 15 mins and then the scan was run in a potential window of – 0.2 V to 1.0 V. All experiments were performed at room temperature (30 °C) unless otherwise mentioned. Blanks for all the samples were run in 2.5 M H<sub>2</sub>SO<sub>4</sub>, in the same potential window. The samples were studied for methanol oxidation with respect to three different scan rates of 10, 50 and 100 mVs<sup>-1</sup>. Similar scans were run for the OMS-2 samples and some composite electrodes using Pt-NR and 5% Ru-C, the results of which are presented in Table 5.10.

### 5.9.2 Results and Discussion:

Cyclic voltammetry technique can be used as a tool for comparing relative electrocatalytic activity. For methanol oxidation, a better electrocatalyst will show oxidation of methanol at a lower positive potential. Figure 5.9 gives blank profile in sulphuric acid alone (curve a) as well as for methanol oxidation in sulphuric acid

medium (curve b) at a sweep rate of  $10 \text{ mVs}^{-1}$  on Pt-NR electrode a. In curve (a) the region  $0 - 0.3 \text{ V}$  is hydrogen underpotential deposition (upd) region. These peaks get suppressed in the presence of methanol (curve b) due to the formation of adsorbed CO on the hydrogen adsorption sites. The current for methanol oxidation was observed to occur around  $0.4 \text{ V}$  in the forward scan. The peak at  $\sim 0.64 \text{ V}$  is associated with initial dehydrogenation of methanol to form  $(\text{CO})_x$  type adsorbed species, followed by  $\text{Pt}-\text{OH}_{(\text{ads})}$  formation. On the reverse scan the oxidized Pt surface gets reduced and catalyses methanol oxidation peak which is seen to peak at  $\sim 0.3 \text{ V}$ . These peaks are not clearly discernible at higher scan rates as evident in Figure 5.10.

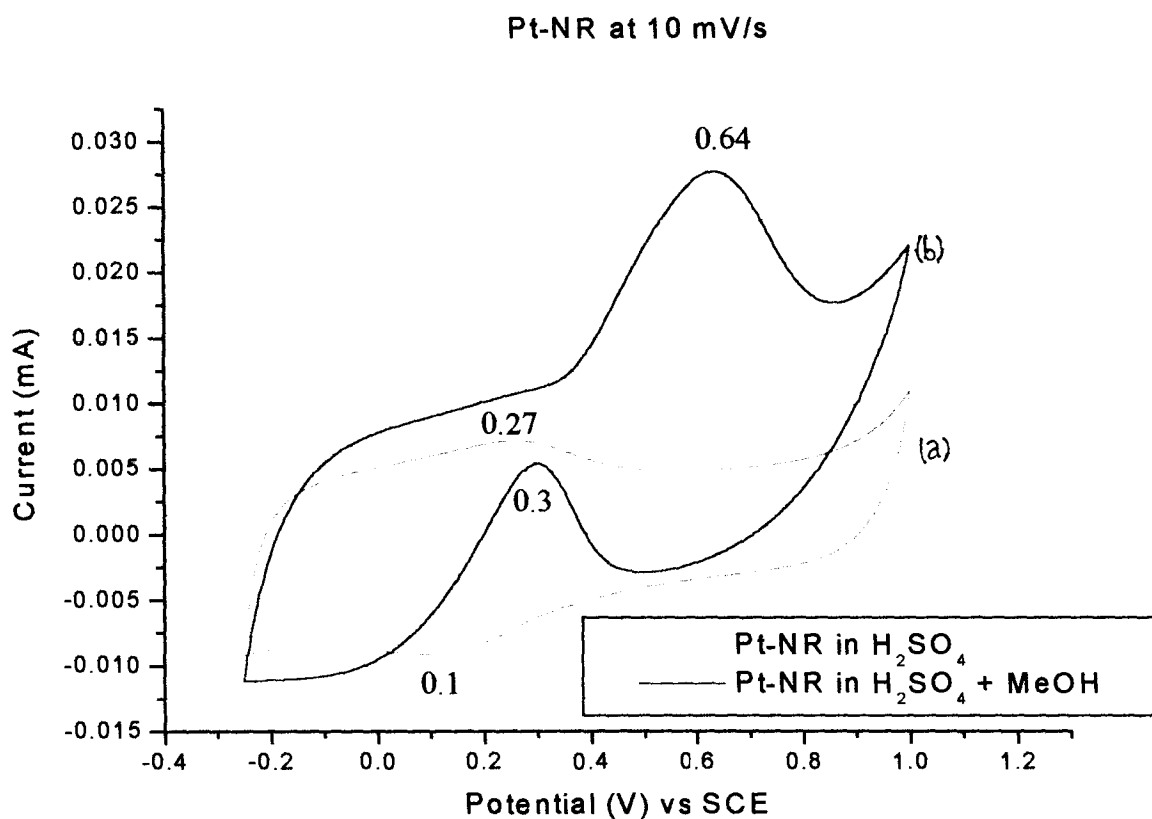


**Figure 5.9:** Cyclic Voltammograms of Pt/C catalyst in  $(2.5 \text{ M}) \text{H}_2\text{SO}_4$  ( ) and  $(2.5 \text{ M}) \text{H}_2\text{SO}_4 + (1\text{M})$  methanol (—)

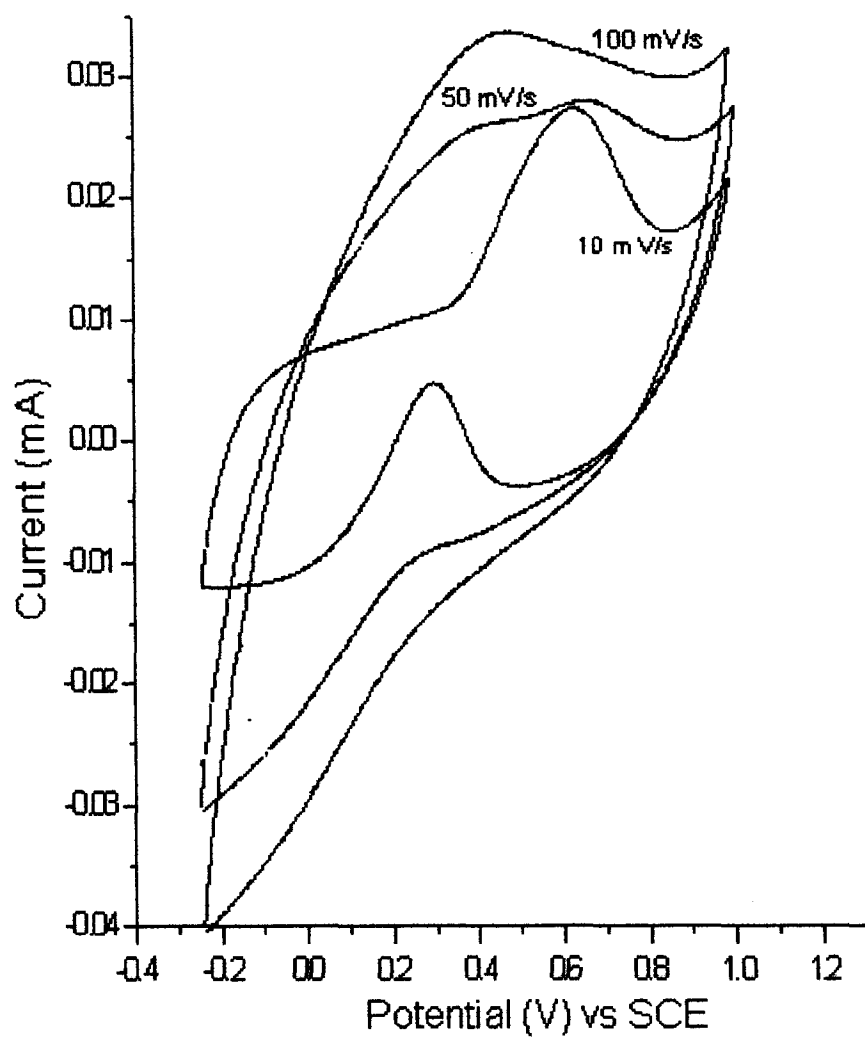


**Figure 5.10:** Cyclic Voltammograms of Pt/C catalyst at various scan rates of 10, 50 and 100 mVs<sup>-1</sup>

Figures 5.11 – 5.13 show profiles for methanol oxidation on various electrodes, when OMS-2 was combined with Pt-NR catalyst or Ru-C catalyst. Table 5.10 summarizes the potentials of the main methanol oxidation peaks (obtained from CV data) in relation to the relative current densities (obtained earlier from Tafel plots and the current densities therein in Tables 5.3 and 5.4) for these catalysts. It can be seen that in catalysts, which show methanol oxidation potentials lower in the CV profiles, those catalysts exhibit higher exchange current densities. Thus CV technique can also be conveniently used for measurement of relative electrocatalytic activity.

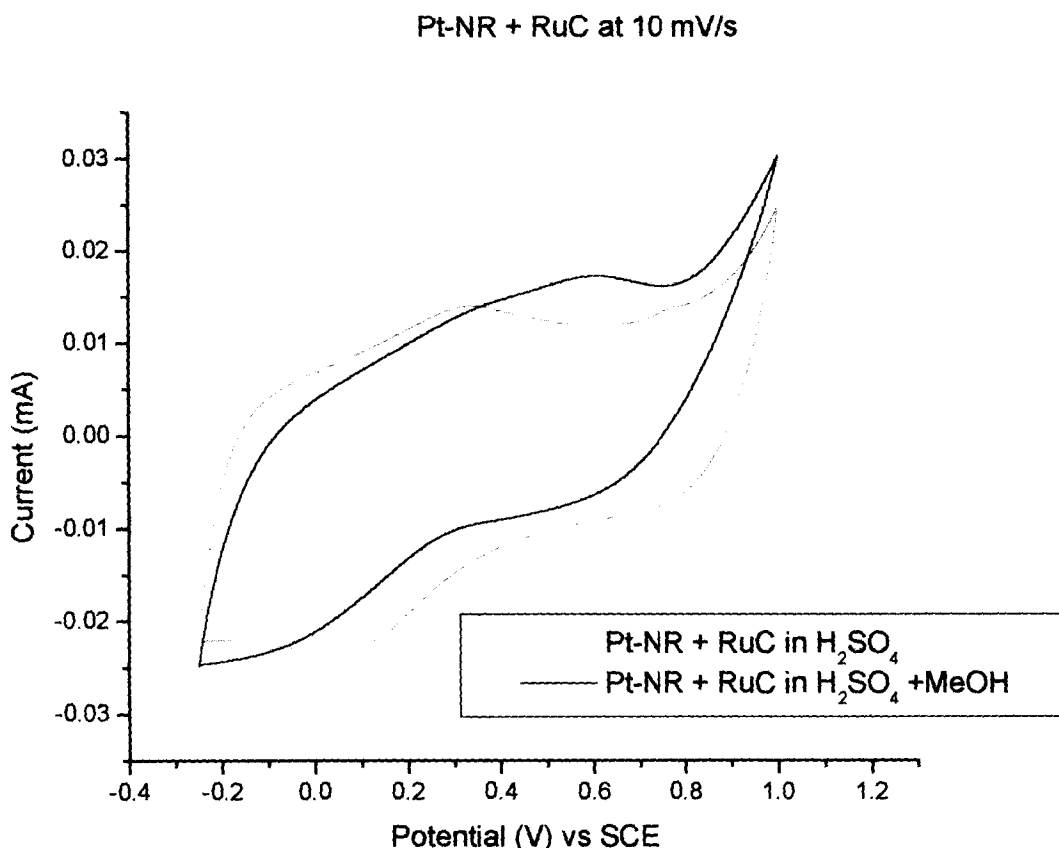


**Figure 5.11:** Cyclic Voltammograms of Pt-NR + Ru-C catalyst in (2.5 M)  $H_2SO_4$  ( - - ) and (2.5 M)  $H_2SO_4$  + (1M) methanol (—)

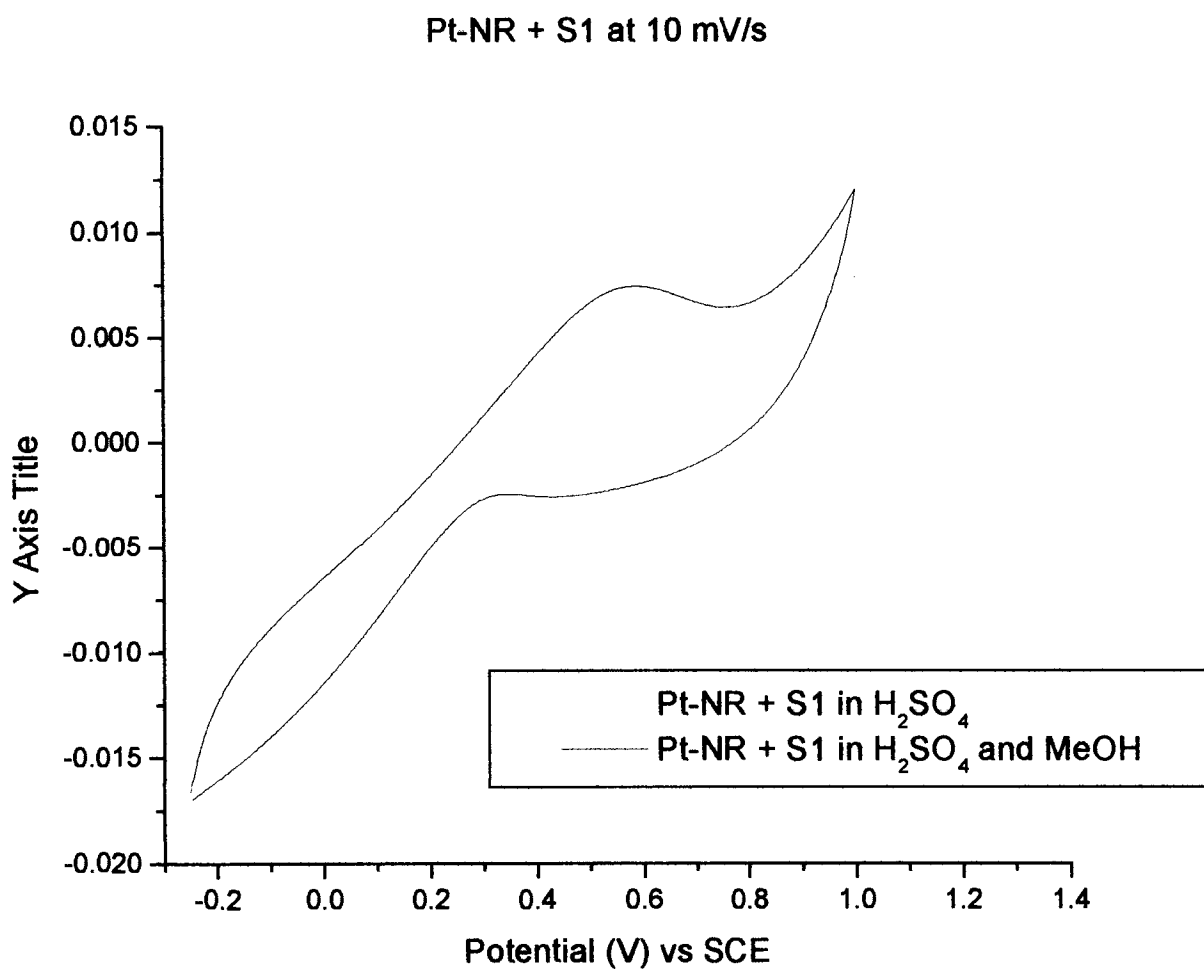


**Figure 5.12:** Cyclic Voltammograms of Pt-NR + S catalyst in (2.5 M) H<sub>2</sub>SO<sub>4</sub> ( - - ) and (2.5 M) H<sub>2</sub>SO<sub>4</sub> + (1M) methanol (—)

S1 + RuC (50% MM) at 10 mV/s

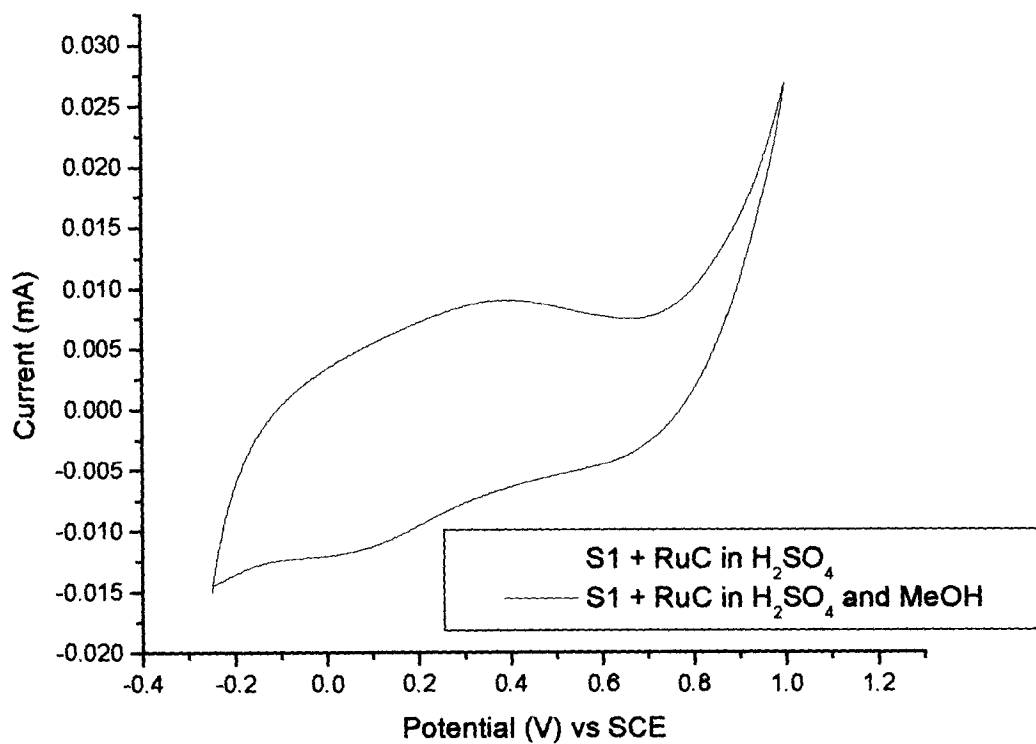


**Figure 5.13:** Cyclic Voltammograms of OMS-2 (S) + Ru-C catalyst in (2.5 M)  $H_2SO_4$

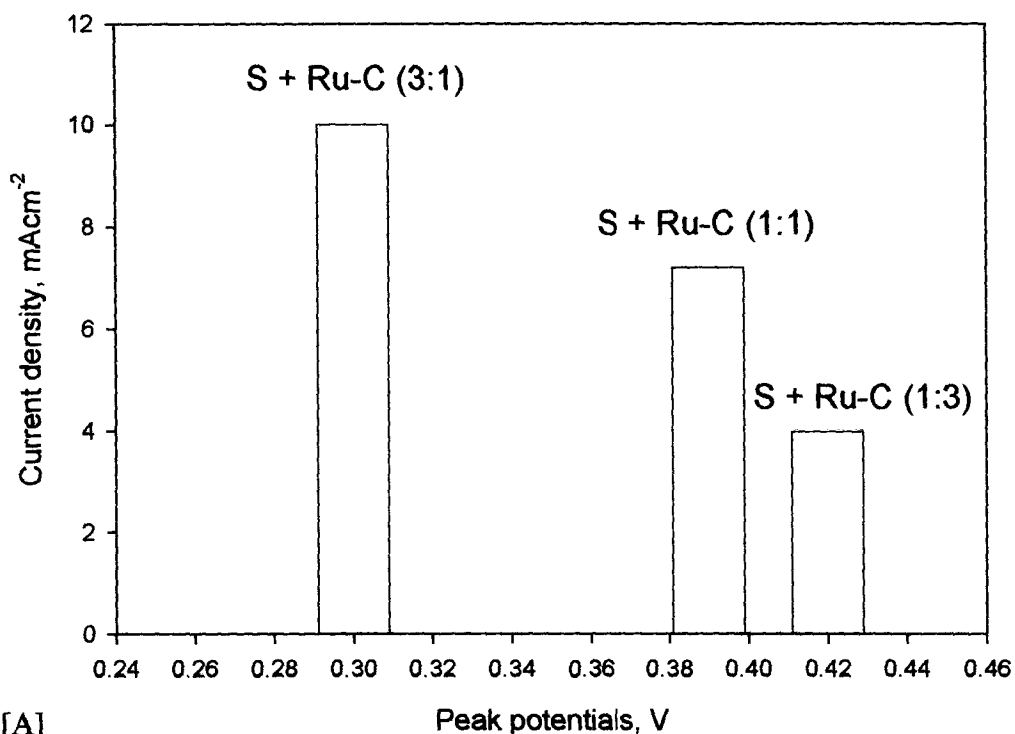
( ) and (2.5 M)  $H_2SO_4$  + (1M) methanol (—)



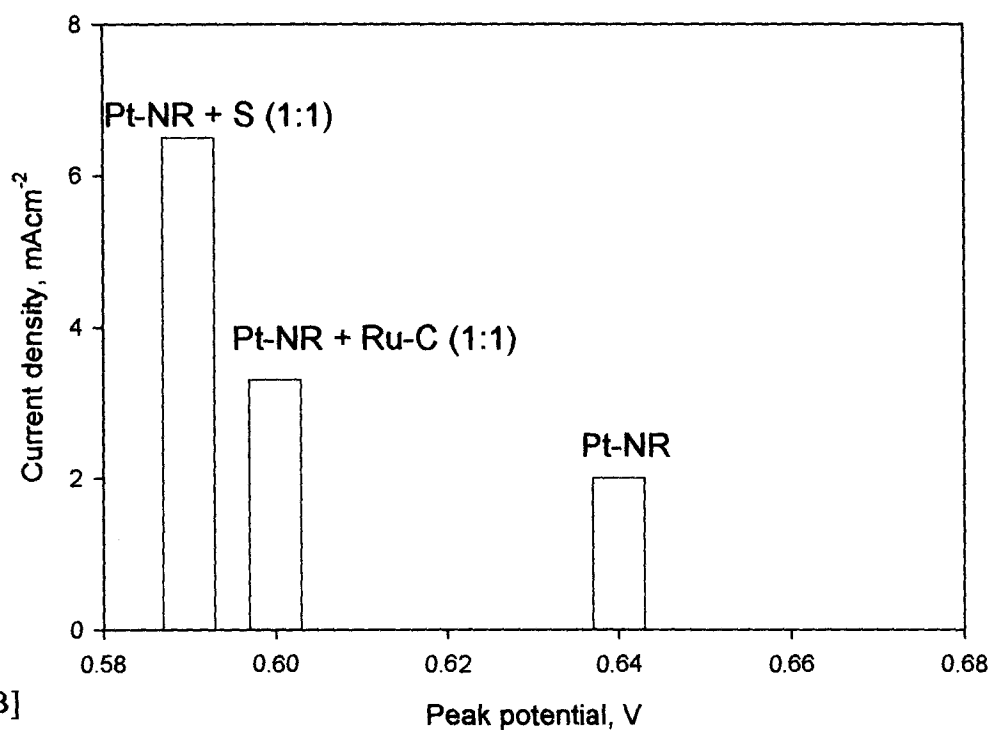
**Table 5.10:** Methanol oxidation peak potentials of forward scan from CV data for various catalysts at scan rate of 10 mVs<sup>-1</sup>

Catalyst	E (V)	$i_{150}$ (mA cm <sup>-2</sup> )
Pt-NR	0.64	2.1
Pt-NR + Ru-C (50% MM)	0.6	3.3
Pt-NR + S1 (50% MM)	0.59	6.7
S1+ Ru-C (25% MM)	0.42	3.98
S1+ Ru-C (50% MM)	0.39	7.2
S1+ Ru-C (75% MM)	0.3	10

An interesting correlation was observed between the peak potentials obtained from cyclic voltammetry data and the current densities deduced from the Tafel plots (Tables 5.3 and 5.4) for the various catalysts as seen in Figure 5.14. The results could be divided into two groups; [A] showing the effect of various amounts of OMS-2 on Ru-C and [B] showing effect of Ru-C and OMS-2 on Pt-NR. Thus S + Ru-C (3:1 mixture) showed highest current density (10 mAcm<sup>-2</sup>) at the lowest peak potential (0.3 V) in that group with the current density decreasing with decrease in amount of OMS-2 in the mixture with a corresponding increase in peak potentials. Similarly in the other group, Pt-NR showed a higher current density (6.7 mAcm<sup>-2</sup>) and at lower potential (0.59V) in combination with OMS-2 than it showed with Ru-C (3.3 mAcm<sup>-2</sup>, 0.6 V). Thus composites with high electrocatalytic activity show methanol oxidation peak at lower potentials.



[A]



[B]

**Figure 5.14:** Correlation between peak potentials obtained from cyclic voltammetry and current densities at overpotential of 150 mV obtained from Tafel plots of various catalysts; [A] various amounts of OMS-2 + Ru-C and [B] Effect of Ru-C and OMS-2 on Pt-NR

### 5.10: Conclusions:

- (a). In case of OMS-2 materials in combination with 5% Ru-C (whether *in situ* generated phase on the Ru-C or 1:1 mixture), Ru enhances oxidation of CO to CO<sub>2</sub> significantly.
- (b). Methanol oxidation kinetics improved with temperature.
- (c). Increasing amount of OMS-2 in a mixture with 5% Ru-C showed increase in current.
- (d). Reduction studies revealed that the OMS-2 material shows maximum activity under reducing atmosphere by hydrogen upto 120 °C and is not stable beyond 300 °C.
- (e). The high activity of the manganese oxide was associated with presence of Mn<sup>4+</sup>/Mn<sup>3+</sup> redox couple. The extent of participation of lattice oxygen played an important role in methanol oxidation reaction.
- (f). Cyclic voltammetry studies showed that active OMS-2 composites allowed oxidation of methanol at a lower positive potential.

## References:

1. C.T. Kresge, M.E. Leonowicz, W.J. Roth, J.C. Vartuli, J.S. Beck, *Nature*, 359, **1992**, 710.
2. C.F. Cheng, Z. Luan, J. Klinowski, *Langmuir*, 11, **1995**, 2815.
3. A. Monnier, F. Schuth, Q. Huo, D. Kumar, D. Margolese, R.S. Maxwell, G.D. Stucky, M. Krishnamurthy, P. Petroff, A. Firouzi, M. Janicke, B.G. Chmelka, *Science*, 261, **1993**, 1299.
4. Q. Huo, J.L. Feng, F. Schuth, G.D. Stucky, *Chem. Mater.*, 9, **1997**, 14.
5. Q. Huo, D. Margolese, U. Ciesla, P. Feng, T.E. Gier, P. Sieger, R. Leon, P. Petroff, F. Schuth, G.D. Stucky, *Nature*, 368, **1994**, 317.
6. U. Ciesla, D. Demuth, R. Leon, P. Petroff, G.D. Stucky, K. Unger, F. Schuth, *Chem. Commun.*, **1994**, 1387.
7. D. Mantonelli, J.Y. Ying, *Angew. Chem.*, 107, **1995**, 2202.
8. I.M. Varentsov, In *Manganese Ores of Supergene Zone: Geochemistry of Formation*, Kluwer Publishers, Boston, **1996**.
9. J.E. Post, *Proc. Natl. Acad. Sci. USA*, 96, **1999**, 3447.
10. S. L. Suib, *Chemical Innovation*, 30, **2000**, 27.
11. S.L. Brock, N. Duan, Z.R. Tian, O. Giraldo, H. Zhou, S. L. Suib, *Chem. Mater.*, 10, **1998**, 2619.
12. S. Fritsch, J.E. Post, S. L. Suib, A. Navrotsky, *Chem. Mater.*, 10, **1998**, 474.
13. Z.R. Tian, W. Tong, J.Y. Wang, N. Duan, V.V. Krishnan, S. L. Suib, *Science*, 276, **1997**, 926.
14. W.T.Jr. Lankford, N.L. Samways, R.F. Craven, H.E. McGannon, In *The Making, Shaping and Treating of Steel* (Assoc. of Iron and Steel Engineers, Pittsburg, PA), **1984**.

15. D.A. Crerar, H.L. Barnes, *Geochim. Cosmochim. Acta*, 38, 1974, 279.
16. A.M. Bystrom, *Acta Chem. Scand.*, 3, 1949, 163.
17. S. Turner, Ph.D. Thesis, Arizona State University, Tempe, 1982.
18. J.E. Post, D.E. Appleman, *Am. Cryst. Assoc. Abstr.*, 16, 1988, 46.
19. J.E. Post, D.E. Appleman, *Am. Mineralogist*, 73, 1988, 1401.
20. J.E. Post, D.R. Veblen, *Am. Mineralogist*, 75, 1990, 477.
21. B.J. Aronson, A.K. Kinser, S. Passerini, W.H. Smyrl, A. Stein, *Chem. Mater.*, 11, 1999, 949.
22. Y.F. Shen, R.P. Zerger, R.N. DeGuzman, S.L. Suib, L. McCurdy, D.I. Potter, C.L. O'Young, *Science*, 260, 1993, 511.
23. R.N. DeGuzman, Y.F. Shen, E.J. Neth, S.L. Suib, C.L. O'Young, S. Levine, J.M. Newsam, *Chem. Mater.*, 6, 1994, 815.
24. R. Giovanoli, B. Balmer, *Chimia*, 35, 1981, 53.
25. J. Luo, S.L. Suib, *J. Phys. Chem. B*, 101, 1997, 10403.
26. Q. Feng, E.H. Sun, K. Yanagisawa, N. Yamasaki, *J. Ceram. Soc. Jpn.*, 105, 1997, 564.
27. Q. Feng, E.H. Sun, K. Yanagisawa, N. Yamasaki, *Chem. Commun.*, 1996, 1607.
28. T. Rhiza, H. Gies, J. Rius, *J. Eur. J. Mineral*, 8, 1996, 675.
29. J. Dai, S.F.Y. Li, K.S. Siow, Z. Gao, *Electrochim. Acta*, 45, 2000, 2211.
30. R. Jothiramalingam, T.K. Varadarajan, *Bull. Cat. Soc. India*, 3, 2004, 94.
31. S. Ching, J.L. Roark, N. Duan, S.L. Suib, *Chem. Mater.*, 9, 1997, 750.
32. S. Ching, D.J. Petrovay, M.L. Jorgensen, S.L. Suib, *Inorg. Chem.*, 36, 1997, 883.
33. L.J. Garces, B. Hincapie, V.D. Makwana, K. Laubernds, A. Sacco, S.L. Suib, *Micropor. Mesopor. Mater.*, 63, 2003, 11.

34. Q. Zang, J. Luo, E. Vileno, S.L. Suib, *Chem. Mater.*, **9**, **1997**, 2090.
35. J. Brenet, *J. Power Sources*, **39**, **1992**, 349.
36. M.H. Rossouw, D.C. Liles, M.M. Thackeray, *Prog. Batteries Battery Mater.*, **15**, **1996**, 8.
37. C.S. Johnson, D.W. Dees, M.F. Manusetto, M.M. Thakeray, D.R. Vissers, D. Argyriou, C.-K. Loong, L. Christensen, *J. Power Sources*, **68**, **1997**, 570.
38. M.Y. Liao, J.M. Lin, J.H. Wang, C.T. Yang, T.L. Chou, B.H. Mok, N.S. Chong, H.Y. Tang, *Electrochem. Comm.* **5**, **2003**, 312.
39. L.I. Hill, A. Verbaere, D. Guyomard, *J. Power Sources*, **226**, **2003**, 119.
40. J.C. Villegas, L.J. Garces, S. Gomez, J.P. Durand, S.L. Suib, *Chem. Mater.*, **17**, **2005**, 1910.
41. X. Chen, Y.F. Shen, S.L. Suib, C.L. O'Young, *Chem. Mater.*, **14**, **2002**, 940.
42. G. G. Xia, J. Y. Wang, Y. G. Yin, S. L. Suib, In *Catalysis of Organic Reactions*; Herkes, F. E., Ed.; Marcel Dekker: New York, **1998**, 615.
43. J. Y. Wang, G. G. Xia, Y. G. Yin, S. L. Suib, In *Catalysis of Organic Reactions*; Herkes, F. E., Ed.; Marcel Dekker: New York, **1998**, 621.
44. H. Zhou, Y.F. Shen, J.Y. Wang, X. Chen, C.L. O'Young, S.L. Suib, *J. Catal.*, **176**, **1998**, 321.
45. J.Y. Wang, G.G. Xia, Y.G. Yin, S.L. Suib, C.L. O'Young, *J. Catal.*, **176**, **1998**, 275.
46. H. Zhou, J.Y. Wang, X. Chen, C.L. O'Young, S.L. Suib, *Micropor. Mesopor. Mater.*, **21**, **1998**, 315.
47. V.D. Makwana, L.J. Garces, J. Liu, J. Cai, Y.C. Son, S.L. Suib, *Catal. Today*, **85**, **2003**, 225.
48. S.L. Suib, *Stud. in Surf. Sci. Catal.*, **102**, **1996**, 47.

49. V.V. Krishnan, S.L. Suib, *J. Catal.*, **184**, **1999**, 305.
50. E.N. Tolentino, Z.R. Tian, H. Zhou, G. Xia, S.L. Suib, *Chem. Mater.*, **11**, **1999**, 1733.
51. J. Y. Wang, G. G. Xia, N. Duan, Y. Ma, S.L. Suib, In *Shape Selective Catalysis, Chemicals Synthesis and Hydrocarbon Processing*, ACS Symposium Series 738, C. Song, J. M. Garces, Y. Sugi, Eds., American Chemical Society: Washington, DC, **1999**, 80.
52. J. Luo, Q. Zhang, A. Huang, S.L. Suib, *Micropor. Mesopor. Mater.*, **37**, **2000**, 243.
53. X. Chen, Y.F. Shen, S.L. Suib, C.L. O'Young, *J. Catal.*, **197**, **2001**, 292.
54. R. Ghosh, Y.C. Son, V.D. Makwana, S.L. Suib, *J. Catal.*, **224**, **2004**, 288.
55. S. R. Segal, S. L. Suib, X. Tang, S. Satyapal, *Chem. Mater.*, **11**, **1999**, 1687.
56. G.G. Xia, Y.G. Yin, W.S. Willis, J.Y. Wang, S.L. Suib, *J. Catal.*, **185**, **1999**, 91.
57. S.R. Segal, S.L. Suib, L. Foland, *Chem. Mater.*, **9**, **1997**, 2526.
58. S.R. Segal, S.H. Park, S.L. Suib, *Chem. Mater.*, **9**, **1997**, 98.
59. M. Polverejan, J.C. Villegas, S.L. Suib, *J. Am. Chem. Soc.*, **126**, **2004**, 7774.
60. J.B. Fernandes, B.D. Desai, V.N. Kamat Dalal, *Electrochim. Acta*, **29**, **1984**, 181.
61. Y. Chabre, J. Pannetier, *J. Prog. Solid State Chem.*, **23**, **1995**, 1.
62. M.A. Scibioh, B. Rajesh, B. Viswanathan, *PINSA*, **68 A**, **2**, **2002**, 99.
63. K. Metkemeijer, P. Achard, *Int. J. Hydrogen Energy*, **19**, **1994**, 535.
64. [www.dmf.com/images](http://www.dmf.com/images).
65. A. Hamnett, *Catalysis Today*, **38**, **1997**, 445.
66. T. Iwasita, *J. Braz. Chem. Soc.*, **13**, **2002**, 401.

67. H.A. Gasteiger, N. Markovic, P.N. Ross, E.J. Cairns, *J. Electrochem. Soc.*, 141, **1994**, 1795.
68. T. Iwasita, H. Hoster, A. John-Anacker, W.F. Lin, W. Vielstich, *Langmuir*, 16, **2000**, 522.
69. M. Watanabe, S. Motoo, *J. Electroanal. Chem.*, 60, **1975**, 267.
70. P.A. Christensen, A. Hamnett, J. Munk, E. Skou, *J. Appl. Electrochem*, 401, **1996**, 215.
71. M. Krausa, W. Vielstich, *J. Electroanal. Chem.*, 279, **1994**, 307.
72. B.J. Kennedy, A. Hamnett, *J. Electroanal. Chem.* 283, **1990**, 271.
73. J.B. Goodenough, A. Hamnett, B.J. Kennedy, R. Manoharan, S.A. Weeks, *J. Electroanal. Chem.*, 240, **1988**, 133.
74. J.O'M. Bockris, A.K.N. Reddy, M.G. Aldeco, In *Modern Electrochemistry*, Vol. 2A, Plenum Publishers, New York, **2000**, 1284.
75. J.O'M. Bockris, A.K.N. Reddy, In *Modern Electrochemistry: An Introduction to an Interdisciplinary Area*, Plenum Publishing Corporation, **2000**, 1166
76. F. Carrette, K.A. Friedrich, U. Stimming, *J. Chem. Phys. Chem.*, 1, **2000**, 162-193.
77. J. Greeley, M. Mavrikakis, *J. Am. Chem. Soc.*, 124, **2002**, 7193.
78. J. Greeley, M. Mavrikakis, *Surf. Sci.*, 540, **2003**, 215.
79. J. Greeley, M. Mavrikakis, *J. Am. Chem. Soc.*, 126, **2004**, 3910.
80. H. Idriss, *Platinum Metal Review*, 48, **2004**, 105.
81. K.Y. Chen, A.C.C. Tseung, *J. Electrochem. Soc.*, 143, **1996**, 2703.
82. A. Hamnett, S.A. Weeks, B.J. Kennedy, G.L. Troughton, P.A. Christensen, *Ber. Bunsenges. Phys. Chem.*, 94, **1990**, 1014.
83. D.R. Rolison, P.L. Ragans, K.E. Swider, J.W. Long, *Langmuir*, 15, **1999**, 774.



84. S.A. Campbell, R.J. Parsons, *J. Chem. Soc. Farad. Tran.*, **88**, **1992**, 833.
85. A. Hamnett, B.J. Kennedy, *Electrochim. Acta*, **33**, **1988**, 1613.
86. H.J. Nakajima, *J. Chem. Tech. Biotech.*, **50**, **1991**, 555.
87. R.Ya Shaidullin, A.P. Semenova, G.D. Vovchenko, Yu B. Vasillev, *Zh. Fiz. Khim*, **57**, **1983**, 1019.
88. S.Ya Vasina, S.A. Stuken, O.A. Petrii, I.L. Gogichadz, V.A. Mukhin, *Electrokhimiya*, **23**, **1987**, 1127.
89. Manoharan, R.; Goodenough, J. B. *J. Mater. Chem.*, **2**, **1992**, 875.
90. K.W. Park, J.H. Choi, B.K. Kwon, S.A. Lee, Y.E. Sung, H.Y. Ha, S.A. Hong, H. Kim, A. Wieckowski, *J. Phys. Chem. B*, **106**, **2002**, 1869.
91. A. Kawahima, T. Kanda, K. Rashimoto, *Mat. Sci. Eng.*, **99**, **1988**, 521.
92. S. Senkan, *Angew. Chem. Int. Ed.*, **40**, **2001**, 312.
93. E. Reddington, A. Sapienza, B. Gurau, R. Viswanathan, S. Sarangpani, E.S. Smotkin, T.E. Mallouk, *Science*, **280**, **1998**, 1735.
94. S. Jayaraman, A.C. Hillier, *Meas. Sci. Technol.*, **16**, **2005**, 5.
95. A. Hamnett, B.J. Kennedy, S.A. Weeks, *J. Electroanal. Chem.*, **240**, **1988**, 355.
96. A. Hamnett, P. Stevens, G.L. Troughton, *Catal. Today*, **7**, **1990**, 219.
97. P.K. Shen, A.C.C. Tseung, *Proc. 186<sup>th</sup> Meeting of Electrochem. Soc. Ext. Abstr.*, Hawaii, May 16-21, **1993**, 576.
98. A.K. Shukla, M.K. Ravikumar, A.S. Arico, G. Candiano, V. Antonucci, N. Giordano, A. Hamnett, *J. Appl. Electrochem*, **25**, **1995**, 528.
99. K. Lasch, L. Jorissen, J. Garche, *J. Power Sources*, **84**, **1999**, 225.
100. O. Savadago, P.J. Beck, *New Materials for Fuel Cell and Modern Battery Systems II*, Montreal, Canada, July 6-10, **1997**.
101. P.V. Samant, J.B. Fernandes, *J. Power Sources*, **79**, **1999**, 114.

102. J.H. White, A.F. Sammells, *J. Electrochem. Soc.*, 140, **1993**, 2167.
103. K.L. Machida, M. Enyo, G.Y. Adachi, J. Shiokawa, *Bull. Chem. Soc. Jap.*, 60, **1987**, 411.
104. W.T. Napporn, H. Lahorde, J.M. Leger, C. Lamy, *J. Electroanal. Chem.*, 153, **1996**, 4049.
105. A.M. Castro Luna, *J. Appl. Electrochem*, 30, **2000**, 1137.
106. M.F. Strike, M. DeRoos, H. Kouldelka, M. Ulmann, J. Augustynski, *J. Appl. Electrochem*, 22, **1992**, 922.
107. M. Hepel, *J. Electrochem. Soc.*, 145, **1998**, 124.
108. S. Swathirajan, Y.M. Mikhail, *J. Electrochem. Soc.*, 139, **1992**, 2105.
109. C.H. Lee, C.W. Lee, D. Kim, S. Bae, *Int. J. Hydrogen Energy*, 27, **2002**, 445.
110. Y. Liu, X. Qiu, Y. Huang, W. Zhu, *J. Power Sources*, 111, **2002**, 160.
111. E. Yasumoto, K. Hatoh, T. Gamou, U.S. Patent No. **5,702,838** (December 30, **1997**).
112. P.V. Samant, J.B. Fernandes, *J. Power Sources*, 125, **2004**, 172.
113. M. Shelef, U.S. Patent No. **6,117,581** (September 12, **2000**).
114. S. Surampudi, A. Frank, R. Narayanan, W. Chun, B. Jeffries-Nakamura, A. Kindler, G. Halpert, U.S. Patent No. **2,001,005,0230** (December 13, **2001**).
115. <http://neon.cm.utexas.edu/stevenson/catalysis.html>
116. Joint Committee on Powder Diffraction Standards (JCPDS), File 20-908.
117. J. Koshiba, S. Nishizawa, In *Electrochemistry of MnO<sub>2</sub> & MnO<sub>2</sub> Batteries In Japan*, Eds. K. Takahashi et al., Vol. II, **1971**, 23.
118. F.A. Julian, *J. Am. Chem. Soc.*, 15, **1893**, 113.
119. W.F. Cole, P.D. Wadsley, A. Walkley, *Trans. Electrochem. Soc.*, 92, **1947**, 133.
120. B.D. Desai, Ph.D. Thesis, University of Bombay, India, **1980**.

121. J.B. Fernandes, B.D. Desai, V.N. Kamat Dalal, *Electrochim. Acta*, 28, **1983**, 309.
122. R. K. Sorem, E. N. Cameron, *Econ-Geol.*, 55, **1960**, 278.
123. P. M. De Wolff, *Acta Cryst.*, 12, **1959**, 341.
124. J.B. Brenet, K. Traore, M. Kappler, *Proc. MnO<sub>2</sub> Symp., Cleveland, OH, U.S.A.*, A. Kozawa, R.J. Brodd (Eds.), 1, **1975**, 290.
125. J. B. Fernandes, B. D. Desai, V. N. Kamat Dalal, *J. Appl. Electrochem.*, 15, **1985**, 351.
126. R.A. Sheldon and J.K. Kochi, In *Metal-Catalyzed Oxidation of Organic compounds*, Academic Press, New York, **1981**.
127. M. Hudlicky, In *Oxidations In Organic Chemistry*, Am. Chem. Soc., Washington, DC, **1990**.
128. R.C. Larock, In *Comprehensive Organic Transformations*, VCH, New York, **1989**.
129. G. Cainelli, G. Cardillo, In *Chromium Oxidations in Organic Chemistry*, Springer, Berlin, **1984**.
130. P. Capdevielle, D. Sparfel, J.B-Lafont, N.K. Cuong, M. Maumy, *J. Chem. Res.*, 10, **1993**, 1993.
131. M. Munakata, S. Nishibayashi, H. Sakamoto, *J. Chem. Soc. Chem. Commun.*, **1980**, 219.
132. T. Nishimura, T. Onoue, K. Ohe, S. Uemura, *J. Org. Chem.*, 64, **1999**, 6750.
133. R. Lenz and S.V. Ley, *J. Chem. Soc. Perkin trans.*, 1, **1997**, 3291.
134. A. Dijkman, I.W.C.E. Arends and R.A. Sheldon, *Chem. Commun.*, **1999**, 1591.
135. T. Mallat and A. Baiker, *Catal. Today*, 19, **1994**, 247.

136. R. Sumathi, K. Johnson, B. Viswanathan, T.K. Varadarajan, *Indian J. Chem.*, **36A**, **1997**, 874.
137. R. Sumathi, K. Johnson, B. Viswanathan, T.K. Varadarajan, *Appl. Catal. A: General*, **1**, **1998**, 4250.
138. R. Sumathi, K. Johnson, B. Viswanathan, T.K. Varadarajan, *Indian J. Chem.*, **38A**, **1999**, 40.
139. R. Sumathi, K. Johnson, B. Viswanathan, T.K. Varadarajan, *Indian J. Chem.*, **41A**, **2002**, 1349.
140. R.B.C. Pillai, *J. Indian Chem. Soc.*, **74**, **1997**, 169.
141. U.R. Pillai, E.S-Demessie, *J. Catal.*, **211**, **2002**, 434.
142. W.K. Scok, *Bull. Korean Chem. Soc.*, **20**, **1999**, 395.
143. G.J. tenBrink, I.W.C.E. Arends, R.A. Sheldon, *Science*, **287**, **2000**, 1636.
144. M. Hulce, D.W. Marks, *J. Chem. Educ.*, **78**, **2001**, 66.
145. N. Kakiuchi, T. Nashimura, M. Inone, S. Uemura, *Fourth Int Electronic Conf (ECSOC-4)* [www.mdpi-org/ecsoc-4.htm](http://www.mdpi-org/ecsoc-4.htm).
146. H. Ji, K. Ebitani, T. Mizugaki, K. Kaneda, *React. Kinet. Catal. Lett.*, **78**, **2003**, 73.
147. S.T. Oyama, A.N. Desikan, J.W. Hightower, In *Catalytic Selective Oxidation*, Eds. S.T. Oyama, J.W. Hightower; ACS symposium Series 53, Washington DC, **1993**, 6.
148. K.M. Myles, C.C. McPheeters, *J. Power Sources*, **9**, **1990**, 311.
149. J. Janata, *J. Chem. Rev.*, **90**, **1990**, 691.
150. H.H. Kung, In *Stud. Surf. Sci. Catal.: Transition metal oxides*, **45**, Elsevier: Amsterdam, **1989**.

151. J.F. Brazdil, In *Characterization of Catalytic Materials*, I.E. Wachs, Butterworth-Heinemann (Eds.), Boston, **1992**.
152. <http://www.webelements.com/webelements/elements/text/radii.html>
153. M. Hirano, S. Yakabe, H. Chikamori, J.H. Clark, T. Morimoto, *J. Chem. Res. (S)*, **1998**, 308.
154. V.D. Makwana, Y.C. Son, A.R. Howell, S.L. Suib, *J. Catal.*, 210, **2002**, 46.
155. S. Fritsch, J.E. Post, S.L. Suib, A. Navrotsky, *Chem. Mater.*, 10, **1998**, 474.
156. Y.G. Yin, W.Q. Xu, S.L. Suib, *Inorg. Chem.*, 34, **1995**, 4187.
157. S. Bakardjieva, P. Bezdika, T. Grygar, P. Vorm, *J. Solid State Electrochem.*, 4, **2000**, 306.
158. Q. Feng, H. Kanoh, K. Ooi, *J. Mater. Chem.*, 9, **1999**, 319.
159. P.M. De Wolff, *Acta Crystallogr.*, 12, **1959**, 341.
160. K. Kordesch, J. Gsellmann, M. Peri, K. Tomantschger, R. Chemelli, *Electrochim. Acta*, 26, **1981**, 1495.
161. Y.F. Yao, N. Gupta, H.S. Wroblowa, *J. Electroanal. Chem.*, 233, **1987**, 107.
162. H. Morimoto, T. Esaka, S. Takai, *Mater. Res. Bull.*, 32, **1997**, 1359.
163. W. Li, W.R. McKinnon, J.R. Dahn, *J. Electrochem. Soc.*, 141, **1994**, 2310.
164. H. Kanoh, Q. Feng, Y. Miyai, K. Ooi, *J. Electrochem. Soc.*, 142, **1995**, 702.
165. L.C. Ferracin, F.A. Amaral, N. Bocchi, *Solid State Ionics*, 130, **2000**, 215.
166. S. Franger, S. Bach, J.P. Pereira-Ramos, N. Baffer, *J. Electrochem. Soc.*, 147, **2000**, 3226.
167. K. Nagayama, K. Kamioka, E. Iwata, H. Oka, Y. Tokunaga, T. Okada, *Electrochemistry*, 69, **2001**, 6.
168. N.A.M. Deraz, H.H. Salim, A.A. El-Aal, *Mater. Lett.*, 53, **2002**, 102.

169. M.H. Rossouw, D.C. Liles, M.M. Thakeray, W.I.F. David, S. Hull, *Mat. Res. Bull.*, 27, **1992**, 221.
170. A. Kozawa, *Progr. Batt. Sol. Cells*, 2, **1983**, 309.
171. A. Kozawa, J. F. Yeager, *J. Electrochem. Soc.*, 115, **1968**, 1003.
172. D. T. Ferrel, W. C. Vosburgh, *J. Electrochem. Soc.*, 98, **1951**, 334.
173. S. W. Donne, G. A. Lawrance, D. A. J. Swinkels, *J. Electrochem. Soc.*, 144, **1997**, 2949.
174. W.H.L.-Valbuena, A. de Souza, V.A. Paganin, C.A.P. Leite, F. Galembeck, E.R. Gonzalez, *Fuel cells*, 2, **2003**, 159.

## **ACHIEVEMENT**

- i. OMS-2 could be synthesized in a facile manner
  - without the need of presence of  $K^+$  ion.
  - $SO_4^{2-}$  ion was found to play a crucial role in OMS-2 phase formation.
- ii. OMS-2 as well as its metal modified forms have been found to be active for benzyl alcohol oxidation. A mechanism has been proposed for the enhanced activity towards the oxidation of benzyl alcohol to benzaldehyde.
- iii. **OMS-2 has been successfully tested for the first time as anode material for use in direct methanol fuel cells.**

### **Publications:**

- (1) "Thermal analysis: An important tool to explain enhanced catalytic activity of manganese oxides",  
**Jeanette S. Rebello** and Julio B. Fernandes  
G.A. Rama Rao, S.C. Parida (Eds.), Proceedings of Thermans-2006, University of Rajasthan, Jaipur, 6<sup>th</sup>-8<sup>th</sup> February 2006
- (2) "Enhanced electrocatalytic activity of Carbon supported MnO<sub>x</sub>/Ru catalysts for oxidation of methanol in Fuel cells"  
**Jeanette S. Rebello**, Purnakala V. Samant, José Luis Figueiredo and Julio B. Fernandes  
Journal of Power Sources, 153, 36-40, 2006
- (3) "SO<sub>4</sub><sup>2-</sup> ion induced synthesis of manganese oxide octahedral molecular sieves (OMS-2)"  
**Jeanette S. Rebello** and Julio B. Fernandes  
Microporous and Mesoporous Materials, 77, 189-192, 2005
- (4) "Catalytic oxidation of benzyl alcohol by Al<sup>3+</sup> doped manganese oxide type OMS-2 using molecular oxygen or air"  
**Jeanette S. Rebello**, Sajo P. Naik and Julio B. Fernandes  
Indian Journal of Chemistry, Vol. 43A, 1676 - 1679, 2004
- (5) "Enhanced activity of OMS-2 samples towards oxidation of methanol",  
**Jeanette S. Rebello**, and Julio B. Fernandes  
S. K. Aggarwal, J. Kamat (Eds.), ELAC-2004, Goa, 18-23<sup>rd</sup> January 2004

### **Papers presented at International Symposia:**

- (1) "Anodic activity of different supports for use in DMFCs",  
**Jeanette S. Rebello**, Purnakala V. Samant and Julio B. Fernandes  
FUELCELLS-2004, Munich, Germany, 6<sup>th</sup>-7<sup>th</sup> Oct 2004.
- (2) "Enhanced electrocatalytic activity of Carbon supported MnO<sub>x</sub>/Ru catalysts for oxidation of methanol in Fuel cells",  
**Jeanette S. Rebello**, Purnakala V. Samant, J.L. Figueiredo and Julio B. Fernandes  
CARBOCAT-2004, Lausanne, Switzerland, 18<sup>th</sup> – 20<sup>th</sup> July 2004.
- (3) "Enhanced activity of OMS-2 samples towards oxidation of methanol",  
**Jeanette S. Rebello**, and Julio B. Fernandes  
ELAC-2004, International Center, Dona Paula, Goa, 18-23<sup>rd</sup> Jan 2004.



**Papers presented at National Symposia:**

- (2) "Thermal analysis: An important tool to explain enhanced catalytic activity of manganese oxides",  
**Jeanette S. Rebello** and Julio B. Fernandes  
Thermans – 2006, University of Rajasthan, Jaipur, 6<sup>th</sup> – 8<sup>th</sup> February 2006.
- (3) "Synthesis of catalytically active Fe-doped OMS-2",  
**Jeanette S. Rebello** and Julio B. Fernandes  
ISCAS – 2005, Goa University, 1<sup>st</sup> – 3<sup>rd</sup> December 2005.
- (4) "Oxidation Benzyl alcohol by Fe-doped OMS-2",  
**Jeanette S. Rebello** and Julio B. Fernandes  
Advances in Catalysis, Loyola College, Chennai, 6<sup>th</sup> – 7<sup>th</sup> Jan 2004.
- (5) "Anodic oxidation of methanol by Fe-doped OMS-2 catalyst",  
**Jeanette S. Rebello** and Julio B. Fernandes  
NCE-11, Tiruchirapalli, Tamil Nadu, 26<sup>th</sup> - 27<sup>th</sup> Dec. 2003.
- (6) "Electrocatalytic Oxidation of Methanol by pure and doped OMS- 2 for use in Fuel Cells",  
**Jeanette S. Rebello** and Julio B. Fernandes  
New Frontiers in Chemistry, Goa University, 26<sup>th</sup> February 2003.
- (7) "Influence of  $\text{SO}_4^{2-}$  ions on the synthesis of OMS-2 materials",  
**Jeanette S. Rebello** and Julio B. Fernandes  
K.J. Somaiya College, Mumbai, 7<sup>th</sup> & 8<sup>th</sup> February 2003.
- (8) "Synthesis of a catalytically active  $\text{Al}^{+3}$  doped OMS-2",  
**Jeanette S. Rebello** and Julio B. Fernandes  
RACS-2002, Kerala, 18<sup>th</sup>- 21<sup>st</sup> December 2002.

